University of Strathclyde

Strathclyde Institute of Pharmacy and Biomedical Sciences

BIODEGRADABLE NANOPARTICLES FOR ORAL DELIVERY OF CICLOSPORIN

BY

DHAWAL DHIRAJLAL ANKOLA

A thesis presented in fulfillment of the requirements for the degree of

Doctor of Philosophy

2010

DEDICATION

I would like to dedicate this work to my wife Mili, my brother Rishit and my parents for their love, care and encouragement.

TABLE OF CONTENT

ACKNOWLEDGMENT

I take this opportunity to express my deepest feelings for my supervisor, Professor M. N. V. Ravi Kumar for his constant support, valuable guidance and continuous enthusiasm.

I also express my sincere thanks to my co-supervisor, Professor R. M. Wadsworth for his help and guidance.

I also would like to thank Professor R. Solaro (University of Pisa, Pisa, Italy) for his valuable support and guidance.

PhD studentship from Faculty of Science, University of Stracthclyde is duly acknowledged.

Post-graduate fellowship in Nanoscience and Nanotechnology sponsored by Ministry of Education, University and Research of the Republic of Italy (MIUR) for research at Department of Chemistry and Industrial Chemistry, University of Pisa, Pisa, Italy is acknowledged.

Thanks to Dr. G. A. Buxton and Dr. E. W. Durbin for in silico release modelling.

Thanks to J. Schäfer and Professor U. Bakowsky for AFM analysis.

Words are hard to come to express my thankfulness for Jagdish, Gaurav Vivek, Girish, Venkat and all the friends who made my time very memorable and enjoyable.

My beloved wife and my parents have been my greatest source of inspiration. Their love, care, scarifies, support, motivation and contribution have made me what I am today.

Finally I would like to thank God for his blessings.

ABSTRACT

Ciclosporin (CsA), a potent immunosuppressant has demonstrated immense potential in the field of transplantation and autoimmune disorders however, the drug associated side effects such as nephrotoxicity and hypertension have been a concern. Attempts were made to reduce CsA mediated nephrotoxicity by nanoparticulate and antioxidant adjuvant approaches. The therapeutic effects and nephrotoxicity of CsA seems to be C_{max} dependent and preliminary data with poly(lactide-*co*-glycolide) (PLGA) nanoparticles (20% drug loading) at 15 mg/Kg dose led to ~3 times lower C_{max} in rats then commercial formulation Neoral®, thereby reduced nephrotoxicity. In the present investigation, the primary objective was to achieve a comparable C_{max} to Neoral® and understand their nephrotoxic behaviour. Various PLGA nanoparticulate formulations were developed with different drug loading leading to varied entrapment efficiency which demonstrated different pharmacokinetic behaviour. The nanoparticles at 30% loading at 30 mg/Kg dose produced comparable C_{max} to that of Neoral® at 15 mg/Kg. The developed formulation in spite of higher kidney burden of CsA demonstrated lower nephrotoxicity indicated by lower blood urea nitrogen, plasma creatinine and glomerular damage, probably due to slow release of the drug from the nanoparticles. The nephrotoxicity of CsA is thought to be free radical mediated, therefore co-entrapped CsA-Coenzyme Q10 (CoQ10) nanoparticles were developed to have better control on nephrotoxic behaviour. Various formulation parameters affected the particle characteristics of co-entrapped nanoparticles with a strong influence of CoQ10 on CsA entrapment. However on *in vivo* evaluation, co-entrapment of CoQ10 provided no added benefits in reducing the nephrotoxicity, compared to CsA nanoparticles. Polymer architecture including the functionalities,

hydrophilicity and molecular weight affect the drug loading and release behaviour, therefore efforts were put in designing a new polymer with an overall objective to reduce the dose of CsA. Multiblock copolymer containing periodically spaced side–chain carboxyl groups was synthesised by a two–step synthesis involving the preparation of ABA triblock pre–polymers of lactic acid (A block) and ethylene glycol (B block) followed by chain extension to $(ABA)_n$ multiblock copolymers by reaction with pyromellitic dianhydride (PMDA) and characterised thoroughly. The new carboxylated polymer when processed into nanoparticles was able to deliver CsA orally, achieving higher C_{max} than PLGA nanoparticles with enhanced tissue levels. The investigation unlocks the potential of polymeric nanoparticles in oral delivery of CsA.

PUBLICATIONS

Ankola, D. D., Battisti, A., Solaro, R. and Kumar, M. N. V. R., 2010. Nanoparticles made of multiblock copolymer of lactic acid and ethylene glycol containing periodic side–chain carboxyl groups for oral delivery of cyclosporine A. Journal of Royal Society Interface, 7, S475-S481.

Ankola, D. D., Durbin, E. W., Buxton, G. A., Schäfer, J., Bakowsky U. and Kumar, M. N. V. R., 2010. Preparation, characterization and *in silico* modeling of biodegradable nanoparticles containing Cyclosporine A and Coenzyme Q10. Nanotechnology, 21, 065104.

Ankola, D. D., Kumar, M. N. V. R**.,** Chiellini, F. and Solaro, R., 2009. Multiblock copolymers of lactic acid and ethylene glycol containing periodic side–chain carboxyl groups: Synthesis, characterization and nanoparticle preparation. Macromolecules, 42, 7388–7395.

LIST OF ABBREVIATIONS

AFM	Atomic force microscopy
Apt	A10 RNA aptamer
ATP	Adenosine triphosphate
AUC	Area under curve
BP	Blood pressure
BUN	Blood urea nitrogen
C_{max}	The maximum concentration of a drug observed after its adminstration
CoA	Coenzyme A
CoQ10	Coenzyme Q10
CsA	Ciclosporin
CYP3A4	Cytochrome P-450 3A4
DBP	Diastolic blood pressure
DL	Drug loading
DMAB	Didodecyldimethylammonium bromide
DNA	Deoxyribonucleic acid
DSC	Differential scanning calorimetry
EDTA	Ethylenediaminetetraacetic acid Sodium
EE	Entrapment efficiency
EGCG	Epigallocatechin gallate
ET-1	Endothelin-1
FAE	Follicle-associated epithelium
FDA	Food and drug adminstration
GALT	Gut associated lymphoid tissue
GIT	Gastrointestinal tract
HMG-CoA	3-hydroxy-3-methyl-glutaryl-CoA
HPLC	High performance liquid chromatography

IL2	Interleukin 2
LDL	Low density lipoproteins
MPS	Mononuclear phagocyte system
MW	Molecular weight
NADPH	Nicotinamide adenine dinucleotide phosphate
NFAT	Nuclear factor of activation of T-cells
NMR	Nuclear magnetic resonance
NP(s)	Nanoparticle(s)
PBS	Phosphate buffer saline
PC	Plasma creatinine
PCL	Polycaprolactone
PDI	Polydispersity index
PEG	Poly(ethylene glycol)
P-gp	P-glycoprotein
PLA	Polylactide
PLGA	Poly(lactide-co-glycolide)
PMDA	Pyromellitic dianhydride
POM	Polarised optical microscopy
PP	Peyer's patches
PSMA	Prostate specific membrane antigen
PVA	Poly(vinyl alcohol)
RA	Rheumatoid arthritis
RAS	Renin-angiotensin system
RES	Reticulo-endothelial system
ROS	Reactive oxygen species
RSD	Relative standard deviation
S.D.	Standard deviation
S.E.M	Standard error of mean

SBP	Systolic blood pressure
SD	Sprague Dawley
SEC	Size exclusion chromatography
SHR	Spontaneously hypertensive rats
TEA	Triethylamine
TGA	Thermal gravimetric analysis
TGF-β	Transforming growth factor-beta
T_{max}	The time after administration of a drug when the maxium blood concentration is reached
ZP	Zeta potential

1. GENERAL INTRODUCTION

1.1 Ciclosporin

Over the past few decades, Ciclosporin (also known as Cyclosporine A) is seen as a breakthrough drug in the field of organ transplantation to prevent graft rejections (Cecka and Terasaki 1991). Originally Ciclosporin (CsA) was obtained from the extracts of the fungus *Tolypocladium inflatum Gams* and its immuno-suppressive effect was discovered in 1970's at Sandoz (Borel *et al*., 1976). The use of CsA for prevention of transplant rejection was approved by Food and Drug Administration (FDA) in 1983 and in 1984 the complete chemical synthesis of CsA was reported (Wenger, 1984). CsA is an extremely hydrophobic cyclic peptide (Figure 1.1) with a molecular formula of $C_{62}H_{111}N_{11}O_{12}$ (molecular weight of 1202.64 Da). In addition to graft prevention (Starzl *et al*., 1981), CsA found several applications in treatment of psoriasis, Crohn's disease and rheumatoid arthritis. CsA has also demonstrated neuroprotective effect by preventing cortical damage following traumatic brain injury (Sullivan *et al*., 2000).

1.1.1 Mechanism of action

CsA exerts its pharmacological actions by inhibition of T-cells mediated immunity (Scheiber *et al*., 1992; Reynolds and Al-Daraji, 2002) by intra-cellular interaction with cytoplasmic receptor protein present in thymus derived (T) lymphocytes, cyclophilin (Figure 1.2). The CsA-cyclophilin complex inhibits activation of calcineurin, which acts as a secondary messenger in dephosphorylation of the nuclear factor of activation of T cells (NFAT). NFAT regulates interleukin-2 (IL2). Hence, inhibition of calcineurin prevents translocation of NFAT from cytoplasm to nucleus that results in

inhibition of IL2 production and leads to arrest of T-cell mediated immune response (Schumacher and Nordheim, 1992).

1.1.2 Therapeutic indications of CsA

Introduction of CsA transformed the field of organ transplantation by specifically inhibiting the early phase T-cell mediated immune response while leaving the remaining immunity unchanged, hence minimising the risk of unwarranted infections (Kahan, 1989). Early studies demonstrated its immunosuppressive activity in murine models (Borel *et al*., 1976). Later several clinical trials in renal transplant patients established CsA's potential as immunosuppressant, improving graft survival rates (European multicentre trial group, 1983; Merion *et al*., 1984; The Canadian multicentre transplant study group, 1986). In subsequent years CsA established itself as a founding stone of solid organ transplantation. In addition to kidney and liver transplants, CsA increased the survival rates of heart (Emery *et al*., 1986) and lung (Toronto lung transplant group, 1986) transplants.

In addition to transplantation, CsA found application in treatment of various auto-immune disorders. Table 1.1 depicts various therapeutic applications of CsA. Several clinical trials demonstrated the effectiveness of CsA in rheumatoid arthritis (RA). At an initially low dose of 2.5 mg/Kg, which was cautiously stabilised to 3.8 mg/Kg, CsA significantly improved patient conditions in a randomised trial consisting of 144 patients with severe RA (Tugwell *et al.,* 1990). CsA was also found to have beneficial effects in treatment of psoriasis. On administration at intermittent short durations, CsA successfully controlled the plaque psoriasis along with improving patient's quality of life by reducing the disease symptoms (Ho *et al*., 1999; Touw *et al.,* 2001). CsA was also found to be useful in patients with chronic

Crohn's disease resistant to corticosteroid therapy (Brynskov *et al.*, 1989). Patients with severe corticosteroid-resistant ulcerative colitis also responded to CsA therapy (Lichtiger *et al.*, 1994). Several clinical trials also demonstrated the effectiveness of CsA in dry eye syndrome (Sall *et al.*, 2000; Stonecipher *et al.*, 2005).

During the last two decades of its existence CsA was tested for various other indications other than organ transplantation however, the potential of CsA is not realised yet due to its adverse effects. Further adding to the complications, the vehicle cremophore® EL (polyoxyethylated castor oil) present in the current marketed formulations is reported to cause anaphylactic reactions (Dye and Watkins, 1980; Theil *et al.*, 1988).

1.1.3 Adverse effects associated with CsA treatment

CsA is associated with various toxicities of which dose-dependent nephrotoxicity is its most characteristic and limiting adverse effect. CsA is also associated with various other adverse effects such as neurotoxicity and hypertension. Table 1.2 enlists various adverse effects of CsA of which the most commonly seen effects viz., nephrotoxicity and hypertension are described below.

1.1.3.1 Nephrotoxicity

In spite of CsA's clinical applicability, its use has generated considerable concerns due to its nephrotoxic effects. Administration of CsA causes renal dysfunction causing functional abnormality and histological deformity characterised by increased plasma creatinine and blood urea levels. The incidences of nephrotoxicity being observed in ~75% of patients receiving CsA (Mihatsch *et al.*, 1994; Toki *et al.*, 1999). CsA induced damage is

associated with reduced glomerular filtration rate and renal blood flow (Myers *et al.,* 1988; Hansen *et al.,* 1997). Most of the functional irregularities are reversible (Andoh and Bennett, 1998) however chronic administration causes irreversible structural changes in kidney. Histological changes are mainly characterised by glomerular damage, tubular atrophy, tubulointerstitial fibrosis and arteriolopathy (Mihatsch *et al*., 1988; Andoh and Bennett, 1998; Rezzani, 2004).

1.1.3.2 Hypertension

Chronic administration of CsA is reported to cause hypertension. A transient rise in blood pressure was observed in healthy volunteers on administration of single dose of CsA (Hansen *et al.,* 1997). Similarly administration of CsA increased hypertension in autoimmune (Bach, 1999) and transplant patients (Taler *et al.,* 1999). The incidences of increased blood pressure were 29-54 and 71-100 % in autoimmune and transplant patients respectively.

Several mechanisms have been proposed for CsA induced renal damage and hypertension. CsA administration markedly reduces glomerular filtration rate and renal blood flow due to its vasoconstriction actions. Several factors contribute to CsA induced vasoconstriction (Conger *et al*., 1994; de Mattos *et al*., 2000).

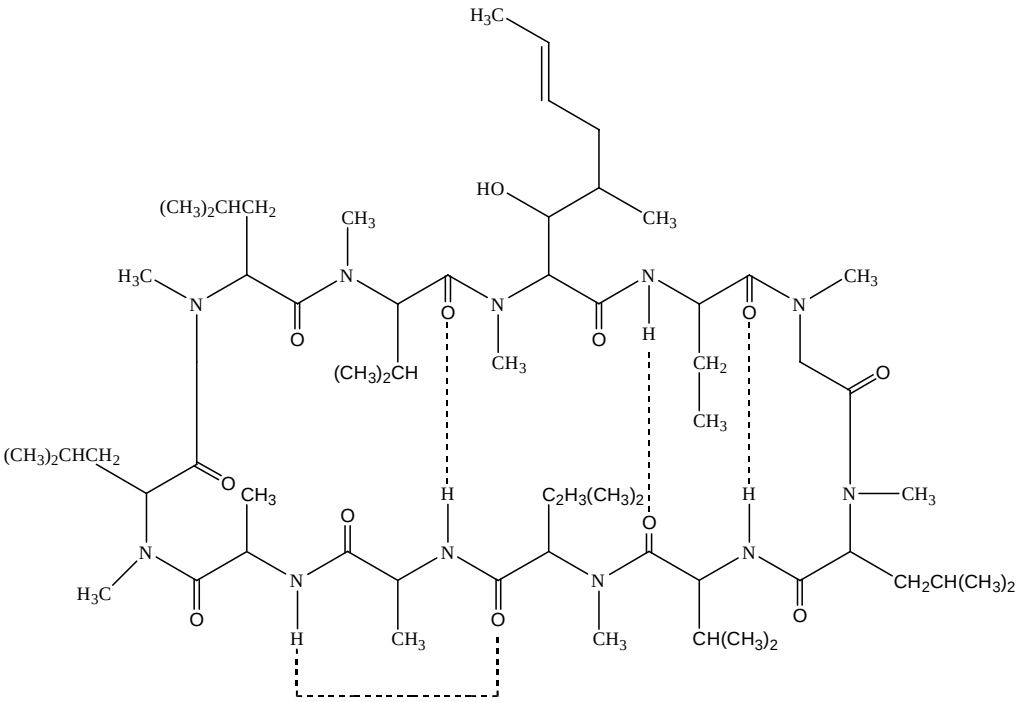

Figure 1.1 Chemical structure of CsA consisting of neutral cyclic peptide with eleven amino acids of which seven are N-methylated.

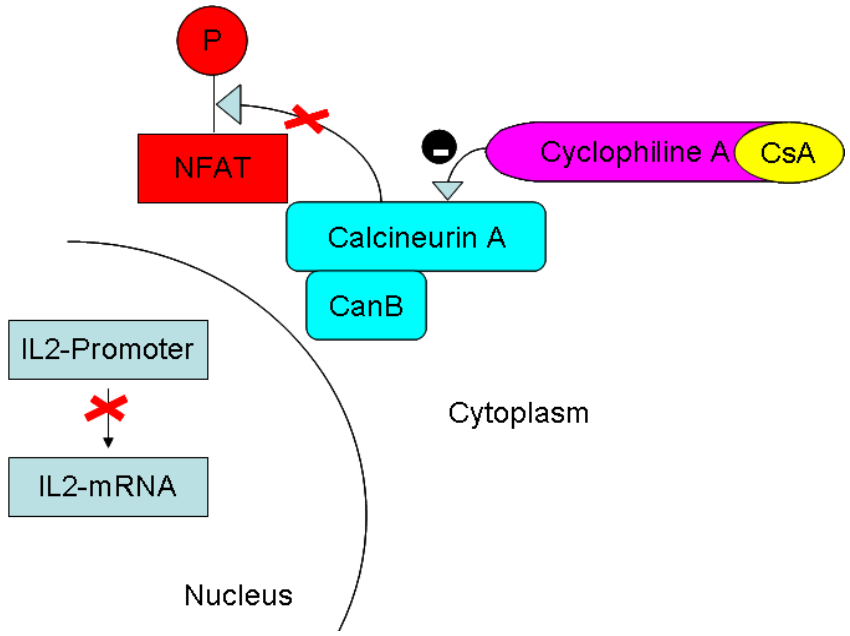

Figure 1.2 Mechanism of action of CsA is based on inhibition of calcineurin which prevents translocation of NFAT to the nucleus, resulting in inhibition of IL2 production and arrest of T-cell mediated immune response. (Adapted from Rezzani, 2004)

CsA causes renin release from juxtaglomerular cells which activates intrarenal and systemic renin-angiotensin system (RAS). RAS by its haemodynamic activity causes vasoconstriction (Lee, 1997). Angiotensin II release causes fibrosis and extra-cellular matrix deposition via stimulation of growth factors (Ruiz-Ortega and Egido, 1997). Endothelin-1 (ET-1) has been found to be associated with CsA toxicity. CsA causes hypersecretion of ET-1 which can cause vasoconstriction and renal damage (Perico *et al*., 1990; Lanese and Conger, 1993).

In addition to RAS and ET-1, CsA is found to stimulate systemic and renal transforming growth factor-beta (TGF-β) expression. Over expression of TGF-β causes renal fibrosis by it actions on extra-cellular matrix components (Shihab *et al*., 2002; Ling *et al*., 2003). In addition to above, thromboxane A_2 (Conger *et al*., 1994) and nitric oxide (Malyszko *et al*., 1996) were also involved in CsA induced toxicity.

Several investigations have also revealed the role of free radicals in CsA induced toxicity. Several animal assessments have observed increased systemic and renal free radical levels on CsA administration. Systemic administration of antioxidants has resulted in amelioration of CsA induced toxicities (Cristol *et al*., 1995; Chander *et al*., 2005).

Various formulation strategies have been attempted to maximise the therapeutic potential of CsA and minimise its toxic effects. The beneficial effect of antioxidants when used in combination with CsA was elegantly demonstrated. The following sections highlight the advances in CsA delivery and the combination approaches.

Table 1.1 Therapeutic indications of CsA

Graft rejection prevention: liver, kidney, lung, heart and bone marrow
Systemic and local immune- associated diseases: Crohn's disease, ulcerative colitis, rheumatoid arthritis, psoriasis, dry eye syndrome, vernal keratoconjunctivitis, atopic dermatitis, myasthenia gravis, aplastic anaemia, autoimmune hepatitis

(Modified from Italia *et al*., 2006)

Table 1.2 Adverse effects of CsA

Urinary system: Acute and chronic nephrotoxicity characterised by increased fluid retention, raised blood urea and plasma creatinine concentrations with histological changes
Cardiovascular system: Cardiovascular complications characterised by increased blood pressure, hypermagnesaemia and hyperkalaemia along with thrombo-embolic complications,
Central nervous system: Adverse effects consist of tremors, ataxia, confusion, convulsions, leucoencephalopathy, cortical blindness
Other include: hepatotoxicity, reduced insulin production, gum hyperplasia and hypertichosis

(Modified from Italia *et al*., 2006)

1.1.4 Delivery aspects of CsA

Considering the fact that CsA therapy in transplant or autoimmune patients requires administration of the drug for longer durations and in certain cases life-long, oral delivery remains the primary route for CsA administration. However, in critical care, CsA is also administered by parenteral routes. In addition to oral and parenteral route, CsA is used for topical applications in treatment of localised autoimmune disorders like dry eye syndrome and psoriasis.

Development of CsA formulations is challenging due to its poor aqueous solubility. CsA has a very unique rigid cyclic structure with eleven amino acids, seven of them being N-methylated. The extensive methylation and hydrophobic character of the amino acid residues together with four intra-molecular hydrogen bonds provides a high rigidity to the cyclic structure along with limiting its aqueous solubility (6.6 μg/ml and log P of 2.92) (Petcher *et al*., 1976; Wegner, 1984; El-Tayar *et al*., 1993). The solubility limiting factor does not allow CsA to be formulated conventionally and further adding to these complications, CsA also does not offer any ionisable functional groups that can lead to improvements in the form of salt formation or pH dependent solubility. CsA prodrugs to improve its solubility have been attempted (Hamel *et al*., 2004; Lallemand *et al*., 2005; Lallemand *et al*., 2007). The very low solubility of CsA qualifies it as a BCS Class II drug (Amidon *et al*., 1995; Chiu *et al*., 2003). In addition to its low solubility, the high molecular weight of CsA reduces it permeability across gastrointestinal tract (GIT) and other biological membranes such as skin and cornea.

Along with CsA's poor aqueous solubility, its extensive metabolism by the cytochrome P-450 3A4 (CYP3A4, cytochrome enzyme system in the

endoplasmic reticulum) presents a challenge in designing oral formulations (Wu *et al*., 1995). CsA metabolises into 15-30 different metabolites by CYP3A4, the biological activity of which are significantly lower than CsA (Kelly *et al*., 1999). The metabolism takes place in the liver along with gastrointestinal tract and the kidney, with intestinal metabolism accounting up to 50% on oral administration of CsA (Hebert, 1997). Additionally, CsA being a P-glycoprotein (P-gp) substrate is effluxed within enterocytes, which seems to cause interpatient variations in oral bioavailability (Lown *et al*., 1992; Fricker *et al*., 1996). The above issues present a challenge in developing CsA formulations with improved bioavailability and reduced variability.

1.1.5 Current CsA formulations Neoral® and Sandimmune®

The formulation initially developed and marketed for CsA was Sandimmune® (Novartis, Switzerland). Sandimmune® is an oil based formulation which forms oil/water mixture, which prior to absorption undergoes emulsification by bile salts. However, its dependence on bile salts results in large interpatient and intrapatient variability in CsA absorption, affecting the therapeutic outcome of CsA and increasing the risk of graft rejection (Mehta *et al*., 1988). Taking into account the disadvantages of Sandimmune®, a new dosage form Neoral® (Novartis, Switzerland) was designed and marketed. Neoral® is available as a soft gelatin capsule or oral solution containing micro-emulsion pre-concentrate. Neoral® on contact with aqueous fluid rapidly emulsifies without the critical actions of bile salts (Ritschel *et al*., 1990). Neoral® formulation was found to have reduced interpatient and intrapatient variability along with improved bioavailability, rapid absorption and linear dose response as compared with Sandimmune® (Mueller *et al*., 1994). Neoral® also demonstrated better correlation between

its blood trough concentrations and Area Under Curve (AUC) with better graft prevention (Lindholm and Kahan, 1993; Freeman *et al*., 1995; Kahan, 2004). In addition to Sandimmune® and Neoral®, some generic CsA formulations have been marketed which include Cicloral (Sandoz/Hexal) and Gengraf (Abbott). Retasis® (Allegran), a topical emulsion of CsA has also been introduced for treatment of dry eye syndrome.

1.1.6 Pharmacokinetics and therapeutic drug monitoring of CsA

The bioavailability of CsA formulations is highly variable, ranging from less than 10% to as high as 89% in various patients. However, Neoral® was found to produce more reliable and reproducible concentrations and on average 30% higher bioavailability with ~ 1 h lower T_{max} and ~50% higher C_{max} (Lindhlom, 1991; Dunn *et al*., 2001) to Sandimmune®. On administration, CsA has a volume of distribution of 3-5 L/Kg, with a clearance of 6 ml/min/Kg and half life of 10 h (Lindhlom, 1991; Fahr, 1993). In blood, CsA primarily binds to lipoproteins and erythrocytes. The unbound fractions of CsA are found to be highly variable (1.4-12%) due to high variability of erythrocytes and lipoproteins in transplant patients (Legg and Rowland, 1987; Legg *et al*., 1988). CsA undergoes extensive metabolism in liver (>99%). Hepatic metabolism of CsA is mainly via CYP3A4. Elimination of the metabolites is mainly through bile. Less than 1% of CsA is recovered in urine in unchanged form. (Kronbach *et al*., 1988; Fahr, 1993; Dunn *et al*., 2001). Several drugs may interact with CsA therapy. The first group of drugs are agents like aminoglycosides antibiotics and amphotericin B, which are known to cause nephrotoxicity and potentially increase the incidences of renal damage when administered along with CsA (Lindhlom, 1991; Dunn *et al*., 2001). The second groups of agents are those which cause either inhibition or induction of

CYP3A4 which results into increased or decreased bioavailability of CsA, respectively (Gomez *et al*., 1995; Spoendlin *et al*., 1998).

Over or under exposure of the CsA which is a narrow therapeutic index drug, greatly affects the outcome of the therapy. Over exposure to CsA results in toxicity while under exposure causes graft rejection. Its critical nature and variable bioavailability underlines the need for therapeutic monitoring of its concentrations and its dose adjustment (Lindholm and Kahan, 1993; Kahan, 2004). Conventionally pre-dose trough levels (C_0) were used to determine dosing as it represented the lowest concentration during dosing interval. However, several studies have demonstrated that steady state concentration obtained at 2 h after dose (C_2) correlated better with the AUC than C_0 levels. Additionally C_2 was also associated with lower incidence of graft rejections (Grant *et al*., 1999; Pollard, 2004). Currently C_2 levels are used to determine dosing regimen for Neoral®.

1.1.7 Delivery systems for CsA

In spite of advancements made by launch of Neoral®, in improving bioavailability and reducing variability in absorption of CsA, there still exists a degree of interpatient and intrapatient variability in the absorption of the CsA which can affect the therapeutic outcome of CsA treatment (Lindholm and Kahan 1993). In addition, the Cremophor® EL present in Neoral® is found to be associated with anaphylactic reactions, hypersensitivity and toxicity (Dye and Watkins, 1980; Theil *et al*., 1988). Considering the clinical significance of CsA as an immunosuppressant, considerable efforts have been put in designing oral formulations with enhanced and reliable bioavailability along with reducing its nephrotoxicity.

Recent improvements in drug delivery technology together with a better understanding of the molecular nature of CsA have allowed the development of a number of promising delivery systems for this peptide. Table 1.3 summarises potential delivery systems investigated for CsA delivery. Solid dispersions of CsA-sodium lauryl sulphate dextrin were prepared by spray drying. The prepared solid dispersion microspheres were found to improve the rate of dissolution and oral bioavailability of CsA in comparison to free drug powder; however, demonstrated similar bioavailability when compared to Sandimmune® (Lee *et al*., 2001). CsA loaded polymeric micelles of polysaccharides (polyoxyethylene cetyl ether grafted dextran and hydroxypropylcellulose) enhanced CsA's permeability across Caco-2 monolayer cell lines. In addition, the micelles demonstrated superior stability in gastric and intestinal fluids (Francis *et al*., 2005). CsA loaded hyaluronic microspheres were found to improve the solubility of CsA but produced similar pharmacokinetic profile to that of Neoral® (Woo *et al*., 2007).

Nanotechnology based formulations of CsA have received significant attention in recent years. As CsA mediates its actions through T lymphocytes circulating in lymphatic system, targeting the lymphatic system by nanoparticulate formulations has been a potential approach to enhance CsA's therapeutic effects. Several polymeric nanoparticulate formulations of CsA have been investigated. The CsA loaded nanoparticles made up of pH sensitive copolymer poly(methacrylic acid/methacrylate) were found to have improved bioavailability in comparison to Neoral® (Dai *et al*., 2004). CsA loaded polycaprolactone (PCL) and poly(isobutyl-2-cyanoacrylate) nanoparticles were prepared by precipitation and polymerisation respectively. The prepared nanoparticles had enhanced immunosuppressive activity investigated by inhibition of lymphocyte proliferation. However,

drug free nanoparticles also demonstrated significant immunosuppressive activity (Guzman *et al*., 1993). PCL nanoparticles were also found to enhance oral bioavailability and lymphatic uptake of CsA without corresponding increase in renal toxicity, compared to Sandimmune® (Varela *et al*., 2001). Poly(lactic acid)–poly(ethylene glycol) (PLA– PEG) and PLA nanoparticle were investigated for CsA delivery. The PLA-PEG nanoparticles demonstrated a better control on CsA release over conventional PLA nanoparticles (Gref *et al*., 2001). Positively charged nanoparticles of chitosan HCl, gelatine-A and sodium glycocholate were explored for oral CsA delivery. Chitosan nanoparticles demonstrated highest bioavailability. The relative bioavailability of CsA increased by 73% and 18% for chitosan and gelatin nanoparticles respectively in comparison to Neoral®. However for sodium glycocholate the bioavailability decreased by 36% (El-Shabouri, 2002). CsA loaded lipospheres were found to improve the *in vitro* immunosuppressive activity of CsA. Bioavailability studies in human revealed a correlation between AUC and C_{max} of CsA to the particle size of the liposphere dispersion (Bekerman *et al*., 2004). Glyceryl monooleate/poloxamer 407 cubic nanoparticles were explored for CsA delivery. The cubic nanoparticles demonstrated 178% relative bioavailability compared to Neoral® in beagle dogs (Lai *et al*., 2010).

In addition to polymeric nanoparticles, solid lipid nanoparticles (SLN) also represent a potential delivery system for CsA. CsA loaded SLN demonstrated a plasma profile curve with no initial blood peaks to those observed in Neoral® with low variation in bioavailability (Mueller *et al*., 2006). Due to its hydrophobic properties, CsA seems to be an ideal molecule for incorporation into liposomes. Numerous efforts have been made to take advantage of liposomes as carrier systems of CsA to lower its side effects, as

liposomes appear to avoid the kidneys (Freise *et al*., 1994) but are preferentially cleared by the reticuloendothelial system and tend to accumulate in the spleen (Fahr *et al*., 1995). Although the lipid bilayers of vesicles are unstable in the gastrointestinal tract (which may lead to uncontrolled drug release and its precipitation), encapsulation of CsA in liposomes has resulted in improved oral absorption of CsA with lower variability (Venkataram *et al*., 1990; Al-Meshal *et al*., 1998; Guo *et al*., 2001; Shah *et al*., 2006). In addition to oral delivery various other modes such as parenteral (Aliabadi *et al*., 2008), pulmonary (Iacono, *et al*., 1997; Tam *et al*., 2008) and topical (Newton *et al*., 1998; Kim *et al*., 2009) delivery have been explored.

Very recently, results from this laboratory has reported on poly(lactide-*co*-glycolide) (PLGA) nanoparticles for oral delivery of CsA with an overall objective of improving oral bioavailability and minimise drug associated nephrotoxicity. The developed formulations, in spite of an improved AUC values demonstrated a better safety profile when compared to Neoral®, in chronic nephrotoxicity model (30 days daily dosing) at 15 mg/Kg dose. One of the possible reasons for low nephrotoxicity could be the lower C_{max} of 448.5 ng/ml of PLGA nanoparticles against a C_{max} of 1448.4 ng/ml attained for Neoral® (Italia *et al*., 2007). In literature several investigations have demonstrated the correlation of CsA concentrations to incidence of side effects. The toxicity was found to depend on C_{max} of the drug (Perico *et al*., 1992; David-Neto *et al*., 2000), which warrants further investigations to have a better insight on the role of C_{max} in toxicity.

Table 1.3 Overview of CsA delivery systems

Route	Formulation/Delivery system	Highlights
Oral	Emulsion pre-concentrate	Marketed by Novartis as Sandimmune® with high solubilising efficiency but with low and variable bioavailability
	Microemulsion pre-concentrate	Marketed by Novartis as Neoral® which has improved bioavailability and reduced variability
	Microemulsion based on Solutol HS 15	Improved solubilisation
	Self-dispersing gels	High CsA solubilisation with similar bioavailability to Neoral®
	Microspheres of sodium lauryl sulfate dextrin	Improved solubility and bioavailability than CsA powder but with similar bioavailability to Sandimmune®
	Stearic acid nanoparticles	Sustained CsA release
	Micellar formulation of polyoxyethylene cetyl ether-grafted dextran	Enhanced permeability
	Nanoparticles of Poly(isobutyl-2-cyanoacrylate)	Enhanced in vitro immunosuppression
	Micro- and nanoparticles of PLGA, PLA with additive fatty acid ester	Polymer matrix and additive affecting release characteristics
	PLGA nanoparticles prepared using DMAB	Better bioavailability and lower nephrotoxicity than Neoral®
	PLA-PEG particles	Improved stability and controlled CsA release
	Polycaprolactone nanoparticles	Enhanced lymphatic uptake and improved bioavailability with no increase in toxicity
	pH sensitive nanoparticles of Eudragit® S100 and	pH dependent CsA release and improved bioavailability

	Hydroxypropyl methylcellulose phthalate	
	Positively charged nanoparticles of chitosan	Improved bioavailability with lower variability
	Polyelectrolyte nanoparticles	Enhanced oral uptake
	Glyceryl monooleate/poloxamer 407 cubic nanoparticles	Improved oral bioavaibility than Neoral®
	Solid dispersions containing polyoxyethylene stearate	Improved CsA dissolution and bioavailability comparable to that of Neoral®
	Solid lipid nanoparticles	Controlled drug release, high entrapment efficiency, consistent bioavailability
	Hyaluronic microspheres	Similar pharmacokinetic profile to Neoral®
	Lipospheres	Correlation between particle size of the dispersion to pharmacokinetic profile
	Cyclodextrins	Improved bioavailability with reduced variability in absorption
	Prodrugs	High solubility in water but with unknown pharmacokinetics
Intravenous	CsA solution in Cremophore® EL and ethanol	Marketed by Novartis
	Liposomes	Reduced nephrotoxicity, rapid clearance from systemic circulation
	PEO-b-PCL micelles	Less nephrotoxic with reduced distribution to kidney
Intramuscular	PLA microsphere	Sustained CsA release
Pulmonary	Propylene glycol aerosol	Effective in lung transplant patients
	Liposomes	Higher CsA retention in lungs
Topical	Penetration enhancer	Improved dermal delivery

	Lecithin vesicles	Enhanced CsA deposition into skin
	Iontophoresis with lecithin vesicles	Enhanced transdermal delivery
Ocular	Penetration enhancers	Improved corneal permeation
	Anionic microemulsion	Marketed by Allergan Pharmaceuticals as Restasis® for treating dry eye syndrome
	Cationic microemulsions	Improved conjunctival and corneal levels
	PCL nanocapsules	Improved corneal uptake
	PLGA microspheres	Higher corneal levels
	Chitosan nanoparticles	Longer retention with higher CsA levels in cornea and conjunctiva

(Modified from Italia *et al*., 2006 and Czogalla, 2009)

1.1.8 Protective role of antioxidants in CsA mediated toxicity

Many experimental studies have demonstrated the role of reactive oxygen species (ROS)/free radical in the pathogenesis of CsA mediated renal toxicity. The vasoconstriction effect of CsA in kidney causes a hypoxia-reoxygenation situation involving free radicals (Zhong *et al*., 1998). Considering the role of free radicals in the CsA mediated nephrotoxicity, several exogenous antioxidants have been explored to prevent the same. Vitamin E was found to inhibit the CsA mediated lipid peroxidation. In addition to lowering free radical mediated damage, Vitamin E improved renal functions such as creatinine clearance and renal blood flow (Durak *et al*., 1998). In addition to Vitamin E several antioxidants such as N-acetyl cysteine, Vitamin C, Melatonin and Selenium were found to be beneficial in reducing the adverse effects of CsA.

Several newer generation antioxidants such as ellagic acid, epigallocatechin gallate (EGCG) and resveratrol have demonstrated their potential in ameliorating CsA induced nephrotoxicity. Resveratrol, when administered per-orally at 5 and 10 mg/Kg was able to prevent CsA mediated nephropathy in rats receiving CsA at 20 mg/Kg (s.c. for 21 days). Resveratrol prevented renal oxidative stress and structural damage (Chander *et al*., 2005). Similarly administration of ellagic acid at 10 mg/Kg for 21 days markedly normalised the CsA induced liver and heart malondialdehyde (MDA) levels, liver catalase (CAT) activities and glutathione peroxidase (GSH-Px) activities and partially ameliorated the structural damages in the kidney, liver and heart tissues in rats receiving CsA (15 mg/Kg, s.c. for 21 days) (Yuce *et al*., 2008). In recent reports from our group, ellagic acid and EGCG entrapped in polymeric nanoparticles were found to be more potent than simple suspensions. Ellagic acid loaded PLGA nanoparticles were able to prevent

CsA mediated kidney damage at three times lower dose than the suspension form (Sonaje *et al*., 2007). Similarly, EGCG loaded PLGA nanoparticles were found to prevent CsA mediated kidney damage. Orally administered nanoparticles of EGCG (50 mg/Kg once in three days) were found to have similar potency to EGCG administered i.p. (50 mg/Kg daily) in preventing renal damage in rats receiving CsA in the form of Neoral® at 15 mg/Kg for 30 days. Orally administered EGCG solution was found to be ineffective in ameliorating the CsA mediated nephrotoxicity (Italia *et al*., 2008).

In addition to toxicity, the oxidative stress generated by CsA is found to be associated with pathogenesis of kidney graft rejection. Association of chronic graft rejection with oxidative stress was investigated in kidney transplant patients receiving CsA and steroids. It was found that patients with renal transplantation had elevated level of oxidative stress with decreased antioxidant defence mechanism. The oxidative markers were predominantly elevated in transplant patients with chronic rejections, indicating towards the role of free radicals in chronic graft rejection (Cristol *et al*., 1998). Similarly, the role of oxidative stress in kidney fibrosis in rat renal allograft model was observed (Djamali *et al*., 2005).

In addition to renal complications mediated by free radicals, the role of oxidized low density lipoprotein (LDL) in cardiovascular complications has generated great interest in transplant patients (Apanay *et al*., 1994), as oxidized LDL may result in atherosclerosis. Administration of CsA to renal transplant patients caused an increase in total cholesterol and plasma triglycerides levels with an increase in small dense LDL which can be easily oxidized. A greater LDL oxidation rate was observed in transplant patients than control.

The above reports widely open up an area for use of antioxidant as co-adjuvant for prevention of CsA mediated disorders.

1.1.9 CsA and newer generation immunosuppressants

The immunosuppressive therapy has transformed over time, from use of non-specific drugs like steroids and azathioprine to more selective molecules. Calcineurin inhibitors, CsA and tacrolimus which inhibit T-cells mediated immune response became the choice of drugs. Tacrolimus which was introduced after CsA in late 1980's, differs from CsA as it binds to FK506 binding proteins (FKBP) 12 rather than cyclophilin. Tacrolimus demonstrated 100 times more potency than CsA *in vitro* but established similar efficacy to CsA in graft prevention due to their similar mechanism of actions. In addition, tacrolimus is also associated with similar renal and hepatic toxicities to CsA (Suzuki *et al*., 1990; Manez *et al*., 1995; Ghasemian *et al*., 2001).

Recently, sirolimus (marketed as Rapamune® by Wyeth) which is an inhibitor of mammalian targets of rapamycin (mTOR) has gained considerable attention due to its lack of nephrotoxicity (Kahan, 2008). In spite of its non-nephrotoxic characteristics, use of sirolimus is limited by its inability act in high risk patients. It is mostly used in patients at moderate risk and is mostly prescribed in combination with CsA or steroids during initial stages of immunotherapy (Woodroffe *et al*., 2005). In addition, sirolimus is also associated with several adverse effects which include hyperlipidemia, leucopenia and thrombocytopenia (Hong and Kahan, 2000; Morrisett *et al*., 2002).

Daclizumab and basiliximab which are CD25 (alpha chain of the IL-2 receptor) monoclonal antibodies (IL-2 antagonist) have been used as

prophylactic and inductive agents in acute rejections. However, these antibodies have also been associated with several side effects which include hyperglycemia, hypertension, neurotoxicity, anaemia and impaired wound healing. In addition, they also require simultaneous administration of CsA for desired immunosuppression (Gorantla *et al*., 2000; Woodroffe *et al*., 2005). In addition to above, mycophenolate mofetil, which is inosine monophosphate dehydrogenase inhibitor, has found limited applications (Gorantla *et al*., 2000). In spite of the introduction of several immunosuppressants, CsA remains the back bone of immunotherapy.

1.2 Coenzyme Q10- A potential antioxidant

Coenzyme Q10 (CoQ10), also known as ubiquinone, is an oil soluble substance found in every cell of human body, mainly present in mitochondria. CoQ10 is biosynthesised in all the tissues of body through a complex process involving several vitamins, trace elements and the amino acid tyrosine. The quinone ring and polyisopreniod chain of CoQ10 are derived from the amino acid tyrosine and acetyl coenzyme A (CoA) respectively, resulting into a benzoquinone with isoprenoid units attached at sixth position with number of isoprene units varying depending upon the species. In humans the bezoquinone is attached to 10 isoprene units hence Q10 (Folker *et al*., 1986; Aberg *et al*., 1992). Figure 1.3 represents chemical structure of CoQ10. The 10 isoprene units attached at position 6 to its benzoquinone ring makes CoQ10 a high molecular weight compound (MW 863 Da) with lipophilic nature. It is a yellow crystalline powder and practically insoluble in water.

CoQ10's bioenergetic actions are of great significance as it acts as coenzyme in the metabolic pathways required for energy production and is found

abundantly in organs such as heart and brain which have highest oxygen consumption (Crane *et al*., 1957; Carne, 2001). CoQ10 acts as a medium for transfer of electrons from nicotinamide adenine dinucleotide phosphate (NADPH) and succinate dehydrogenase to the cytochromes system, an essential process in synthesis of adenosine triphosphate (ATP). CoQ10 acts as a cofactor for mitochondrial enzymes (complexes I, II and III) which are part of oxidative phosphorylation, acting as the only non-protein element involved in electron transport chain transferring electrons between flavoproteins and cytochromes (Aberg *et al*., 1992; Carne, 2001). In addition to CoQ10's role in energy production, it acts as powerful antioxidant, inhibiting lipid peroxidation and protecting mitochondrial deoxyribonucleic acid (DNA) from oxidative stress (Quiles *et al*., 2004) along with prolonging the antioxidant effects of α-tocopherol by its recycling (Quinn *et al*., 1999). Over the years, numerous investigations have demonstrated the beneficial role of CoQ10 in diseases involving free radicals and oxidative stress in their pathology like cardiovascular disorder, cancer and neurodegenerative disorders (Reiter *et al*., 2009; Littaru and Tiano, 2010).

1.2.1 Antioxidant potential of CoQ10

Literature documents an age-dependent decrease in CoQ10 levels in human body. The peak CoQ10 levels are found at age of 19-21 years which gradually decreases by 65% at the age of 80. Furthermore, drugs like 3-hydroxy-3-methyl-glutaryl-CoA (HMG-CoA) reductase inhibitors also cause depletion of endogenous CoQ10 levels (Folkers *et al*., 1990; Andersson *et al*., 1995). Deficiency of CoQ10 has also been reported in a variety of disorders such as hypertension, cancer, Parkinson's disease, periodontal diseases, chronic obstructive pulmonary disease and acquired immunodeficiency syndrome.

Various clinical and animals studies have demonstrated the beneficial role of CoQ10 in above mentioned disorders (Greenberg and Frishman, 1990; Lockwood *et al*., 1994; Beal, 1999).

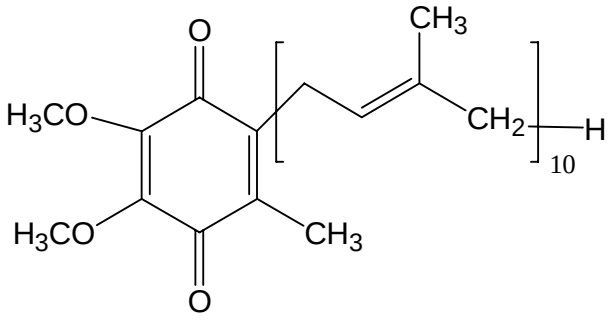

Figure 1.3 Chemical structure of CoQ10 (2,3-dimethoxy-5-methyl-6-decaprenly-1,4-benzoquinone)

1.2.1.1 Hypertension

Several clinical and experimental studies have demonstrated the deficiency of CoQ10 in hypertension and the potential benefits of CoQ10 supplementation. Administration of CoQ10 at 2 and 10 mg/Kg was able to prevent the occurrence of hypertension in unilaterally nephrectomised rats receiving saline and desoxycorticosterone. In addition to prevention of hypertension, CoQ10 administration resulted in lower incidences of glomerulus and tubular epithelia degeneration in the kidney (Igarashi *et al*., 1972). Similarly, administration of CoQ10 in spontaneously hypertensive rats (SHR) and renal hypertensive (Goldblatt method) dogs resulted in suppression of hypertension (Igarashi *et al*., 1974).

Many clinical trials have also demonstrated the beneficial role of CoQ10 in hypertensive patients. Administration of CoQ10 in patients with symptomatic essential hypertension significantly enhanced the systolic and diastolic functions with improvement in left ventricular wall thickness. Along with steady enhancement of clinical functions, 51% of patients required lesser (by 1 to 3) antihypertensive drugs (Yamagami *et al*., 1986). In an another study administration of CoQ10 at 50 mg twice a day, for 10 weeks to 26 patients with essential arterial hypertension resulted in significant decrease of systolic and diastolic blood pressure. (SBP and DBP). The SBP decreased from 165±3 to 147±4 mm Hg while DBP was reduced from 98±2 to 86±1 mm Hg (Digiesi *et al*., 1994). In a meta-analysis of clinical trials data, CoQ10 was found to reduced SBP and DBP by 17 and 10 mm Hg, respectively (Rosenfeldt *et al*., 2007). The beneficial effect of CoQ10 in hypertensive state is associated with a decrease in total peripheral resistance which is due to its direct action on the vascular wall (Okamoto *et al*., 1991) along with improving diastolic function (Langsjoen *et al*., 1993) and reducing

blood viscosity (Kato and Yoneda, 1990). CoQ10 also acts as an antagonist for vascular superoxides, either scavenging them or suppressing their synthesis (McCarthy, 1999).

Recently, the potential of CoQ10 loaded PLGA nanoparticles for management of hypertension was explored by this laboratory. The CoQ10 nanoparticle formulation had the following characteristics, size: 112±7 nm, PDI: 0.10±0.04, Entrapment Efficiency: 82±3 at 20% loading and Zeta potential: 82±1 mV. The Goldblatt 2-kidney 1-clip (2K1C) model was used to assess the potency of different CoQ10 formulations. From the blood pressure recordings on 12th and 15th day after renal clipping it was observed that CoQ10 nanoparticles were more efficacious than the suspension form in treating hypertension at 60% lower dose and more efficacious than the commercial liposomal formulation (Liq-Q-Sorb®) at equal dose (Ankola *et al*., 2007).

1.2.1.2 CoQ10 in free radical mediated drug toxicities

Several studies have established CoQ10's beneficial role in preventing several free radical mediated drug toxicities. Gentamicin, a well known antibiotic exhibits its nephrotoxicity by generation of free radicals which causes lipid peroxidation and depletion of antioxidant enzymes (Walker *et al*., 1999). CoQ10's potential against reducing gentamicin nephrotoxicity was investigated. Administration of CoQ10 (10 mg/Kg/day, i.p.) to rats receiving gentamicin (80 mg/Kg, i.p.) for eight days resulted in significant decrease in nephrotoxic parameters (plasma creatinine and blood urea levels) with reduced free radical damage compared to rats receiving only gentamicin (Upaganlawar *et al*., 2006). Similarly CoQ10's protective role was investigated for cisplatin induced nephrotoxicity. Administration of CoQ10

(125 mg/Kg) to rats for five days resulted in amelioration of cisplatin (7.5 mg/Kg) induced free radical damage associated with cisplatin's acute nephrotoxicity (Sayed-Ahmed *et al*., 1999). Several preclinical and clinical studies have established CoQ10's efficacy in preventing anthracycline-induced cardiotoxicity. CoQ10 by its antioxidant activity prevents the mitochondrial damage in heart caused by anthracyclines daunorubicin and doxorubicin (Conklin, 2005).

In a recent report, CoQ10's role in metabolic syndrome was established. Metabolic syndrome is a disorder characterised by several complications which include hypertension, dyslipidemia and hyperglycemia associated with systemic oxidative stress. Administration of CoQ10 supplemented in diet (0.07%, 0.2% and 0.7%) to rats with metabolic syndrome resulted in lowerer generation of oxidative and inflammatory markers in dose dependent manner in comparison to control animals. In addition to preventing oxidative damage, CoQ10 also lowered the blood pressure and reduced endothelial dysfunction (Kunitomo *et al*., 2008).

1.2.2 Delivery aspects of CoQ10

The high molecular weight and low aqueous solubility of CoQ10 limits its oral absorption (Bhagavan and Chopra, 2007). On administration at 90 mg/day in adults, only 3% of the administered dose was found in the blood. Once absorbed, CoQ10 is taken up by chylomicrons and distributed to liver and gets incorporated into low density lipoprotein and subsequently distributed to tissues. About 40-50% percent of intracellular CoQ10 is found in mitochondria while the rest is distributed in the nucleus (25-30%), microsomes (5-10%) and cytoplasmic matrix (5%). After oral administration T_{max} of CoQ10 is observed after 2-6 h however, some studies have also

observed an additional plasma peak after 24 h which is thought to be due to entero-hepatic circulation and redistribution. CoQ10 has half life of about 34 h with total body clearance about 1.51 to 4.13 L/h. The metabolic process of CoQ10 is indistinctive with very little information available in humans and animals. CoQ10 undergoes metabolism in all tissues and is eliminated through biliary tract (Greenberg and Frishman, 1990; Weis *et al*., 1994; Bhagavan and Chopra, 2006).

CoQ10 due to its poor biopharmaceutical properties presents a challenge to formulation scientist in development of oral formulations. Many formulations of CoQ10 have been investigated of which oil based and powder fill capsules have been commercialised, however bioavailability of these formulations are low with large variability. Several investigations have been performed to determine the bioavailability of various CoQ10 formulations. A 100 mg single dose study in humans showed that CoQ10 when administered as a suspension in soya bean oil shows higher CoQ10 peak values than powder filled capsule or a suspension in soya bean oil with emulsifiers (Weis *et al*., 1994). In a separate study it was observed that administration of CoQ10 as suspension in oil didn't show any significant difference in bioavailability to powder filled capsule over long term supplementation (Kaikkonen *et al*., 1997).

Q-Gel®, a new hydrosoluble CoQ10 formula in softgel (using a new Bio-Solv process) was developed by Chopra and his colleagues (Tischon Corp., Westbury, NY) which had 100% dissolution and its relative bioavailability was compared to other commercially available products. These products represented hard shell capsules containing powder, softgel capsule containing a suspension in oil and tablets based on powder. The relative bioavailabilities were 125%, 100% and 128% respectively. The Q-Gel®

documented vast superiority with relative bioavailability of 319%. Administration of Q-Gel® resulted in sharp increase in plasma CoQ10 levels (2.5 μg/ml) within three to four weeks with further increase over the time (Chopra *et al*., 1998). Although optimal dose of CoQ10 is not known for every pathological condition, researchers during the 9th international conference on CoQ10 in Ancona, Italy came to a common agreement that levels of 2.5 μg/ml and possibly over 3.5 μg/ml are required to have desired therapeutic effects.

Several other delivery strategies such as redispersible dry emulsions, complexation of CoQ10 with cyclodextrins, self-emulsifying drug delivery systems and nanoparticles have been explored for improving CoQ10 bioavailability. Kommuru *et al*., (Kommuru *et al*., 2001) developed and characterised self-emulsifying drug delivery systems of CoQ10 which demonstrated two-fold increase in oral bioavailability in dogs compared to powder formulation. However, the major disadvantage of the formulation was the use of high concentration of surfactants (30-60 %w/w) which causes cell toxicity (Gursoy and Benita, 2004). Several nanoparticulate approaches were also explored for CoQ10 delivery. Preparation and characterisation of CoQ10 loaded solid lipid nanoparticles was reported (Bunjes *et al*., 2001). Other nanoparticulate strategies comprises of CoQ10 loaded poly(ethylene imine) dodecanoate complex (Thunemann and General, 2001) and poly(methyl/methacrylate) nanoparticles (Kwon *et al*., 2002). Polymeric nanoparticles of poly(methyl/methacrylate) also demonstrated superior stability against UV and high temperature mediated degradation compared to oil based formulations (Kwon *et al*., 2002). Recently surfactant free PLGA nanoparticles were explored for CoQ10 delivery which demonstrated a sustained release of CoQ10 over 2 weeks, *in vitro*. (Nehilla *et al*., 2008).

1.3 Nanotechnology in oral delivery

The oral route remains the most convenient and desired route for administrating drugs to the patients. However, upon oral administration, several drug molecules when given in conventional dosage form results in poor bioavailability. The low oral bioavailability results from poor biopharmaceutical properties associated with the drug molecules which are low aqueous solubility and intestinal permeation; poor intestinal stability; P-gp mediated efflux in enterocytes and pre-systemic metabolism. Over several decades, numerous delivery systems have been explored to overcome the poor biopharmaceutical properties of drugs to result in safe and efficacious formulations.

Over the last decade, nanotechnology based formulations have received great interest due to their ability to cross various biological membranes of the body (Chen and Langer, 1998; Kreuter *et al*., 2003; Panyam and Labhasetwar, 2003). Nanoparticles can be characterised as colloidal systems ranging from 10 to 1000 nm (Speiser and Kreuter, 1976). Of the various explored nanoparticulate approaches, biodegradable polymeric nanoparticles offer wide applications in oral drug delivery (Allemann *et al*., 1998; Hans and Lowman, 2002; Bhardwaj *et al*., 2005). By virtue of their absorption properties through GIT, polymeric nanoparticles offer a platform to deliver various drugs falling under different classes (I-IV) of BCS (Bhardwaj *et al*., 2005). In addition to improving absorption, polymeric nanoparticles offer several advantages like, sustaining the release of drugs, preventing P-gp efflux and pre-systemic metabolism and protecting sensitive molecules from enzymatic metabolism and degradation in the gut. The polymeric nanoparticles have been widely explored for delivery of different classes of drugs which include protein and peptides, chemotherapeutic agents, hormones, antibiotics and

immunomodulators (Tobio *et al*., 1998; Varela *et al*., 2001; Ubrich *et al*., 2004; Mittal *et al*., 2007; Bhardwaj *et al*., 2009) with greater emphasis put in designing nanoparticulate carries for delivery of macromolecules through oral route.

The absorption characteristic of nanoparticles through GIT has been widely investigated (Jani *et al*., 1992; Desai *et al*., 1996; Delie, 1998). The GIT is lined with an epithelium made of a mosaic of cells, among which absorptive cells (enterocytes) and goblet cells (secreting the mucus) may be distinguished. These cells are tightly held together and form a strong barrier covered by a layer of mucus. Lymphoid follicles which are part of the gut associated lymphoid system (GALT) are scattered in the enterocytes layer. Lymphoid follicles may be diffusely distributed or clustered in so-called Peyer's patches (PP), with the number and location of PP varying widely between species and individuals. These follicles are overlaid by the follicle-associated epithelium (FAE), which comprises the M (membranous) cells which are modified with less uniform microvilli and thinner glycocalyx on its apical surface compared to neighbouring enterocytes (Gebert *et al*., 1996). The majority of investigation suggests, M-cells in PP as the site of nanoparticle uptake (Jani *et al*., 1990; Hussain *et al*., 2001; Florence, 2005). On binding with the apical membrane of M-cells, nanoparticles are swiftly internalised (endocytosis) and shuttled to lymphocytes, resulting in systemic delivery of drug (Jani *et al*., 1992; Desai *et al*., 1996; Florence, 2004; des Rieux *et al*., 2006). However, in addition to uptake via M-cells, nanoparticles have been found to be absorbed via other transcellular pathways involving enterocytes and very limited absorption through paracellular route (Desai *et al*., 1996; Florence, 2004; des Rieux *et al*., 2006).

Several investigations have demonstrated the effect of size on nanoparticle uptake. 100 nm particles demonstrated a 2.5 and 6 fold higher uptake than particles of 1 μm and 10 μm in size respectively in Caco-2 cells (Desai *et al*., 1997). It was also found that nanoparticles in the range of 50-100 nm show maximum absorption while particles above 1 μm in size were trapped in PP (Jani *et al*., 1990). The 50 and 100 nm particles were absorbed to an extent of 34 and 26% respectively. In addition to size, several other parameters such as particle surface charge and hydrophobicity/hydrophilicity of particles have found to affect their uptake through GIT.

1.3.1 Formulation parameters

Selection of excipients is crucial in designing a nanoparticulate system. The excipients have found to influence various important nanoparticle characteristics critical to the success of technology.

1.3.1.1 Polymer matrix

1.3.1.1.1 Polyesters

Of the various biodegradable polymers explored for nanoparticulate approach, polyesters have received a great deal of attention. Polyester, PLA, Poly(glycolic acid) (PGA) and their copolymer PLGA (Figure 1.4) have been exploited utmost for particulate delivery due to their desired properties of biocompatibility, degradability and ease of fabrication (Kitchell and Wise, 1985; Anderson and Shive, 1997; Bala *et al*. 2004; Mohamed and Van der Walle, 2008; Kumari *et al*., 2010).

Due to the presence of chiral carbon PLA exists as isomers, L-PLA and D-PLA, with equimolar mixture of the two as D,L-PLA which is amorphous in nature. PGA demonstrates high degree of crystallinity and less

hydrophobicity due to absence of methyl groups. The ratios of the monomers have found to affect the characteristics of PLGA nanoparticles. In a recent report by our group it was observed that molecular weight and copolymer composition of PLGA affected the entrapment and release characteristics of estradiol. The C_{max} of estradiol was found to depend on the copolymer composition and molecular weight whereas the release duration was found to be influenced by particle size (Mittal *et al*., 2007).

The degradation of PLGA is found to be affected by various polymer characteristics along with degradation environment. PLGA undergoes hydrolytic degradation by cleavage of ester linkage. On degradation, PLGA breaks down to lactic and glycolic acids which are metabolised and eliminated from the body via Krebs' cycle as carbon dioxide and water (Anderson and Shive, 1997).

From a series of investigations from our laboratory, zero order (Hariharan *et al*., 2006; Italia *et al*., 2007; Mittal *et al*., 2007) and Higuchi's (Shaikh *et al*., 2009) release patterns were observed for various drugs entrapped in PLGA nanoparticles. The investigations suggested that various parameters which include polymer molecular weight, particle size and drugs physicochemical properties affected the release profile of drugs from PLGA nanoparticles (Bala *et al*., 2006; Italia *et al*., 2007; Mittal *et al*., 2007). Similarly, diversified pharmacokinetic behaviour of the drug entrapped PLGA nanoparticles was observed that was also depended on particle size, copolymer composition and drug's physicochemical properties (Italia *et al*., 2007; Mittal *et al*., 2007; Shaikh *et al*., 2009).

In addition to biodegradability and biocompatibility, PLGA also provides requisites physical stability as result of its glass transition temperature (Tg) (45- 55 °C) which is greater than the human body temperature. Considering

the nanoparticulate formulation aspects and FDA approval of products containing PLGA, it has resulted in a widely excepted polymer for nanoparticulate technology.

1.3.1.1.2 Poly(ethylene glycol) based copolymers

The hydrophobicity/hydrophilicity of nanoparticle's surface has been found to influence their *in vivo* behaviour. Hydrophobic particles have been found to be rapidly cleared from systemic circulation by MPS (Mononuclear phagocyte system), limiting their efficiency as carriers (Moghimi, *et al*., 2001; Owens and Peppas, 2006). Several techniques have been deployed to improve the hydrophilicity of hydrophobic polymers, of which, surface modification using poly(ethylene glycol) (PEG) has resulted in great accomplishments. PEG, on adsorption or covalent attachment to polymer chain increases the systemic circulation of nanoparticles and reduces surface adsorption of protein and enzymes, reducing elimination and degradation. Due to its hydrophilicity and steric repulsion, PEG reduces nonspecific interactions which results in reduced opsonisation and phagocytosis with increased circulation time (Gref *et al*., 2000). In addition, PEG has been found to increase the stability of nanoparticles in gastric fluid (Tobio *et al*., 2000) and also facilitate uptake of particles (Gref *et al*., 2000; Vila *et al*., 2002). PEG coating also improved mucosal penetration of large polymeric nanoparticles by reducing electrostatic and hydrophobic interactions (Lai *et al*., 2007). However, pegylated polymers lack functional groups for attaching drug or targeting moiety. In addition to the above polymers, polycaprolactone, poly(alkylcyanoacrylates), poly(ortho-esters), polyanhydrides and polyamides have also been widely explored for various drug delivery and

biomedical applications (Hans and Lowan, 2002; Panyam and Labhasetwar, 2003; Andrieux and Couvreur, 2009).

1.3.1.2 Stabilisers for nanoparticle systems

Stabilisers are used to prevent the formation of agglomerates during nanoparticle preparation. The high interfacial tension because of the large surface area of small droplets always keeps the likelihood of the system to coalescence. Stabilisers, by reducing the interfacial tension, prevent coalescence of nanoparticles. Several stabilisers such poly(vinyl alcohol) (PVA) and Pluronic F68 have been explored. However, recently a new cationic surfactant didodecyl dimethylammonium bromide (DMAB), a double-tail cationic surfactant has generated considerable interest due to its ability to form nanoparticles of smaller size than routinely used stabilisers (Kwon *et al*., 2001; Hariharan *et al*., 2006). The extensive investigations made by our group demonstrates DMAB as a potential stabiliser generating stable particles in range of 100 nm in size irrespective of the drug and polymer composition used (Ankola *et al*, 2007; Italia *et al*., 2007; Mittal *et al*., 2007**)**. In addition, DMAB at a concentration lower than 33 μM was found to be non-toxic (Bhardwaj *et al*., 2009) and DMAB stabilised PLGA nanoparticles when administered to rats were found to be safe with no inflammatory response (Hariharan *et al*., 2006; Italia *et al*., 2007; Mittal *et al*., 2007). In a recent report by Peetla and Labhasetwar, it was observed that DMAB-modified nanoparticles penetrated the endothelial cell model membrane better with enhanced endothelial cell uptake over other cationic surfactants and PVA (Peetla and Labhasetwar, 2009). In addition to smaller particles, use of DMAB induces a high surface charge to nanoparticles necessary for particle stability (> 30 mV) (Hariharan *et al*., 2006).

1.3.1.3 Solvents

Organic solvent plays a crucial role in determining the characteristic of nanoparticles (Sahana *et al*., 2008). Ensuring the complete solubility of the drug and the polymer in the organic solvent is essential for successful preparation of nanoparticles. On the other hand physical properties like vapour pressure, viscosity, surface tension play crucial role in particle characteristics that include particle size and drug entrapment.

The selection of solvents also depends on the method of preparation used. The emulsion/diffusion/evaporation method uses a partially water-soluble solvent, such as ethyl acetate, methylene chloride or chloroform; while the solvent displacement/nanoprecipitation technique uses a water miscible solvent like acetone. Another most important aspect, which must be considered during selection of a solvent, is its toxicity. Influence of solvents on the entrapment efficiency (Sahana *et al*., 2008) and size (Italia *et al*., 2007) of nanoparticles was demonstrated in our recent studies.

In addition to the polymer, stabiliser and solvents, the physiochemical and biopharmaceutical properties of the drug and the dose of drug need to be taken into account while designing nanoparticulate formulations (Bhardwaj *et al*., 2005). The dose to be incorporated into a nanoparticulate system depends on the extent of particle uptake. In general high dose drugs cannot be administered in the form of nanoparticles unless linked with carriers or when particle uptake is not the major mechanism of drug absorption.

1.3.1.4 Methods for nanoparticle preparation

Polymeric nanoparticles can be prepared using either preformed polymers or by in situ polymerisation with incorporation of the drug in the matrix of the nanoparticles. Nanoparticles using preformed polymers can be prepared by

emulsion-evaporation, emulsion-evaporation-diffusion, double emulsion, salting out and solvent displacement (nanoprecipitation) methods. All of the methods have been reviewed extensively (Bala *et al*., 2004; Bhardwaj *et al*., 2005; Mora-Huertas *et al*., 2010). The single emulsion techniques are generally used to entrap hydrophobic drugs while double emulsion and nanoprecipitation techniques are used for water soluble compounds.

1.3.2 Co-entrapped nanoparticles

Conventional combination formulations are widely available in market for treatment of several disorders like tuberculosis. Combination approach has been widely utilised to improve the potency of the drugs or reduce drug toxicity. Traditional combination formulations are generally available as tablets and capsules however; recently attempts have been made to design nanoparticles containing multiple drugs.

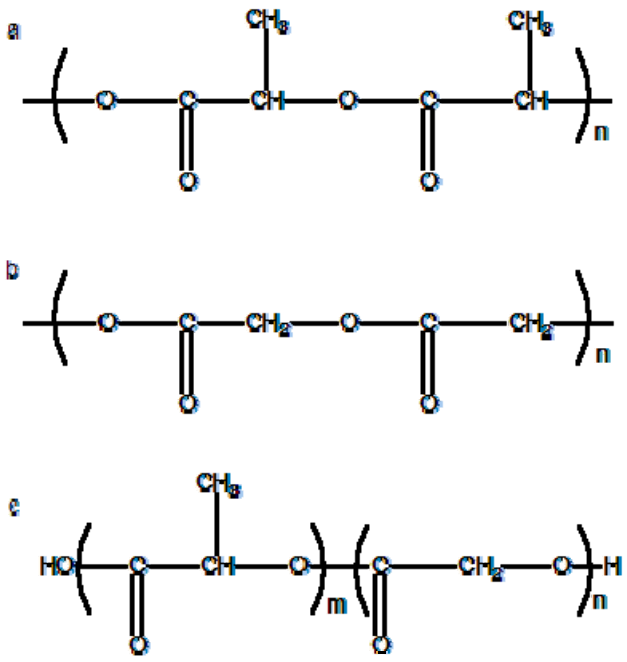

Figure 1.4 Chemical structures of (a) PLA, (b) PGA and (c) PLGA

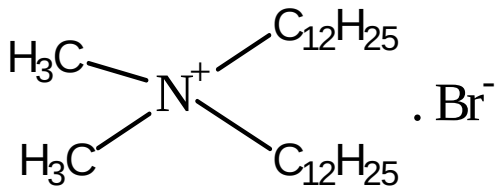

Figure 1.5 Chemical structure of DMAB

Three anti-tubercular drugs pyrazinamide, isoniazid, and rifampicin were encapsulated at 2/3rd therapeutic doses in PLGA nanoparticles. Encapsulation of the anti-tubercular drugs into nanoparticles resulted in reduction of dosing frequency and amount of drug dosage (Sharma *et al*., 2004). In a similar attempt, isoniazid, rifampicin, pyrazinamide and ethambutol encapsulated alginate nanoparticles were prepared by controlled cation-induced gelification of alginate. The anti-tubercular drugs encapsulated in alginate nanoparticles demonstrated superior bioavailability compared to free drugs. In addition to improved bioavailability, the alginate nanoparticles were able to sustain the drugs concentrations in organs above the minimum inhibitory concentration for 15 days, while free drugs lasted for single day (Ahmad *et al*., 2006).

Recently, a new therapeutic strategy to treat diabetes using biodegradable nano-co-encapsulated antioxidant particles (NanoCAPs) of ellagic acid and CoQ10 was proposed by this laboratory. The combination of ellagic acid and CoQ10 showed beneficial effects in ameliorating lipid peroxidation, dyslipidemia and in preventing organ damage in streptozotocin induced diabetic rats (Ratnam *et al*., 2008). Significantly lower dose of ellagic acid and CoQ10 in NanoCAPs showed equal and sometimes more prominent results in comparison to simple suspension suggesting improved efficacy. On further investigation, the NanoCAPs were effective in treating hyperlipidemia in rats at 3 time's lower dose than their suspension form. NanoCAPs were able to lower cholesterol, glucose and triglycerides levels along with improving endothelial function (Ratnam *et al*., 2009).

The co-entrapped nanoparticles can offer several advantages over individual drug loaded nanoparticles, which includes less excipient usage, low cost and less variable uptake from the GIT.

2. AIMS AND OBJECTIVES

2.1 Aims

Considering the impact that CsA has had in the field of organ transplantation and its ever growing new indications, from arthritis to ulcerative colitis, the potential of the drug remains far from conquered. However, with limited success in overcoming CsA's formulation development challenges and its association with significant nephrotoxicity and hypertension which limits the usage of the drug, a need to design a formulation system with improved CsA's safety and efficacy exists.

In support to our previous findings, polymeric nanoparticles will be explored for oral delivery of CsA, with the possibility of using antioxidant CoQ10 as adjuvant in reducing the nephrotoxicity. Role of polymer matrix on CsA release will also be explored.

2.2 Objectives

The overall objective of this dissertation was to develop CsA formulation with reduced nephrotoxicity along with similar plasma profile to that of Neoral®.

The objectives were achieved by the following specific aims:

1. Development and *in vivo* evaluation of PLGA loaded CsA nanoparticles for reduced nephrotoxicity at a C_{max} similar to commercial formulation Neoral®.
2. Formulation, characterisation and *in vivo* evaluation of biodegradable co-entrapped CsA-CoQ10 nanoparticles for oral administration.
3. Development of new biomaterials for better delivery prospects of CsA.

3. PHARMACOKINETICS AND NEPHROTOXICITY EVALUATION OF CICLOSPORIN LOADED PLGA NANOPARTICLES

3.1 Introduction

Association of CsA with nephrotoxicity limits its wider applicability (Faulds *et al*., 1993; Rezzani, 2004) however, considering its clinical potential there remains a scope for development of CsA formulations with reduced/no nephrotoxicity.

Experimental models of CsA nephrotoxicity in rats have been helpful in studying the pathophysiology of CsA mediated renal adverse effects. Acute and chronic forms of CsA nephrotoxicity can be reproduced in rats. The acute form is induced by administration of large doses of CsA (15-50 mg/Kg) while chronic form is induced by administration of similar CsA doses over several days (> 15).

In literature several different models have been used for mechanistic understanding of CsA mediated nephrotoxicity. Normotensive rats on normal-sodium diet (Elzinga *et al*. 1993) and sodium-depleted normotensive rats have been widely used to study CsA nephrotoxicity (Burdmann *et al*., 1995). The SHR model, similar to human essential hypertension has also been widely explored to study CsA mediated increased blood pressure and renal adverse effects (Mervaala *et al*., 1997). However, most formulation and antioxidant screening for nephrotoxicity have been performed using normal Sprague Dawley (SD) rats (Varela *et al*., 2001; Italia *et al*., 2007; Sonaje *et al*., 2007; Aliabadi *et al*., 2008).

The C_{max} of CsA is responsible for it therapeutic actions as well as its nephrotoxicity (David-Neto *et al*., 2000). Therefore, attempts were made to match the C_{max} of Neoral® using PLGA nanoparticles and the impact of

polymeric nanoparticles on CsA's pharmacokinetic and nephrotoxic behavior was studied in normal SD rats.

3.2 Materials and methods

3.2.1 Materials

PLGA (Resomer® RG 50:50, M.W. 35,000-40,000, Boehringer Ingelheim, Ingelheim, Germany), CsA (Fluorochem Ltd. Derbyshire, UK), DMAB (Aldrich), Ethylenediaminetetraacetic acid Sodium (EDTA) (Sigma) and High Performance Liquid Chromatography (HPLC) grade ethanol (Fluka) were used as received. CsA specific EIA KIT was purchased from Immunotech, Czech Republic. All other chemicals used were of analytical grade.

3.2.2 Preparation of nanoparticles

Emulsion-diffusion-evaporation technique optimised previously was used to prepare the CsA loaded nanoparticles (Italia *et al*., 2007). In brief, 50 mg of PLGA and desired CsA amount corresponding to its loading ratio (5, 10 and 15 mg for 10, 20 and 30% loading respectively) were dissolved in 2.5 ml of ethyl acetate at room temperature and stirred for 2 h at 1000 rpm. The organic phase was then emulsified into 3 ml of aqueous phase containing DMAB (0.25% w/v) as stabiliser. The resulting o/w emulsion was sonicated (Soniprep 150, MSE) at 10 microns amplitude for 1 min. 25 ml of water was added to the above emulsion with constant stirring at 1000 rpm, which resulted in nanoprecipitation. The prepared nanoparticles were charaterised for size, zeta potential and entrapment efficiency.

3.2.2.1 Size and zeta potential measurements

The mean particle size of the prepared nanoparticle suspensions was measured by dynamic light scattering (Nano ZS, Malvern, UK) taking the average of five measurements, which represented the hydrodynamic diameter of the particles. The mean size was derived from cumulants analysis of the measured correlation curve, wherein a single particle size is assumed and a single exponential fit is applied to the autocorrelation function. In addition to the mean particle size, the instrument reports the Polydispersity Index (PDI) between 0 (monodispersed particles) and 1 (polydispersed particles). The zeta potential was estimated on the basis of electrophoretic mobility under an electric field as an average of 30 measurements. The frequency shift of an incident laser beam caused by these moving particles is converted to the zeta potential by the application of the Smoluchowski equation. The temperature was kept constant at 25 °C during size and zeta potential measurements.

3.2.2.2 Entrapment efficiency

The percentage of CsA incorporated during nanoparticle preparation was determined by centrifuging the drug loaded nanoparticles at 14,000 rcf for 30 min and separating the supernatant. The pellet obtained was washed twice with 1 ml of water and the CsA was extracted from the pellet using ethyl acetate and acetonitrile followed by an estimation of the CsA in triplicate by the HPLC method as described below. Estimation of CsA was carried out using Hypersil GOLD (15 cm x 4.6 mm, 5 μm) (C18) column and Hypersil 10x4 mm, 5 μm drop in guards connected by UNIGAUARD (Thermo Scientific). Elution of CsA was achieved using isocratic mobile phase (ethanol:water) at 210 nm. The HPLC system consisted of ChromQuest

acquisition software, Autosampler connected with LC Pump and PDA detector (Thermo Finnigan Surveyor System). The analytical method was validated according to the guidelines of the international conference on harmonization (ICH) of technical requirements for registration of pharmaceuticals for human use. Parameters validated included precision (repeatability (intra-day) and intermediate precision (inter-day)) and accuracy. Both the intra- and inter-day relative standard deviations (RSD) of QC standards were less than 5% over the selected range.

3.2.3 Pharmacokinetic and tissue distribution studies

All animal experiments were carried out under a project license issued under the U.K. Home Office Animals (Scientific Procedures) Act 1986.

For plasma profiling and biodistribution studies male SD rats weighing 200–250 g were used. Neoral® was administered at 15 mg/Kg while CsA nanoparticles were administered as varying dose and loads. To study the effect of dose, nanoparticulate formulations were administered at CsA dose of 15, 30 and 45 mg/Kg of body weight at 20% CsA loading and to study the effect of loading, nanoparticles at 10, 20 and 30 % CsA loading were administered at a dose of 30 mg/Kg.

For all the formulations, blood samples were collected from animals by venipuncture of peripheral blood vessel (tail vein) at 0.5, 1, 2, 6, 12, 24, 36, 48 and 72 h in microcentrifuge tubes containing EDTA as anticoagulant. Blood samples were analysed for CsA concentration by CsA specific EIA KIT. At the end of 72 h, animals were sacrificed and all major organs isolated and the CsA concentration was determined. In brief, the organs were isolated and weighed, to which water was added at 1:4 ratio and then homogenised at 10,000 rpm for 3 min to produce a fine homogenate. 200 µl of homogenate

was transferred into a microcentrifuge tube to which 800 µl of acetonitrile was added to extract CsA from the tissues. The tubes were vortexed for 5 min and centrifuged. The samples were concentrated by collecting 800 µl of supernatant and evaporating it to dryness under vacuum at 25 ^{o}C. The obtained pellet was analysed for CsA content by CsA specific EIA KIT. In brief, 1.2 ml of assay buffer with methanol was added to eppendrof tubes containing the pellet. After addition, the tubes were vortexed for 5 min and then incubated for 5 mins. After inducation the samples were analysed by enzyme competition immunoassay based on principle of horseradish peroxidase and the colour intensity was determined at 450 nm using ELISA reader.

3.2.4 CsA distribution profile at its T_{max}

Male SD rats weighing 200–250 g were administered Neoral® (15 mg/Kg) and CsA nanoparticles (30 mg/Kg at 30% loading) and sacrificed at their T_{max} to determine blood and tissue CsA concentration.

3.2.5 Chronic nephrotoxicity study

Eighteen male SD rats weighing 200–250 g were divided into three groups of six each randomly. Animals in group one were kept as control and received saline, animals in group two were administered Neoral® (15 mg/Kg) and animals in group three were administered CsA nanoparticles (30 mg/Kg at 30% loading). All administrations were through peroral route given with the help of oral gavage and administration was continued for 30 days. On 31st day (24 h after 30th dose) all animals were sacrificed and blood and tissues were collected for CsA estimation and analysis of biochemical parameters.

3.2.5.1 Blood CsA levels during chronic nephrotoxicity study

Blood samples were collected from animals treated with Neoral® and CsA nanoparticles by venipuncture of peripheral blood vessel (tail vein) at 2 and 12 h after doses 1, 15 and 30 and analysed as described above.

3.2.5.2 Plasma creatinine and blood urea nitrogen estimation

After euthanasia, blood was collected from the heart in eppendrof tubes containing EDTA. Plasma was isolated by centrifugation of blood at 4000 rpm for 10 min. Plasma creatinine (PC) was analysed using commercially available kit (Creatinine assay kit, BioVision) which was based on quantitative colorimetric creatinine determination at 570 nm. Blood urea nitrogen (BUN) was analysed (QuantiChrom™ urea assay kit) by colorimetric determination at 520 nm.

3.2.5.3 Histopathological evaluation of kidney

After euthanasia, right kidney was isolated and washed with cold phosphate buffer saline and fixed in 10% neutral buffered formalin solution. The tissues were dehydrated using tissue processor (Citadel 1000, Thermo Shandon Ltd, UK) at different ethanol and histoclear solutions as described in table 3.1 and embedded in paraffin wax. The paraffin blocks were cut into 3 μm sections with the microtome and stained for hematoxylin and eosin using the procedure described in table 3.2. The slides were mounted using DPX moutant and observed under light microscope. The morphometric analysis of the histological sections was carried out in a blind fashion. Twenty five glomeruli were photographed from 3-5 sections in unbiased manner. The images were processed using the software ImageJ to determine the area of the glomerular capillary tuft (CA) and the Bowman's capsule (BA) and the

glomerular collapse index was calculated by the ratio CA/BA (Origlia *et al.*, 2006).

3.2.6 Statistical analysis

Statistical analysis was performed by one way ANOVA followed by Tukey's test for multiple comparisons.

Table 3.1 Tissue processing conditions

Solution	**Time (h)**
70% ethanol	2
90% ethanol	2
100% ethanol	2
50:50 ethanol:histoclear	1
100% histoclear	1
100% histoclear	1
Paraffin wax	2
Paraffin wax	2

Table 3.2 Hematoxylin and eosin staining protocol

Step	Solution	Time (min)
1	Histoclear	1
2	Histoclear	1
3	Histoclear	1
4	100% Ethanol	1
5	100% Ethanol	1
6	Distilled water	1
7	Hematoxylin Gill III	1
8	Distilled water	1
9	1% acid alcohol	1
10	Distilled water	1
11	Scott's tap water	2
12	Distilled water	1
13	0.1 % Eosin	1
14	100% Ethanol	1
15	100% Ethanol	1
16	100% Ethanol	1
17	Histoclear	1
18	Histoclear	1
19	Histoclear	1
20	Histoclear	1

3.3 Results and discussion

3.3.1 Preparation of nanoparticles

CsA loaded PLGA nanoparticles were prepared by emulsion-diffusion-evaporation method using DMAB as stabiliser (Italia *et al*., 2007). Effect of loading on particle characteristics was studied (Table 3.3). The increase in the CsA loading (10 to 30 % w/w of polymer) resulted in particle size increase from 107 to 119 nm with increase in entrapment efficiency from 20 to 62 % that led to increase in the amount entrapped from 1 to 9.3 mg per 50 mg of polymer. Results were similar to those as reported earlier by our group (Italia *et al*., 2007). In spite of slight increase in particle size, the particle size distribution of the formulations was similar. Loading above 30% seems to be difficult due to drug precipitation, suggesting the threshold of the polymer under the studied conditions. As the formulated batches were to be used for pharmacokinetic studies, the amount of polymer administered along with CsA for 200 g rat at 30 mg/Kg was extrapolated. The amount of polymer associated with 6 mg of CsA for 10, 20 and 30 % CsA loaded particles, was 300, 65 and 32 mg, respectively (Table 3.3).

Table 3.3 Nanoparticle characteristics as a function of drug loading**.**

CsA loading	Size (nm)	EE (%)	Amt. Entrapped[a]	Amt. of Polymer[b]
10	107±7	20±2	1.0±0.1	300
20	108±7	46±4	4.6±0.4	65
30	119±5	62±4	9.3±0.6	32

[a]Amount entrapped per 50 mg of PLGA; [b]Amount of polymer for 6 mg of CsA; EE-Entrapment efficiency. Zeta potential (ZP) was 71-78 mV at pH 4.0±0.5. PDI of particles was in the range of 0.08-0.16. All data represented as mean±S.D. (n=3).

3.3.2 Pharmacokinetic and tissue distribution studies

The main purpose of this study was to understand the pharmacokinetic behavior of CsA entrapped PLGA nanoparticles as a function of dose and drug loading with an ultimate aim of matching the Neoral® profile, along with reducing the nephrotoxicity. The dose dependent pharmacokinetics was carried out using 20% CsA loaded nanoparticles at 15, 30 and 45 mg/Kg with Neoral® as control at 15 mg/Kg. Figure 3.1 represents plasma profiles of various CsA formulations and Table 3.4 depicts the obtained pharmacokinetic parameters.

It was clear that with increasing the dose an increase in C_{max} and AUC_{0-72} was observed for nanoparticulate formulations, however not in a dose-proportionality manner. With increasing the dose the relative bioavailability decreased in comparison to Neoral®, further strengthening the argument of dose-disproportionality. The relative bioavailability of CsA nanoparticulate formulation at 15, 30 and 45 mg/Kg were 120, 81 and 64 %, respectively. On increasing the dose of nanoparticulate formulation from 15 to 45 mg/Kg, C_{max} increased from 682 to 1073 ng/ml, which was close to that of Neoral®. Further attempts were made to study the effect of CsA loading on pharmacokinetic profile of nanoparticles. Different formulations at 10, 20 and 30% CsA loading were administered at 30 mg/Kg. With increasing the loading from 10 to 30%, an increase in AUC_{0-72} was observed with corresponding increase in relative bioavailability from 31 to 89% (Figure 3.1 and Table 3.4). The C_{max} was also found to increase from 494 to 1101 ng/ml. For all the nanoparticulate formulations, a sustained release of CsA was observed which led to significant increase in T_{max}. For Neoral® the T_{max} was rapid and at 2 h while for all nanoparticulate formulation the T_{max} observed was 24 h except for the

formulations 45 mg/Kg at 20% loading and 30 mg/kg at 30% loading which exhibited a T_{max} of 12 h.

The amount of CsA absorbed through oral route in nanoparticulate formulation was found to depend upon the amount of polymer administered along with the drug. The amount of polymer required to administer 15, 30 and 45 mg/Kg of CsA at 20% loading to a 200 g rat was ~ 33, 65 and 98 mg, on the other hand to administer a dose of 30 mg/Kg for the nanoparticles made at 10, 20 and 30% w/w CsA to polymer, the polymer quantities translates to ~ 300, 65 and 32 mg (Table 3.3). With increasing amounts of nanoparticles, a decrease in bioavailability was observed which may be due to saturation in the uptake of nanoparticles from the GIT. In a recent report by our group, estradiol loaded PLGA nanoparticles were found to follow dose-dependent increase in bioavailability (Mittal and Kumar, 2009), however the dose range of estradiol was 100 to 500 μg/Kg, which is very low compared to CsA dose range of 15-45 mg/Kg further suggesting the possible role of polymer/nanoparticle concentration.

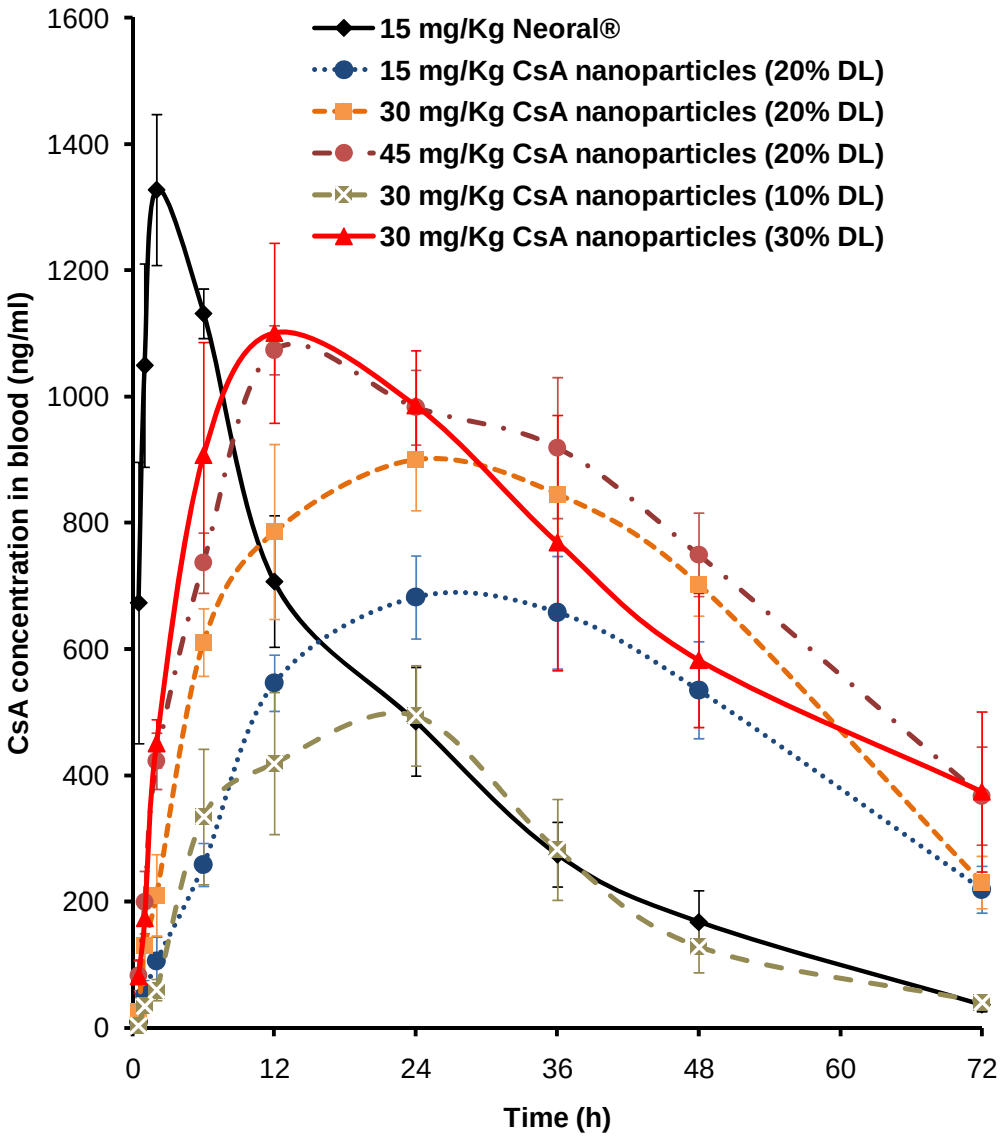

Figure 3.1 Blood CsA levels with time for various formulations. All values represented are mean±S.E.M. (n=3).

Table 3.4 Pharmacokinetic parameters of various CsA formulations.

Formulation	Dose (mg/Kg)	Loading[a]	AUC_{0-72} (ng.h/ml)	C_{max} (ng/ml)	T_{max} (h)	Relative Bioavailability (%)[Ψ]
Neoral®	15	----	29046±1437	1328±120	2	100
CsA NPs	15	20	34854±2157	682±66**[a]	24	120
CsA NPs	30	20	47116±1753	900±81	24	81
CsA NPs	45	20	55322±1537	1073±40	12	64
CsA NPs	30	10	17774±655	494±79***[a]	24	31
CsA NPs	30	30	51763±3812	1101±143	12	89

AUC was calculated by linear trapezoidal rule; [a]% w/w of polymer weight; Ψrelative to Neoral® based on AUC_{0-72}; All data represented as mean±S.E.M. (n=3).
***p < 0.001, **p<0.01; a vs. Neoral® group.

After 72 h the animals were sacrificed and CsA concentration in major organs was determined and tissue distribution coefficient (K_p, ratio of tissue concentration to blood concentration) was calculated (Table 3.5 & 3.6). Nanoparticulate formulation produced CsA tissue concentrations higher than those observed by Neoral® except for the brain at equal dose. With increasing the dose of nanoparticulate formulation an increase in tissue concentration was observed with highest being observed for 45 mg/Kg. Similarly with increasing the load from 10 to 30% for 30 mg/Kg an increase in tissue concentration was observed. Highest concentrations of CsA were seen in the liver for Neoral®, whereas nanoparticulate formulations demonstrated highest CsA concentrations in the kidney. For Neoral® the K_p was large in comparison to those observed for nanoparticles indicating higher fraction of drug being distributed into tissue while for nanoparticles longer circulation of CsA in blood and less tissue distribution. The K_p for all the nanoparticulate formulation were similar for each organ except for CsA nanoparticles administered at 30 mg/Kg at 10% load, where very large K_p was observed. These large K_p maybe because of lower blood levels obtained by incomplete absorption of nanoparticles due to high polymer burden at 10% loading for 30 mg/Kg dose.

Tanaka *et al*. studied CsA tissue distribution kinetics in rats after single dose administration at 1.2, 6, and 30 mg/Kg through 2 min i.v. infusion in cremophore® EL (Tanaka *et al*., 2000). Highest CsA concentrations were observed in liver followed by kidney while lowest levels being observed in brain. The Neoral® group in our investigation followed a similar trend to that observed above, though the route of administration was oral. Tanaka *et al.* also found that the tissue and blood concentration profiles differs widely, however all tissues profiles were comparable to each other for the three

doses studied. On the other hand nanoparticulate CsA differs in the distribution profile with that of Neoral® and the difference could be due to interplay of many factors of which the major factor is the polymer. Similar differences have been documented in the literature with a variety of polymers and drugs (Panagi *et al*., 2001; Aliabadi *et al*., 2005)

The overall aim was to achieve comparable blood levels to Neoral®, therefore, the dose/formulation meeting this requirement as close as possible was selected for subsequent studies. The nanoparticles prepared at 30% initial loading and 30 mg/Kg body weight was selected for further investigation.

Table 3.5 Tissue concentration of various CsA formulations at 72 h

	μg/g of tissue or blood					
Groups	**Neoral®**	**CsA NPs**	**CsA NPs**	**CsA NPs**	**CsA NPs**	**CsA NPs**
Dose (mg/Kg)	**15**	**15**	**30**	**45**	**30**	**30**
Loading[a]	**--**	**20**	**20**	**20**	**10**	**30**
Blood	0.04±0.01	0.22±0.04	0.23±0.04	0.37±0.08	0.04±0.01	0.38±0.13
Brain	3.4±0.7	1.9±0.2	2.5±0.9	2.7±1.1	1.6±0.7	2.8±1.0
Heart	5.0±0.8	6.4±1.5	6.7±1.9	7.7±2.6	7.8±1.5	8.1±2.0
Lung	5.3±0.7	8.9±3.6	9.4±1.8	10.4±1.8	8.7±0.7	11.3±1.8
Kidney	9.9±1.6	14.0±1.3	17.4±1.5	17.6±1.4	12.2±1.4	20.3±2.8
Spleen	6.9±1.8	9.3±2.1	10.4±1.9	11.4±1.4	5.7±1.7	14.9±1.6
Liver	10.7±1.3	11.7±0.8	12.5±0.8	13.1±1.8	9.5±1.2	15.5±1.1
Intestine	6.8±0.8	7.5±1.5	8.9±0.5	11.7±2.1	11.3±2.7	7.7±2.4

[a]% w/w of polymer weight. All data represented as mean±S.E.M. (n=3).

Table 3.6 Tissue distribution coefficient (k_p) of various CsA formulations

	k_p					
Groups	**Neoral®**	**CsA NPs**	**CsA NPs**	**CsA NPs**	**CsA NPs**	**CsA NPs**
Dose (mg/Kg)	**15**	**15**	**30**	**45**	**30**	**30**
Loading[a]	**--**	**20**	**20**	**20**	**10**	**30**
Blood	1	1	1	1	1	1
Brain	85	9	11	7	40	7
Heart	125	29	29	21	195	21
Lung	133	40	41	28	218	30
Kidney	248	64	76	48	305	53
Spleen	173	42	45	31	143	39
Liver	268	53	54	35	238	41
Intestine	170	34	39	32	283	20

[a]% w/w of polymer weight.

3.3.3 CsA distribution profile at its T_{max}

The toxicity of CsA is found to depend upon blood and tissue concentrations in correlation to C_{max} and AUC. Considering the possible differences in *in vivo* distribution between the free drug and the drug entrapped in nanoparticles, T_{max} sacrifice was performed for nanoparticulate formulation of CsA for a dose of 30 mg/Kg at 30% loading and was compared to Neoral®. After administration of the formulations, the rats were sacrificed at 2 and 12 h which corresponded to the T_{max} of Neoral® and CsA nanoparticulate formulation, respectively.

At T_{max}, the tissue distribution profiles for both Neoral® and nanoparticles were very much comparable for all the tissues except intestine (Table 3.7). The T_{max} distribution differs to that of 72 h distribution where much smaller K_p values were observed in comparison to Neoral®, which could be explained due to the delay in the absorption phase for nanoparticles.

The nanoparticulate formulation of CsA prepared at 30% initial loading at a dose of 30 mg/Kg produced similar C_{max} and tissue concentrations in comparison to Neoral® at 15 mg/Kg, therefore, the same doses were used for the nephrotoxicity study.

Table 3.7 Tissue concentrations and distribution coefficient (k_p) of Neoral® and CsA nanoparticles at their T_{max}

Tissue	Neoral® (15 mg/kg) 2h		CsA NPs (30 mg/kg at 30% DL) 12h	
	μg/g of tissue or blood	k_p	μg/g of tissue or blood	k_p
Blood	1.19±0.08	1	1.01±0.08	1
Brain	3.4±1.4	3	3.1±1.1	3
Heart	29.1±2.9	24	23.6±2.8	23
Lung	30.3±3.1	25	24.8±2.1	25
Kidney	32.4±2.8	27	29.6±3.1	29
Spleen	31.7±2.7	27	28.9±2.1	29
Liver	35.5±2.4	30	32.5±2.9	32
Intestine	22.4±5.2	19	29.8±4.7	30

All data represented as mean±S.E.M. (n=3).

3.3.4 Chronic nephrotoxicity study

CsA associated nephrotoxicity is a major concern for its use in various disorders where it has been found to have potential therapeutic applications. CsA induced kidney damage is clinically characterised by measuring BUN and PC levels with histological evaluation of the kidney. Uncharacteristic rise in the BUN and PC levels point towards kidney dysfunction. A 30 day chronic nephrotoxicity study revealed that administration of Neoral® led to significant rise in BUN and PC levels in comparison to that of control groups (Table 3.8). On the other hand, CsA nanoparticles exhibited significantly lower PC and BUN levels indicating lower nephrotoxicity. Similar effects were observed on histological investigation of kidney sections. CsA induced kidney damage is reversible at an early stage but chronic administration leads to irreversible changes in the kidney, most prominent being glomerular collapse, tubular atrophy and interstitial fibrosis. The ratio of areas of glomerular capillary tuft to that of the Bowman's capsule was quantified to determine glomerular collapse (Table 3.8, Figure 3.2). Administration of Neoral® lead to greater glomerular collapse than that observed on administration of CsA nanoparticles, further confirming the lower toxicity of nanoparticulate formulation in comparison to Neoral®.

Determination of blood CsA levels after 1st, 15th and 30th dose showed a gradual increase in CsA concentration on administration of Neoral® and CsA nanoparticulate formulation. The blood concentrations were determined at 2 and 12 h which were corresponding to the T_{max} of Neoral® and nanoparticulate formulation, repectively (Figure 3.3). After 1st and 15th doses, Neoral® and nanoparticulate formulation demonstrated higher CsA concentration at their T_{max} but by 30th day nanoparticulate formulation showed a higher concentration at it's as well as Neoral®'s T_{max}. This high

concentration observed for nanoparticulate formulation may be due to sustained release of CsA. On determination of CsA concentration in the kidney, brain and liver, it was observed that nanoparticulate formulation produced higher levels than those observed in Neoral® group (Figure 3.4).

Table 3.8 Evaluated parameters of chronic nephrotoxicity

Groups	**BUN (mg/dL)**	**Creatinine (mg/dL)**	**Glomerular collapse index**
Control	20.81±1.74	0.497811±0.031	0.8785±0.0109
Neoral® (15 mg/Kg)	35.02±1.65^{***a}	2.129492±0.154^{***a}	0.7499±0.0132^{***a}
CsA NPs (30 mg/Kg)	27.24±1.59^{*a,*b}	1.274491±0.081^{***a,***b}	0.8029±0.0156$^{**a, *b}$

All data represented as mean±S.E.M. (n=6).
***p < 0.001, **p<0.01, *p < 0.05; a vs. Control group; b vs. Neoral® group.

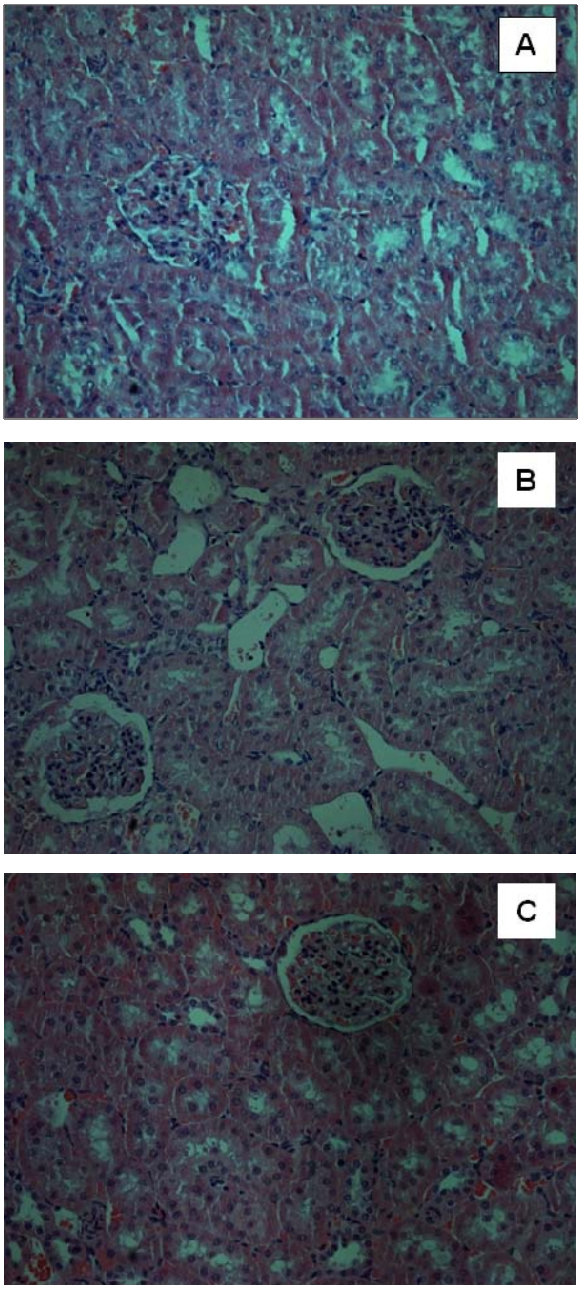

Figure 3.2 Histological sections of rat kidney cortex stained using hematoxylin and eosin (A) control group, (B) Neoral® treated group and (C) CsA nanoparticulate treated group. Glomerular collapse and widespread tubular damage which are characteristic features of CsA induced nephrotoxicity were prominently visible in Neoral® treated group compared to CsA nanoparticulate treated group (x200).

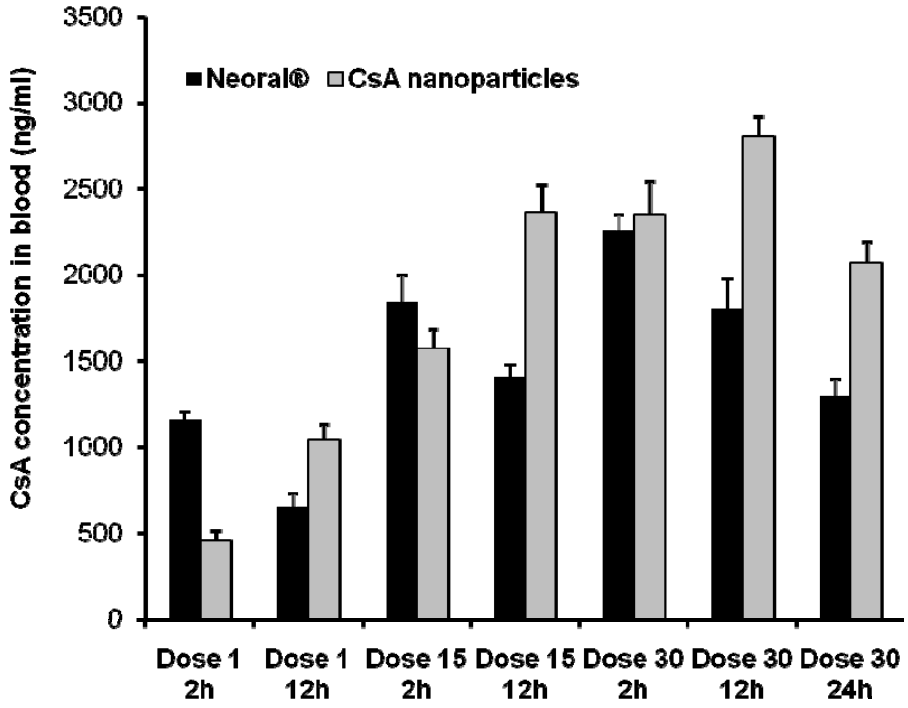

Figure 3.3 Blood CsA levels during the chronic nephrotoxicity study. All values represented are mean±S.E.M. (n=3).

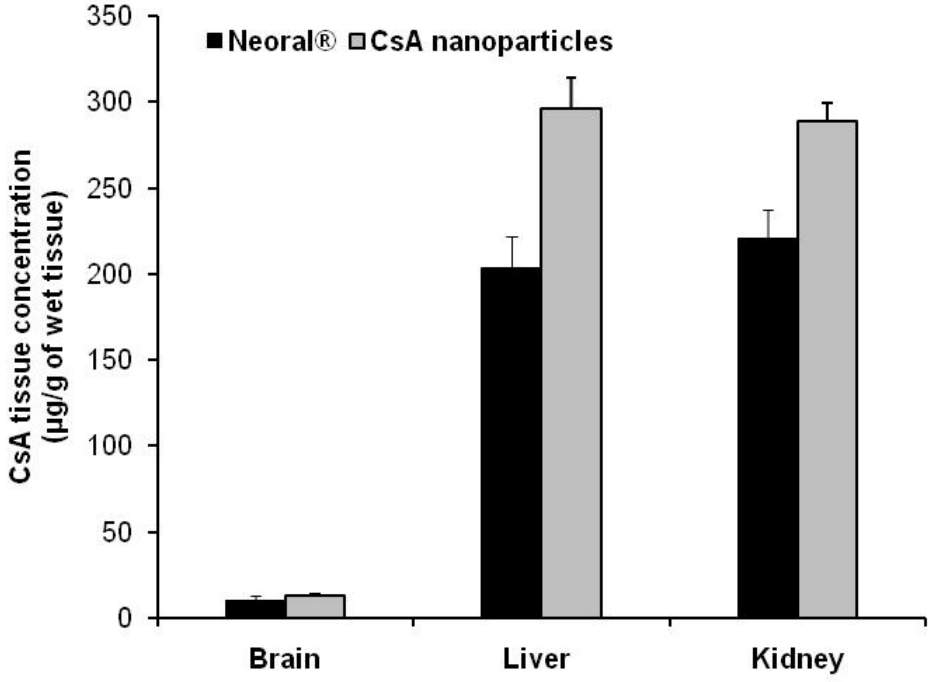

Figure 3.4 CsA levels in brain, liver and kidney observed after 30 days treatment with Neoral® (15 mg/Kg) and CsA nanoparticles (30 mg/Kg, 30% loading). All values represented are mean±S.E.M. (n=3).

In the literature, various formulations have been investigated for reducing CsA nephrotoxicity. CsA loaded liposomes demonstrated reduced nephrotoxicity when administered for 14 days intravenously at a dose of 25 mg/Kg in comparison to CsA administered in cremophore solution, however at similar plasma levels (Smeesters *et al*., 1998). In another report, following intravenous administration CsA loaded liposomes where found to be more potent than commercial formulation in prolonging survival of cardiac allograft in mice and were also less toxic however, a rapid decrease in blood levels with accumulation in the spleen was observed (Górecki *et al*., 1991). Freise *et al*., demonstrated decrease in nephrotoxicity in the ischemic kidney model in rat using liposomes. Pharmacokinetic characterization of formulation demonstrated rapid clearance of liposomes from systemic circulation and higher hepatic uptake (Freise *et al*., 1994). In a recent report, poly(ethylene oxide)-b-poly(e-caprolactone) (PEO-b-PCL) micelles were explored for i.v. delivery of CsA. The formulation was compared to commercial formulation Sandimmune®. On administration of 7 doses at 20 mg/Kg, the micellar formulation was found to be less toxic than Sandimmune® (Aliabadi *et al*., 2008). The observed lower toxicity for the micellar formulation was due to decreased distribution of CsA to kidney.

The current study investigates the preparation of CsA loaded PLGA nanoparticles and its pharmacokinetics and nephrotoxic evaluation in comparison to commercial formulation Neoral®. The developed PLGA nanoparticles were able to hold different amount of CsA based on its loading ratio with minimal effect on size and size distribution. This could be due to the use of the cationic surfactant DMAB as stabiliser for preparation of the nanoparticles and the ability of PLGA matrix to hold such a hydrophobic peptide. The nanoparticulate formulation at 30 mg/Kg at 30% loading

produced a similar C_{max} to that of Neoral® at 15 mg/Kg dose and a higher AUC but demonstrated significantly lower nephrotoxicity. The observed lower nephrotoxicity of CsA nanoparticulate formulation could be due to several reasons. On close examination of the pharmacokinetic profiles, Neoral® was found to follow two-compartment model while nanoparticulate formulations followed one-compartment model, suggesting towards different distribution behavior of CsA in the form of nanoparticulate formulation and could be one of the reasons for the observed lower nephrotoxicity of CsA nanoparticles. In addition to change in distribution patter, Neoral® exhibited a rapid increase in CsA blood levels with C_{max} at 2 h, causing vasoconstriction and kidney damage as result of decrease in glomerular filtration rate (GFR); 30-50% reduction in GFR being observed after 2 h of achieving C_{max} (Perico *et al*., 1992). On the other hand, nanoparticulate formulation was able to provide better control of CsA release with a steady increase in blood concentration with a C_{max} at 12 h, hence a delayed GFR decrease and lower nephrotoxicity. Additionally, administration of nanoparticulate formulation over 30 days resulted in smaller fluctuations of blood CsA concentrations than Neoral®, due to sustain release of CsA from nanoparticles. In spite of higher kidney CsA burden after 30 days, the nanoparticulate formulation exhibited lower nephrotoxicity than Neoral® on histological examination of the kidney. In addition to better control of CsA release, the lower toxicity of nanoparticles would be due to their protective effect as CsA being exposed to the kidney may be entrapped in the nanoparticles. Moreover, nanoparticles entrapping CsA may be eliminated from body before complete release of the drug (Moghimi *et al*., 2001), hence lower toxicity but requires further investigations.

In addition to reduced nephrotoxicity, the PLGA nanoparticles would offer advantage of targeting the lymphatic system by its characteristics absorption properties via M-cell in Peyer's patches, enhancing the CsA's therapeutic effects (des Rieux *et al*., 2006). Additionally, the nanoparticles would reduce the absorption variability of CsA by reducing its intestinal metabolism and P-gp efflux (Bhardwaj *et al*., 2005; Italia *et al*., 2006). The nanoparticulate formulations were able to sustain CsA release and these may further help in reducing dosing frequency. In all, the developed nanoparticulate formulation of CsA represent a potential alternative cremophore® EL free formulation compared to current commercial formulation Neoral®. The less nephrotoxic nanoparticulate formulation would enhance the therapeutic value of CsA. Apart from transplant medicine, it would be widely used in treatment of psoriasis, severe atopic dermatitis and rheumatoid arthritis and many other autoimmune disorders where CsA's association with nephrotoxicity limited its use (Faulds *et al*., 1993; Rezzani, 2004). It is anticipated, that the developed product by minimising the side effects would improve patience compliance. The results obtained from these study leads to a pharmaceutically acceptable product profile and has set the ground for detailed clinical investigations.

In addition to CsA, polymeric nanoparticles have been able to reduced toxicity of various molecules. In recent reports from our group, PLGA particles were able to improve the safety of doxorubicin (Kalaria *et al*., 2009) and atrovastatin (Meena *et al*., 2008). PLGA nanoparticles were also able to improve the efficacy of pharmaceutical challenging molecules like CoQ10 (Ankola *et al*., 2007), ellagic acid (Sonaje *et al*., 2007) and paclitaxel (Bhardwaj *et al*., 2009), demonstrating the potential of DMAB stabilised PLGA nanoparticles for improved oral delivery and suggesting towards potential therapeutic efficacy of CsA nanoparticles in autoimmune disorders.

3.4 Conclusions

The study clearly demonstrates the potential of PLGA nanoparticles for oral delivery of CsA. With dosing and loading variations, PLGA nanoparticles were able to match the C_{max} of Neoral®. Most notably, the CsA nanoparticles demonstrated significant lower nephrotoxicity than Neoral® at higher plasma and tissue concentration, clearly demonstrating the clinical potential of the nanoparticulate formulation.

4. ATTEMPTS TO ERADICATE DELETERIOUS EFFECTS OF CICLOSPORIN BY COMBINATION APPROACH

4.1 Introduction

Combination therapy is gaining importance in treatment of difficult diseases for a variety of reasons. For example, the combination of disease modifying drugs with an antioxidant can offer synergistic effects (Brown *et al.*, 2001) as well as counteract drug induced toxicities (Lexis *et al*., 2006). This is especially true for patients requiring poly-therapy for co-existing disease states or, conversely, in the discovery of unexpected indications for a drug already established in the treatment of another disease. The anti-malarial drug hydroxychloroquine is used to treat rheumatism in arthritis patients but also has a hypoglycemic function that helps these patients avoid diabetic complications (Wasko *et al*., 2007). Conventionally, nanoparticulate systems have been developed for individual drugs; however, more recently, co-entrapment of more than one drug has been attempted successfully (Sharma *et al*., 2004; Ratnam *et al*., 2008).

The CsA loaded PLGA nanoparticles were found to be less nephrotoxic than Neoral®, however still presenting a scope for further reduction. Considering the role of free radicals in the CsA mediated nephrotoxicity (Chander *et al*., 2005; Yuce *et al*., 2008), antioxidant supplementation should benefit the cause. Therefore, attempts were made to develop co-entrapped CsA-antioxidant nanoparticles primarily to eradicate CsA induced nephrotoxicity and hypertension. Our own studies as well as literature reports strongly suggest the ability of CoQ10 in scavenging free radicals as well as preventing hypertension (Igarashi *et al*., 1974; Greenberg and Frishman, 1990; Ankola *et al*., 2007). Therefore, in the present investigation we developed CsA-CoQ10 co-entrapped nanoparticles for reduced CsA toxicity.

4.2 Materials and methods

4.2.1 Materials

CoQ10 was a free gift by Tischon Corp. (Westbury, NY).

4.2.2 Preparation of nanoparticles

CsA-CoQ10 co-entrapped nanoparticles were prepared by emulsion-diffusion-evaporation technique as described in section 3.2.2. Several process parameters, as described below, were optimised with respect to size and entrapment efficiency, aiming to achieve smallest possible size and maximum entrapment.

4.2.2.1 Effect of DMAB concentration on drug entrapment

Four different DMAB concentrations (1, 0.5, 0.25 and 0.1% w/v) were screened to investigate its effect on particle characteristics (CsA loading at 10%, CoQ10 loading at 30% and co-loading of CsA and CoQ10 at 10 and 30% w/w of polymer respectively). The particles were prepared using 5 ml of stabiliser volume and homogenised (Polytron PT4000; Kinematica) at 15,000 rpm for 5 min as a size reduction method.

4.2.2.2 Effect of external phase volume on particle characteristics

Three different external phase volume (5, 3 and 1.5 ml) were screened to investigate its effect on particle characteristics (Co-loading of CsA and CoQ10 at 10 and 30% w/w of polymer respectively). The particles were prepared using 0.1% w/v DMAB concentration and homogenised at 15,000 rpm for 5 min as a size reduction method.

4.2.2.3 Effect of droplet size reduction method on particle characteristics

Homogenisation and probe sonication as size reduction methods were investigated to study their role on particle characteristics (Co-loading of CsA and CoQ10 at 10 and 30% w/w of polymer respectively). The particles were prepared using 3 ml of 0.1% w/v DMAB concentration. Homogenisation was carried out at 15,000 rpm for 5 min while probe sonication at 10 microns amplitude for 1 min.

4.2.2.4 Effect of drug loading on particle characteristics

Several permutations and combinations of drug loading ratios were investigated. CsA loading was varied at 10, 20 and 30% loading, along with varying CoQ10 load from 0 to 70% for each CsA load. The particles were prepared using 3 ml of 0.25% w/v DMAB and probe sonication at 10 microns amplitude for 1 min.

4.2.2.5 Particle size and zeta potential measurements

The particle size and zeta potential measurements were carried out as described in section 3.2.2.1.

4.2.2.6 Entrapment efficiency

The percentage of drug incorporated during nanoparticle preparation was determined by centrifuging the drug loaded nanoparticles at 14,000 rcf for 30 min and separating the supernatant. The pellet obtained was washed twice with water and the drugs were extracted from the pellet using ethyl acetate and acetonitrile followed by an estimation of the drugs in triplicate by a developed HPLC method as described below.

Simultaneous estimation of CsA and CoQ10 was carried out using Hypersil GOLD (15cm x 4.6mm, 5µm) (C18) column and Hypersil 10x4 mm, 5µm drop in guards connected by UNIGAUARD (Thermo Scientific). Elution of both the compounds was achieved using isocratic mobile phase (ethanol:water) at 210 nm for CsA and 275 nm for CoQ10. The HPLC system consisted of ChromQuest acquisition software, autosampler connected with LC Pump and PDA detector (Thermo Finnigan Surveyor System). The analytical method was validated according to the guidelines of the international conference on harmonization of technical requirements for registration of pharmaceuticals for human use. Parameters validated included precision (repeatability (intra-day) and intermediate precision (inter-day)) and accuracy. Both the intra- and inter-day relative standard deviations (RSD) of QC standards were less than 5% over the selected range.

4.2.2.7 Freeze drying of nanoparticles

The CsA, CoQ10 and co-entrapped nanoparticles were freeze dried using previously optimised methods (Kalaria *et al*., 2009; Shaikh *et al*., 2009) for atomic force microscopy (AFM). Trehalose (10% w/v) was added as cryoprotectant before freezing.

4.2.2.8 Atomic force microscopy

Freeze dried particles were re-suspended in distilled water. 100 µl of this particle suspension was diluted with 100 µl water on a glass slide and the residual liquid was removed after 5 min and again rinsed with water to remove stabilisers and dried in air. The particles were then allowed to immobilise on the glass slides for 5 min. Finally, the glass slides were washed with pure water to remove cryoprotectant residues (trelahose) and air dried.

AFM was performed using a vibration-damped NanoWizard (JPK instruments, Berlin, Germany) (Neu *et al*., 2006). Commercial pyramidal Si_3N_4 tips (NSC16 AlBS, Micromasch, Estonia) mounted to a cantilever with a length of 230 μm, a resonance frequency of about 160-170 kHz and a nominal force constant of about 40 N/m were used, and measurements were performed in intermittent contact mode to avoid damage of the sample. The scan speed was proportional to the scan size and the scan frequency was between 0.3 and 0.8 Hz. Images were obtained by displaying the height or amplitude signal in the trace direction (512 x 512 pixels).

4.2.3 Semi-quantitative solid-state solubility of CsA and CoQ10 in the polymer

To determine the solid-state drug–polymer solubility, different quantities of drug solution (stock solution of CsA and CoQ10 in ethyl acetate, 40 mg/ml) were added to polymer solutions of PLGA (40 mg/ml in ethyl acetate), and vortexed, and 75 μL of each drug–polymer solution was spread on a glass slide. The solvent was allowed to evaporate undisturbed overnight at room temperature, and the dried films were observed visually for drug precipitation. Phase separation of drugs from polymers was visible from the opacity of the films, whereas when there was no phase separation, the polymer films remained transparent (Panyam *et al*., 2004).

In the first set of experiments CoQ10 and CsA films were prepared at a concentration of 5, 10, 25, 50, 75 and 100% w/w polymer to determine the load of the drug that PLGA can hold. In second set of experiments the effect of CoQ10 on CsA-PLGA solubility and vice versa were investigated.

4.2.4 *In vitro* drug release studies

Dialysis membrane method was used to determine the release of drugs from the nanoparticulate formulations. Freshly prepared CsA, CoQ10 and CsA-CoQ10 co-entrapped nanoparticle dispersions were centrifuged, redispersed in 1 ml of 5% Labrasol® solution (in pH 7.4 phosphate buffer) and were then transferred to the dialysis bags (Sigma) with a molecular mass cut-off of 12,000 Da. The bags were suspended in vials containing 5 ml of 5% Labrasol® solution (in pH 7.4 phosphate buffer). All the vials were kept in shaker water bath maintained at 37 °C and 50 rpm. The release medium was completely replaced with fresh buffer at every sampling time interval. The sampling points were 6 h followed by sampling at every 24 h for the first 10 days and every 48 h at later stages of release. The CsA and CoQ10 content in the release medium were quantified using a validated HPLC method as described above.

4.2.5 Computer simulation of release

Computer simulations of the release of drugs from a nanoparticle were also performed to provide qualitative insights into our experimental results. In particular, we capture the entropic elasticity of the polymer chains through interactions between cross-link sites and the entropy, and enthalpy, of mixing is captured using Flory-Huggins theory (Flory, 1953). Therefore, we assume the nanoparticles can be described by a collection of cross-linked polymer chains. The Cahn-Hilliard equation is used to diffuse the entrapped drugs. Importantly, the temporal and spatial evolution of the nanoparticle and entrapped drug are coupled throughout. Cross-link sites are randomly distributed within a circular area (the nanoparticle). Potential connections between cross-link sites are determined when the distance between cross-

links is between 0.25 and 0.75 of the cumulative distribution function of the theoretical end-to-end distances. This simply prohibits the creation of polymer chains which are either collapsed or highly stretched, whose occurrence would be unlikely. Polymer chains are created from these potential connections in order of increasing length, while limiting the network connectivity to the functionality (taken here to be 3). To obtain the polymer concentration for the entire nanoparticle, it is necessary to know the local concentration associated with a polymer chain, relative to the end points of the polymer chain. We capture these polymer concentrations using a look-up table of random walk statistics. Therefore, we consider the polymer chains to be ideal and their configurations to be analogous to Brownian motion (corresponding to a random walk). A polymer chain is represented as a random walk of 1000 steps and $1x10^6$ chains are considered. The random configurations are used to create smooth look-up tables of the probabilities of locally finding the polymer, relative to the end points of a polymer chain. The local density is assumed to be proportional to the probability of finding a polymer chain within the cell of the Cahn-Hilliard lattice. The spatial step of our look-up table is taken to be 1/3 of that used when implementing the Cahn-Hilliard equation, to provide a finer representation of polymer concentration than the coarser Cahn-Hilliard lattice. The drug is initially loaded such that polymer and drug concentrations total 0.99. Once we have established the initial nanoparticle configuration, and drug concentrations, we can evolve the system and investigate drug diffusion from the nanoparticle.

The free energy of the system, normalized to k_bT, is given by

$$\frac{U}{k_bT} = \sum_i \left[\frac{R_i^2}{Nb^2} + \frac{Nb^2}{R_i^2}\right] + \sum_j \phi_j \frac{\ln \phi_j}{N_j} + \frac{1}{2}\sum_{i \neq j} \chi_{ij}\phi_i\phi_j + \kappa \sum_j (\nabla \phi_j)^2$$

where the first term describes the entropic stretching of the polymer chains, the second term is from Flory-Huggins theory and the last term provides interfacial tension. R_i is the end-to-end distance of the i^{th} chain, N is the degree of polymerisation and b is the persistence length. $Á_j$ is the concentration of the j^{th} species and $Â_{ij}$ is the interaction parameter between species i and j. The above free energy captures the entropy of chain stretching and, through the Flory-Huggins term, the entropic and enthalpic interactions between the various species (overlapping chains and encapsulated drugs).

The evolution of the position of the i^{th} cross-link site is given by

$$\frac{d\mathbf{r}_i}{dt} = -\frac{DN_e}{k_bTN}\frac{\partial U}{\partial \mathbf{r}_i}$$

where D is the diffusion coefficient of a monomer and N_e is the degree of polymerization when entanglement occurs. The derivative $\partial U/\partial r_i$ for the polymer concentrations can be obtained from $\partial U/\partial r_i = (\partial U/\partial Á_j)(\partial Á_j/\partial r_i)$. The derivative of the polymer concentration with respect to the position of an end point can be obtained directly from the look-up table of polymer concentrations. The drug concentrations are simultaneously updated using the following Cahn-Hilliard equation (Cahn and Hilliard, 1958)

$$\frac{\partial \phi_D}{\partial t} = \nabla \frac{D}{k_bT}\phi_D(1-\phi_D)\nabla\frac{\partial U}{\partial \phi_D}$$

where D is the diffusion coefficient of the drug molecule, which is taken to be the same as a monomer, and the concentration $Á_D$ is the concentration of one of the drugs. The Cahn-Hilliard equation is solved on a discrete lattice of $L^2 = 64^2$, where in lattice units the nanoparticle radius is 20. In order to account for the diffusion of the encapsulated drug beyond this system size we employ extrapolated boundary conditions where the concentration at a point beyond the system is obtained from the linear extrapolation of points inside the system (while ensuring that we do not include negative concentrations). The

simulations progress through the interactive update of both the drug concentration and the polymer crosslink sites. The polymer concentration is subsequently obtained from the positions of the crosslink sites. Therefore, we can simultaneously evolve nanoparticle mechanics and drug diffusion, to capture the release of an encapsulated drug.

4.2.6 Pharmacokinetic and tissue distribution studies

For pharmacokinetic studies male SD rats weighing 200–250 g were used. The effect of co-administration of CoQ10 suspension on pharmacokinetic profile of Neoral® was studied. Neoral® was administered at 15 mg/Kg followed by administration of CoQ10 suspension at 75 mg/Kg after 15 min and was compared to simple Neoral®. The effect of co-entrapped CoQ10 on CsA's pharmacokinetic profile was investigated. Co-entrapped nanoparticles at 30% CsA loading and 70% CoQ10 loading were administered at 30 mg/Kg of CsA that corresponded to 75 mg/Kg of CoQ10. The co-entrapped particles were compared to simple CsA nanoparticles at 30% loading.

Blood samples and tissues were collected from animals and analysed for CsA concentration as described in section 3.2.3.

4.2.7 Chronic nephrotoxicity study

The ability of CoQ10 in preventing CsA induced nephrotoxicity was investigated in a 30 day chronic nephrotoxicity study as described in section 3.2.5. Neoral® was administered at 15 mg/Kg followed by administration of CoQ10 suspension (in carboxymethyl cellulose) at 75 mg/Kg after 15 min and co-entrapped nanoparticles at 30% CsA loading and 70% CoQ10 loading were administered at 30 mg/Kg of CsA that corresponds to 75 mg/Kg of

CoQ10 and compared to simple Neoral®, CsA nanoparticles and control groups.

4.2.7.1 Blood CsA levels during chronic nephrotoxicity study

Blood CsA levels during the chronic nephrotoxicity study were determined as described in section 3.2.5.1

4.2.7.2 Plasma creatinine and blood urea nitrogen

PC and BUN were analysed as described in section 3.2.5.2.

4.2.7.3 Histopathological evaluation of kidney

Histopathological evaluation of kidney was performed as described in section 3.2.5.3.

4.2.7.4 CoQ10 plasma levels

The CoQ10 plasma levels after 30 day chronic nephrotoxicity were determined by liquid chromatography-mass spectroscopy (LC-MS) (Manchala, 2010). In brief, the procedure was as follows. 100 µl of plasma was mixed with 100 µl of Vitamin K1 (internal standard, 10 µg/ml) and 500 µl each of hexane and methanol in microcentrifuge tubes and vortexed. The upper hexane layer was collected by centrifugation at 10,000 rpm for 5 min. The collected hexane layer was evaporated at room temperature and the obtained residue was reconstituted in 100 µl of mobile phase consisting of 5mM ammonium acetate in 95:5 mixture of ethanol and water respectively. The reconstituted samples were analysed by LC-MS in tandem mode (MS/MS) with the orbitrap model using Finnigan LTQ fitted with an Orbitrap detector and X-calibur for data analysis.

4.3 Results and discussion

4.3.1 Preparation of nanoparticles

4.3.1.1 Effect of DMAB concentration on drug entrapment

The amount of stabiliser used for particle preparation is critical to the nanoparticle characteristics, too low concentration leads to the aggregation of the polymer, whereas too much stabiliser affects drug incorporation (Guarrero *et al*., 1996) and similar effects were observed with CsA-DMAB in our preliminary studies (Italia *et al*., 2007). Four different concentrations of DMAB (0.1, 0.25, 0.5 and 1% w/v) were selected and three different sets of particles were prepared using the four concentrations. The three sets of batches included CsA particles at 10% loading, CoQ10 particles at 30% loading and CsA and CoQ10 co-loaded particles at 10 and 30% loading, respectively. Other experimental parameters such as homogenisation at 15,000 rpm for 5 min, external phase volume (5 ml of DMAB solution) were kept constant.

With decreasing DMAB concentration, an increase in particle size and entrapment efficiency was observed for all three experimental sets (Table 4.1). Figure 4.1 shows effect of DMAB concentration on size distribution of CsA and CoQ10 co-loaded nanoparticles. For all batches, the particle size increased from around 100 nm to 200 nm with decreasing DMAB concentration from 1% to 0.1%. A similar phenomenon was observed for estradiol loaded PLGA nanoparticles for DMAB concentration in the range of 0.5 to 3% (Hariharan *et al*., 2006). For CsA, decreasing DMAB concentrations resulted in a significant increase in entrapment efficiency. The entrapment efficiency increased from 10% to 39% as the DMAB concentration dropped from 1 to 0.1%. For CoQ10, an increase in entrapment efficiency was observed, but was not as profound as it was for CsA. For CoQ10 the

entrapment efficiency increased from 63% to 87% as the DMAB concentration dropped from 1 to 0.1%. When CsA and CoQ10 were co-loaded the particle characteristics in terms of size and entrapment remained very similar to their individual particles.

DMAB concentrations had a profound effect on CsA entrapment in comparison to CoQ10, which may be due to the higher solubility of CsA in DMAB solution than CoQ10 (Hariharan *et al*., 2006; Ankola *et al*., 2007), causing excessive partitioning of CsA into the aqueous phase resulting in low entrapment (Italia *et al*., 2007). 0.1% DMAB concentration, which produced particles with the highest entrapment efficiency for CsA, was taken up further to study the effect of external phase volume on co-loaded particle characteristics.

4.3.1.2 Effect of external phase volume on particle characteristics

As DMAB concentration affected the entrapment efficiency, the external phase volume dependent particle characteristics were investigated. 0.1% DMAB concentration was kept constant and the amount of external phase was varied (5, 3 and 1.5 ml). Other process parameters such as homogenisation speed and time were kept constant.

With decreasing external phase volume from 5 to 1.5 ml, entrapment efficiency of CsA increased with increase in size, however the decrease in external phase volume had no effect on CoQ10 entrapment (Table 4.2). Figure 4.2 shows effect of external phase volume on size distribution of CsA and CoQ10 co-loaded nanoparticles. The size increased from 208 nm for 5 ml of external phase volume to 351 nm for 1.5 ml. The entrapment efficiency of CsA increased from 39% to 63% as the volume decreased from 5 to 1.5 ml. This increase in efficiency was due to less amount of DMAB present in

aqueous phase (continuous phase) hence decreasing the solubility and partitioning of CsA into it (Italia *et al*., 2007). The change in external phase volume had no effect on CoQ10 entrapment and it remained around 83%. Considering a balance between entrapment efficiency and particle size 3 ml of 0.1% DMAB solution was used further to investigate the effect of droplet size reduction method on co-loaded particle characteristics.

4.3.1.3 Effect of droplet size reduction method on particle characteristics

It is reported in literature that sonication yields particles with smaller size, while high pressure homogenisation provides more monodisperse particles (Lamprecht *et al*., 2000). In the present study we compared both the processes for their efficiency in reducing the particle size and its effect on entrapment efficiency. Homogenisation was carried out at 15,000 rpm for 5 min, and sonication at 10 microns amplitude for 1 min, while remaining process parameters were kept constant.

Table 4.1 Effect of DMAB concentration on drug entrapment

DMAB Conc (% w/v)	CsA loaded		CoQ10 loaded		Co-loaded (CsA and CoQ10)		
	Size (nm)	EE (%)	Size (nm)	EE (%)	Size (nm)	EE (%) CsA	EE (%) CoQ10
1	105±2	10±5	100±8	63±7	109±13	10±2	63±4
0.5	131±5	13±3	139±7	76±4	142±14	13±3	73±5
0.25	161±6	17±2	167±7	85±6	170±5	18±2	81±7
0.1	196±5	39±3	206±9	87±3	208±9	39±6	85±8

CsA 10 % and CoQ10 30% initial loading w/w of polymer for individual as well as co-loaded formulations. ZP was 69-86 mV at pH 4.5±0.5. PDI of particles was 0.08-0.15. All values represented as mean±S.D. (n=3).

Table 4.2 Effect of external phase volume on particle characteristics

Volume of external phase (ml)	CsA loading	CoQ10 loading	Size (nm)	CsA		CoQ10	
				EE (%)	Amt. Entrapped (mg)	EE (%)	Amt. Entrapped (mg)
5	10	30	208±9	39±6	1.9±0.3	85±8	12.7±1.2
3	10	30	247±16	56±8	2.8±0.4	83±1	12.4±0.4
1.5	10	30	351±25	63±6	3.2±0.3	82±3	12.4±0.5

ZP was 50-85 mV at pH 4.5±0.5. PDI of particles was 0.15-0.29. All values represented as mean±S.D. (n=3).

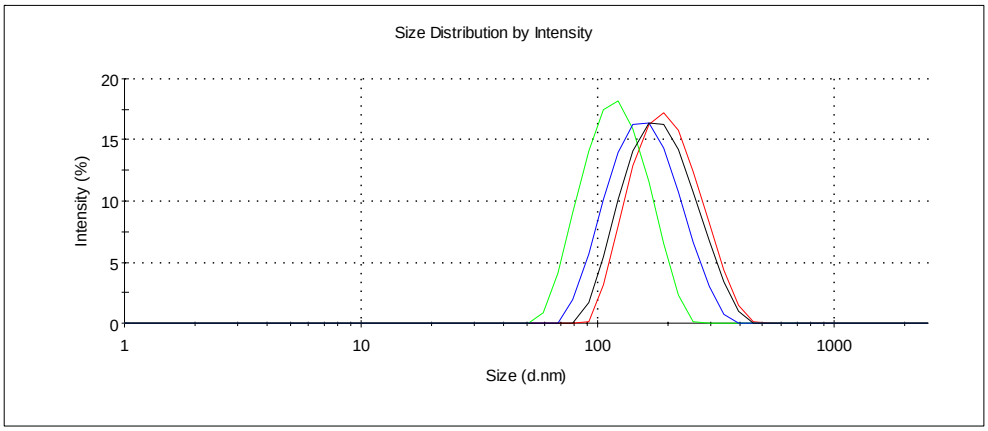

Figure 4.1 Size distribution intensity graph showing the effect of DMAB concentration on CsA-CoQ10 co-loaded size distribution curve. Green-1%, Blue-0.5%, Black-0.25% and Red-0.1% of DMAB concentration.

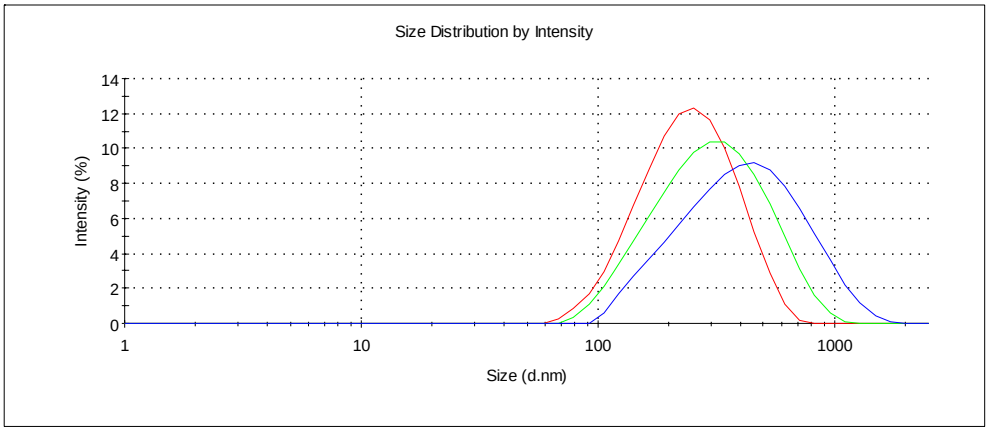

Figure 4.2 Size distribution intensity graph showing the change in size distribution curve with change in external phase volume; Red-5 ml, Green-3 ml, Blue-1.5 ml of 0.1% DMAB solution.

Sonication produced particles of smaller size, by providing very high mechanical energy to the system in the form of sonic waves, leading to improved particle droplet size reduction than that observed during homogenisation. Particles of 247 nm with % entrapment of 56 and 83 for CsA and CoQ10, respectively, were produced using homogenisation while sonication resulted in particles of 156 nm with high % entrapment of 74 and 94 for CsA and CoQ10, respectively (Table 4.3). The high entrapment observed for particles prepared using sonication could be due to the larger surface area exposed, as a consequence of their smaller size, which increased their interactions with the drugs, in comparison to those produced through homogenization.

A fresh batch was investigated using 0.25% DMAB solution and compared to 0.1% batch using probe sonication as the size reduction method. 0.25% DMAB batch produced particles of 116 nm in size with % entrapment of 36 and 83 for CsA and CoQ10 respectively in comparison to 156 nm particles with % entrapment of 74 and 93 for 0.1% DMAB concentration (Table 4.3). Figure 4.3 shows the effect of size reduction method on particle size distribution. In spite of the smaller size particles produced by sonication for 0.25% DMAB, the entrapment of drugs decreased, which may be due to a higher diffusion of drugs into the aqueous phase as a result of higher DMAB concentration.

An optimal nanoparticulate formulation consists of desired sized particles and entrapment efficiency. We have observed that particles of order 100 nm have been most suitable for oral drug delivery (Hariharan *et al*., 2006; Ankola *et al*., 2007; Italia *et al*., 2007; Mittal *et al*., 2007). Therefore, considering the lowest size and moderate % entrapment, 3 ml of 0.25% DMAB solution as the external phase and probe sonication as the size reduction method were

selected for preparing further batches which involved different loading studies.

4.3.1.4 Effect of drug loading on particle characteristics

Dose is a critical factor in designing particulate delivery systems for oral delivery (Bhardwaj *et al*., 2005). For combination formulations, the proportion of one component to another is critical for maximum beneficial effects. CsA is a low dose (2-15 mg/Kg) drug while CoQ10 is a high dose (10-100 mg/Kg) antioxidant, therefore entrapment of both molecules in a polymeric system at a desired proportion can be challenging as CsA's entrapment is highly dependent on DMAB concentration and loading ratio while CoQ10 entrapment is more robust in nature due to its very high lipophilicity and minimal solubility in DMAB solution. Considering the challenges in encapsulating a desired ratio between CsA and CoQ10, due to their varied physicochemical properties, several loading combinations were studied.

Table 4.3 Effect of droplet size reduction method on particle characteristics

DMAB conc. (% w/v)	**Method**	**Size (nm)**	**CsA**		**CoQ10**	
			EE (%)	**Amt. Entrapped (mg)**	**EE (%)**	**Amt. Entrapped (mg)**
0.1	Homogenisation	247±16	56±8	2.8±0.4	83±1	12.4±0.9
0.1	Probe sonication	156±3	74±4	3.7±0.2	94±3	14.1±0.4
0.25	Probe sonication	116±2	36±2	1.8±0.1	83±4	12.4±0.6

CsA 10 % and CoQ10 30% initial loading w/w of polymer. ZP was 73-78 mV at pH 4.5±0.5. PDI of particles was 0.08-0.18. All values represented as mean±S.D. (n=3).

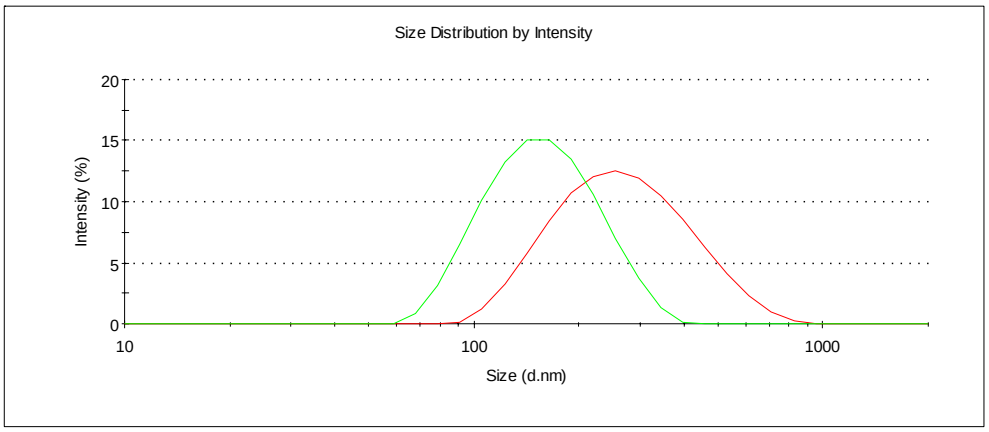

Figure 4.3 Size distribution intensity graph showing the change in size distribution curve as a effect of using homogenization and probe sonication as size reduction method; Red- Homogenization, Green- Probe sonication.

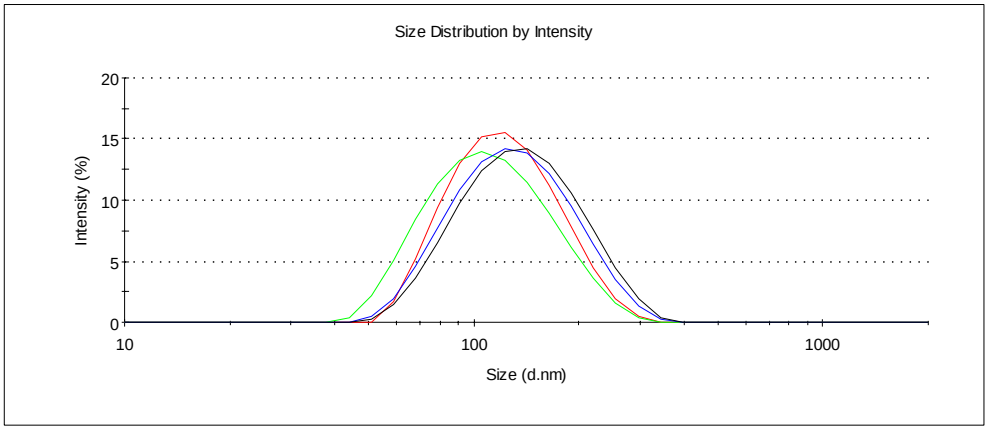

Figure 4.4 Size distribution intensity graph showing the change in size distribution curve as a result of increasing CoQ10 loading; Green- 10%, Red-30% Blue-50% and Black-70% w/w of CoQ10 loads, respectively.

In the first set CsA loading was kept constant at 10 %w/w of polymer and CoQ10 loading was varied at 0, 10, 30, 50 and 70%. With increasing CoQ10 loading from 0 to 70% at 10% constant CsA loading, particle size increased from 107 to 130 nm. The entrapment efficiency of CsA increased with increasing CoQ10 load in the particle. The entrapment of CsA increased from 20 to 51% as the CoQ10 load increased from 0 to 70%. The entrapment of CoQ10 also increased slightly from 79% to 91% with increasing loading from 10 to 70% (Table 4.4). Figure 4.4 demonstrates the effect of co-loading on size distribution pattern. The entrapment efficiency was translated to amount of drug entrapped per 50 mg of polymer. Due to increase in entrapment efficiency of CsA, amount entrapped also increased from 1 to 2.6 mg with increasing CoQ10 load. For CoQ10 the amount entrapped increased corresponding to its % entrapment and load. It increased from 3.9 to 31.9 mg with increase in load from 10 to 70%. Considering the amount of CsA and CoQ10 entrapped in particles, ratio between CsA and CoQ10 was determined. The ratio (CsA:CoQ10) was from 1:2.6 to 1:12.6.

In the second set, keeping CsA loading constant at 20 %w/w, CoQ10 loading was varied similarly as above. With increasing CoQ10 loading from 0 to 70% particle size increased from 108 to 132 nm. The entrapment efficiency of CsA increased with increasing CoQ10 load in the particle. The entrapment of CsA increased from 46 to 63% with the increase in CoQ10 load from 0-70%. The entrapment of CoQ10 remained constant around 85% for different loadings. Considering the amount of CsA and CoQ10 entrapped in particles, ratio between CsA and CoQ10 was determined. The ratio (CsA:CoQ10) was from 1:0.9 to 1:4.8.

In the third set CsA loading was kept constant at 30 %w/w of polymer and CoQ10 loading was varied. With increasing CoQ10 loading from 0 to 70% at

30% constant CsA loading, particle size increased from 119 to 135 nm. The entrapment efficiency of CsA increased with increasing CoQ10 load in the particle. The entrapment of CsA increased from 62 to 81% as the CoQ10 load increased from 0 to 70%. The entrapment of CoQ10 remained constant at around 87% for different loads. Due to increase in entrapment efficiency for CsA amount entrapped also increased from 9.3 mg to 12.1 mg with increasing CoQ10 load from 0 to 70% respectively. For CoQ10 the amount entrapped increased corresponding to its % entrapment and load. It increased from 4.4 to 30.6 mg as the load increased from 10-70%. Considering the amount of CsA and CoQ10 entrapped in particles, ratio between CsA and CoQ10 was determined. The ratio (CsA:CoQ10) was from 1:0.4 to 1:2.5. The particles were found to have low PDI (0.1-0.2) for all the batches and zeta potential was found to be in the range of 67-87 mV.

The size and surface morphology of freeze dried CsA, CoQ10 and co-entrapped nanoparticles were analysed by AFM. From AFM images it appears that the nanoparticles were uniform and spherical in shape (Figure 4.5). Loading of either moieties or their combination had no significant effect on PLGA nanoparticles morphology. The size range of nanoparticles observed under AFM was similar to that observed by dynamic light scattering.

From the foregoing studies it is evident that in the presence of CoQ10 the entrapment of CsA increased, and with increasing CoQ10 a further increase in CsA entrapment was observed. This may be due to several reasons. Considering the high lipophilicity of CoQ10, the presence of CoQ10 in the polymer matrix may have increased the lipophilicity of the system hence making it more conducive for the partitioning of CsA into the polymer matrix, rather than the diffusion into the aqueous phase. Other possibility

may be a better inter-molecular arrangement of CsA in PLGA matrix in presence of CoQ10, leading to a better entrapment of CsA. Another possibility could be a chemical/physical interaction between the drug molecules and polymer. Further studies were, therefore, planned to elucidate these peculiar effects. Firstly, the lipophilicity phenomenon was investigated by determining the semi-quantitative solubility of CsA and CoQ10 in PLGA, and their effects on each other.

Table 4.4 Effect of drug loading on particle characteristics

CsA loading	CoQ10 loading	Size (nm)	CsA		CoQ10		Ratio CsA:CoQ10
			EE (%)	Amt. Entrapped (mg)	EE (%)	Amt. Entrapped (mg)	
10	0	107±7	20±2	1.0±0.1	----	---	---
10	10	104±3	31±3	1.5±0.2	79±3	3.9±0.1	1:2.6
10	30	116±2	36±2	1.8±0.1	83±4	12.4±0.6	1:6.9
10	50	117±3	48±1	2.4±0.1	90±2	22.6±0.4	1:9.5
10	70	130±4	51±6	2.6±0.3	91±5	31.9±1.6	1:12.6
20	0	108±7	46±4	4.6±0.4	---	---	---
20	10	111±5	50±3	5±0.3	85±4	4.3±0.2	1:0.9
20	30	124±3	53±5	5.3±0.5	85±5	12.7±0.7	1:2.4
20	50	126±3	59±3	5.9±0.3	85±4	21.3±0.9	1:3.6
20	70	132±7	63±4	6.3±0.4	85±5	29.9±1.7	1:4.8
30	0	119±5	62±4	9.3±0.6	---	---	---
30	10	121±2	74±6	11.2±0.9	88±4	4.4±0.2	1:0.4
30	30	127±1	75±6	11.3±0.7	87±7	13.1±0.9	1:1.2
30	50	131±2	77±1	11.6±0.1	88±5	22±1.3	1:1.9
30	70	135±4	81±2	12.1±0.2	87±5	30.6±1.1	1:2.5

ZP was 67-87 mV at pH 4.5±0.5. PDI of particles was 0.1-0.2. All values represented as mean±S.D. (n=3).

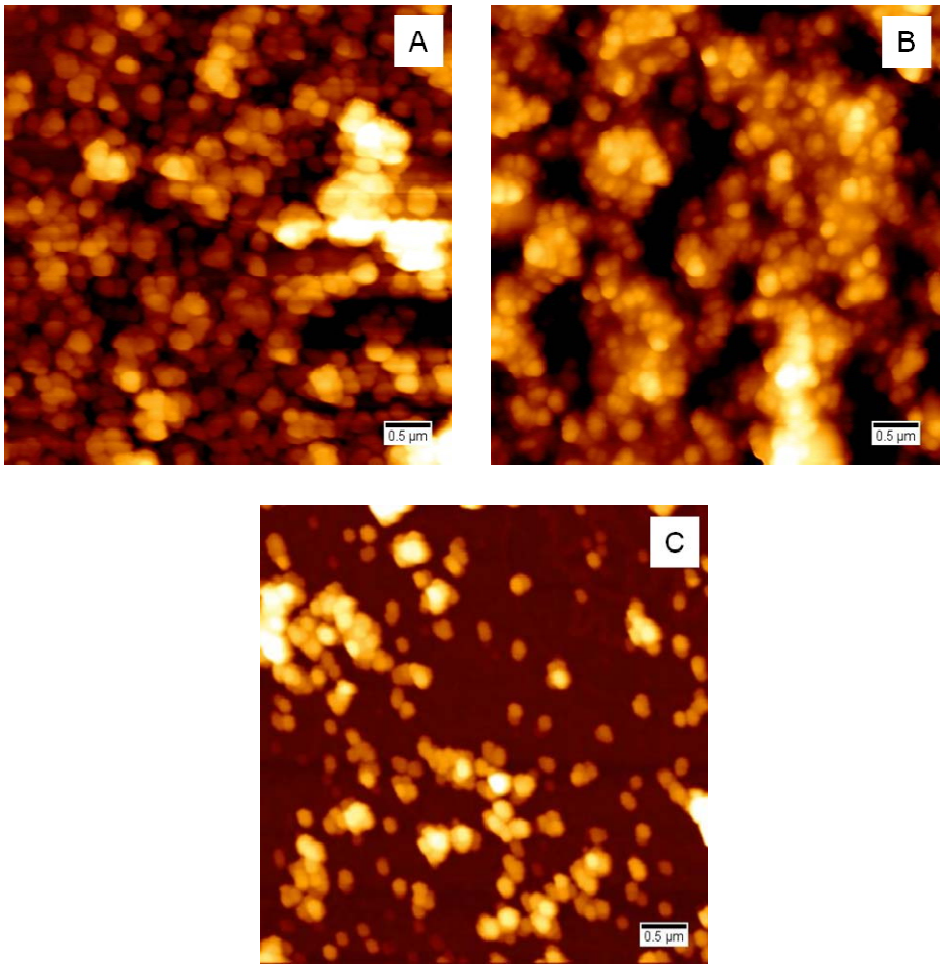

Figure 4.5 AFM images of freeze dried nanoparticles A) CsA nanoparticles, B) CoQ10 nanoparticles and C) Co-entrapped nanoparticles; (Scan size: 10x10µm)

4.3.2 Semi-quantitative solid-state solubility of CsA and CoQ10 in the polymer

The semi-quantitative solid-state solubility of CsA and CoQ10 in PLGA films at different concentrations was determined. The concentrations used were 5, 10, 25, 50, 75 and 100% w/w of polymer for CsA and CoQ10. Concentration above 75% w/w of polymer for CsA and CoQ10 resulted in opaque films while all concentrations below that produced transparent films based on visual inspection.

As observed during nanoparticle preparation, an increase in CoQ10 load results in an increase in % CsA entrapment. So CsA at 75 % w/w of polymer was fixed and gradually the CoQ10 concentration was increased from 5 to 50% w/w of polymer. The transparency/opacity of the film was visually observed. With increasing CoQ10 concentration, the film of CsA (at 75% w/w of polymer) started to become transparent (Figure 4.6A) indicating a possible increase in solubility of CsA in the polymer, due to the presence of CoQ10. Effects of CsA concentration on CoQ10 solubility in PLGA were also similarly determined. With increasing CsA concentration, the film of CoQ10 (at 75% w/w of polymer) started to become transparent (Figure 4.6B) indicating a possible increase in solubility. The possible increase in mutual solubility of CsA and CoQ10 in presence of each other can be due to several reasons but one of the possible theories is that both of them increases the lipophilicity of the polymer by their presence which would result in more partitioning of the other drug in polymer matrix during particle formation.

In a solvent evaporation technique, such as emulsion-diffusion-evaporation used here, the ethyl acetate containing the dissolved polymer and the drug is emulsified in an external phase containing DMAB. Water is added to this emulsion to cause the diffusion of ethyl acetate, and is then stirred to

evaporate the ethyl acetate, which results in the nanoprecipitation of PLGA in which the drug is entrapped. As the ethyl acetate evaporates from the emulsion, the drug distributes between the polymeric droplets and the aqueous phase containing DMAB (continuous phase), which can solubilise the CsA and CoQ10. The drug diffused into the continuous phase by miscibility of ethyl acetate precipitates once the solvent evaporates which then deposits onto the particle surfaces. Based on the above theory, drug loading in particulate systems prepared by the emulsion-diffusion-evaporation technique would depend on the solubility of the drug in the polymeric and continuous phases and drug's separation as a solid in the continuous phase and its deposition onto the nanoparticle surface (Panyam *et al*., 2004). As CsA has a high solubility in DMAB, this can be one of the factors affecting the entrapment of CsA, while CoQ10 has very low solubility in DMAB so its effect on CoQ10 entrapment may be negligible. The free and surface adhered drug is removed by washings before proceeding with the drug entrapment studies and this entrapment is certainly dependent on the partitioning of the CsA between polymer and the continuous phases (Tse *et al*., 1999). Hence, in this study, we determined the solid state solubility of CsA and CoQ10 in a polymer as a function of each other. The increasing solubility of CsA in the presence of CoQ10 may be one of the reasons for higher entrapment of CsA in a polymer matrix in the presence of CoQ10. The CoQ10's solubility also increased in presence of CsA but no major change in entrapment was observed, this could be due to its inherent low solubility in continuous phase and high partitioning in PLGA.

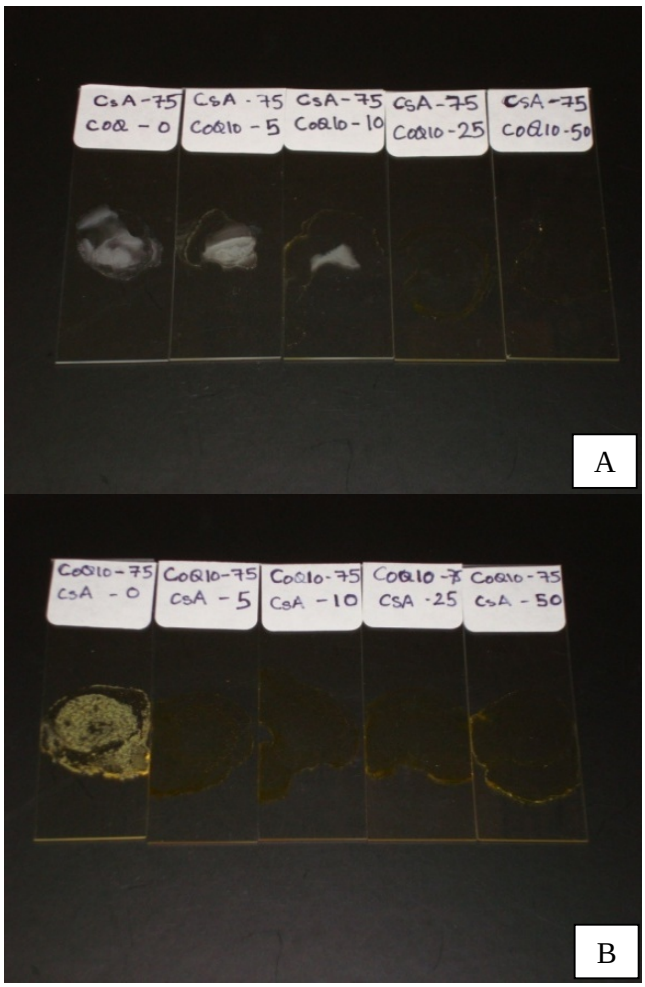

Figure 4.6 A) Effect of CoQ10 on solubility of CsA in PLGA. With increasing CoQ10 concentration the solubility of CsA increased in PLGA as observed visually by decrease in opacity and increase in transparency of film. **B)** Effect of CsA on solubility of CoQ10 in PLGA. With increasing CsA concentration the solubility of CoQ10 increased in PLGA as observed visually by decrease in opacity and increase in transparency of film.

4.3.3 *In vitro* drug release studies

The prepared nanoparticles were further evaluated for *in vitro* drug release. This is challenging for a number of technical reasons, the foremost being the creation of sink conditions for highly lipophilic CoQ10 and CsA. For poorly soluble CsA and CoQ10, an adequate release medium providing sink conditions was not obtained with aqueous solutions within physiological pH. For this reason, an aqueous solution containing a surfactant/solubiliser was used to enhance its solubility. Labrasol® (Caprylocaproyl Macrogolglycerides (Polyoxylglycerides)) commonly used as solubiliser/bioavailability enhancer for oral formulations was used as the release medium at 5% w/v in phosphate buffer pH 7.4. The saturation solubility of CsA and CoQ10 at 37 ^{o}C in the release medium was determined and found to be 726±76 and 29±5 μg/ml for CsA and CoQ10, respectively. Complete release medium replacement was followed to maintain sink conditions.

The release pattern of CsA and CoQ10 were observed from individual and co-entrapped particles. About 14% of CsA was released from individual nanoparticles in 24 h while 12% CsA was released from co-entrapped nanoparticles. The release pattern of CsA from CsA nanoparticles was faster as compared to co-entrapped particles. For the first 48 h no visible difference in release rate was observed but from the 3rd day onwards a clear difference was observed (Figure 4.7). About 86% of CsA was released by the 18th day from CsA nanoparticles, but only 64% of CsA was released from co-entrapped particles. This slower release of CsA from nanoparticles containing CoQ10 may be due to the fact that CoQ10, being a very hydrophobic molecule prevented the partitioning of CsA from the polymer matrix to the release medium and the penetration of the release medium into

the matrix, hence, slowing down the processes of CsA diffusion and polymer degradation and resulting in a slower release of CsA.

The release of CoQ10 from CoQ10 nanoparticles and co-entrapped particles was found to be very slow. Only around 15% of CoQ10 was released over 18 days. This slow release may be due to the inability of CoQ10 to partition and diffuse into release medium. Similarly, slow and low release of CoQ10 was observed earlier using Tween 20 as a release medium (Ankola *et al*., 2007). After 18 days the amount of CoQ10 remaining in the particles was determined. About 50% of CoQ10 was found remaining in particles determined by HPLC after extraction using ethyl acetate and dilution with ethanol. About 35% of CoQ10 was lost from mass balance which could possibly be due to the degradation of CoQ10 in the release medium, as CoQ10 was found to degrade by 16% in the release medium over four days (Figure 4.8). CoQ10 is a highly sensitive molecule which undergoes degradation quite rapidly in the presence of light, so the possibility of CoQ10 degradation in the release medium cannot be ruled out.

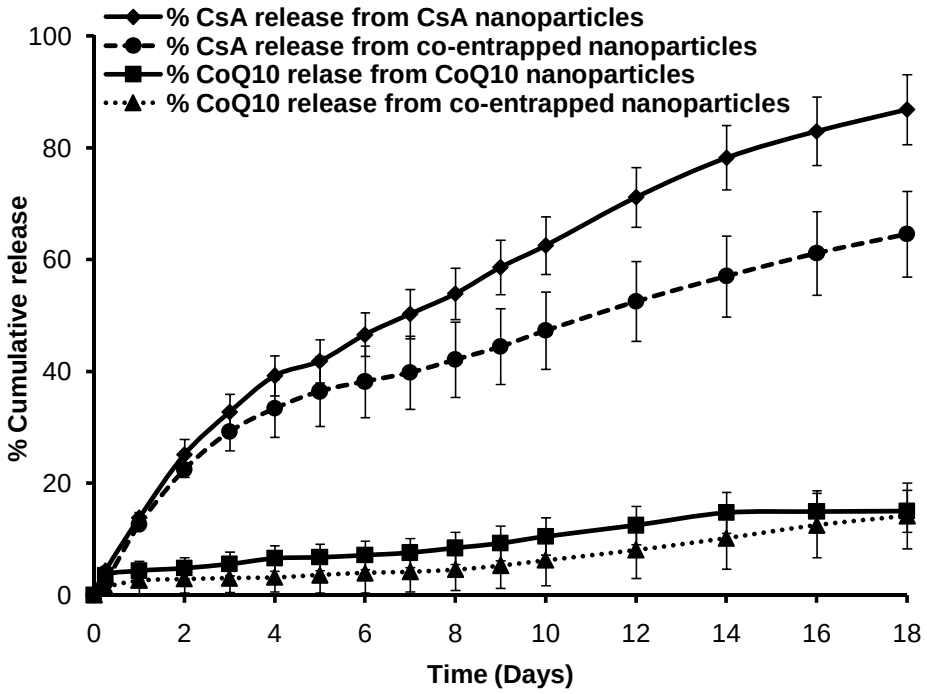

Figure 4.7 *In vitro* release pattern of CsA from CsA nanoparticles; CoQ10 from CoQ10 nanoparticles and CsA and CoQ10 from co-entrapped nanoparticles. All values represented as mean±S.D. (n=3).

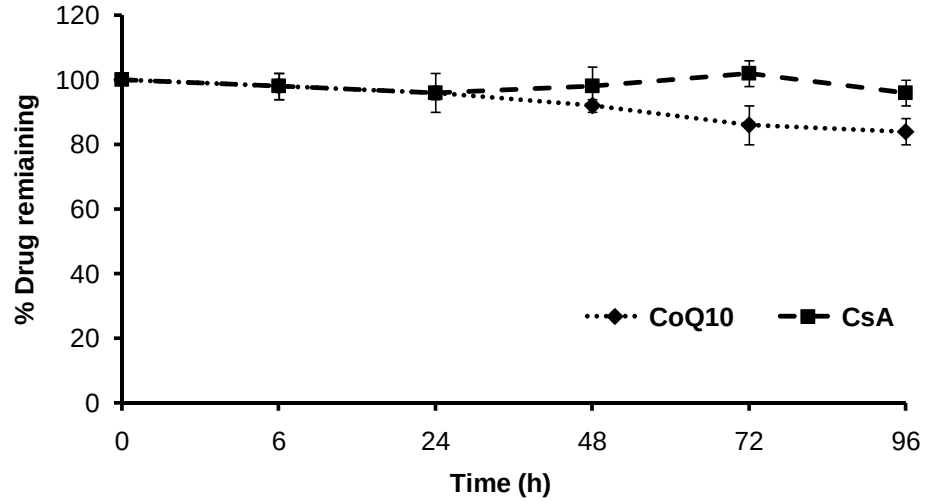

Figure 4.8 Stability of CsA and CoQ10 in 5% Labrasol® solution (In pH 7.4 Phosphate buffer). All values represented as mean±S.D. (n=3).

In an attempt to gain additional insights into the release phenomenon, a qualitative computer model of the co-entrapment of two drugs inside a polymer nanoparticle was investigated (Ankola *et al*., 2010). The entropic elasticity of the polymer chains through interactions between cross-link sites and the entropy, and enthalpy, of mixing was captured using Flory-Huggins theory and the Cahn-Hilliard equation was used to diffuse the entrapped drugs (Flory, 1953; Cahn and Hilliard, 1958; Buxton, and Clarke, 2007).

The interaction between the polymer and release medium is characterised by a chi-parameter of $\hat{A}_{P\{RM\}} = 3.6$ (PLGA-water). The entrapment of two drugs, labeled here drugs A and B, is simulated. Drug A has chemical properties similar to the polymer, with drug B considered to be similar to the release medium. The chi-parameter between drug A and the polymer is zero, and between drug A and the release medium is $\hat{A}_{P\{RM\}}$. Conversely, the chi-parameter between drug B and the polymer is $\hat{A}_{P\{RM\}}$, and between drug B and the release medium is zero. The effects of varying the interaction between drug A and drug B is considered. Logically, the chi-parameter between drugs A and B, $\hat{A}_{AB}$, might be expected to be equal to $\hat{A}_{P\{RM\}}$, considering drug A is similar to the polymer matrix and drug B is similar to the release medium. The release pattern of drug A and drug B were predicted from single loaded particles and co-entrapped particles.

Figure 4.9 shows the single loaded release for drug A (solid black line) and for drug B (dashed black line). As expected the more lipophilic drug B, similar to CoQ10, has a slow release rate while the more hydrophilic drug A, similar to CsA is released relatively quickly. The release pattern from co-entrapped particles is also considered. Drug A is associated with the solid lines, and drug B with the dashed lines, while the chi-parameter between the two drugs was taken to be $\hat{A}_{P\{RM\}}$ (red lines), 0 (green lines) and $-\hat{A}_{P\{RM\}}$ (blue

lines). The red lines, therefore, indicate the situation when the two drugs dislike each other and the co-entrapment results in the drugs pushing each other out of the particle. In this case, both release patterns indicate that the drugs are released faster than in the single loaded particles. Next, we consider the case when the chi-parameter between the two drugs is zero. In this case, the two drugs are compatible and the more hydrophilic drug A is not pushed out of the particle by drug B. However, the release of drug A in to the surrounding release medium encourages an increase in the release of drug B, as now the surrounding fluid contains both the release medium (which dislikes the lipophilic drug B) and drug A (which, here, is compatible with drug B). In order to observe qualitatively similar results to what was observed experimentally (Figure 4.7) it was necessary to consider a negative chi-parameter. The blue lines show the release pattern from a simulation were both drugs are attracted to each other. Here, drug A is both pushed out of the nanoparticle through its interaction with the polymer and, essentially, pulled inwards by its attraction to drug B. This results in a significant decrease in drug release. It should be noted, however, that the current model does not include the effects of polymer degradation and the comparisons between simulations and experiments were qualitative. The simulations indicate that there may be an attraction between CsA and CoQ10 which improves their co-entrapment inside a polymer nanoparticle.

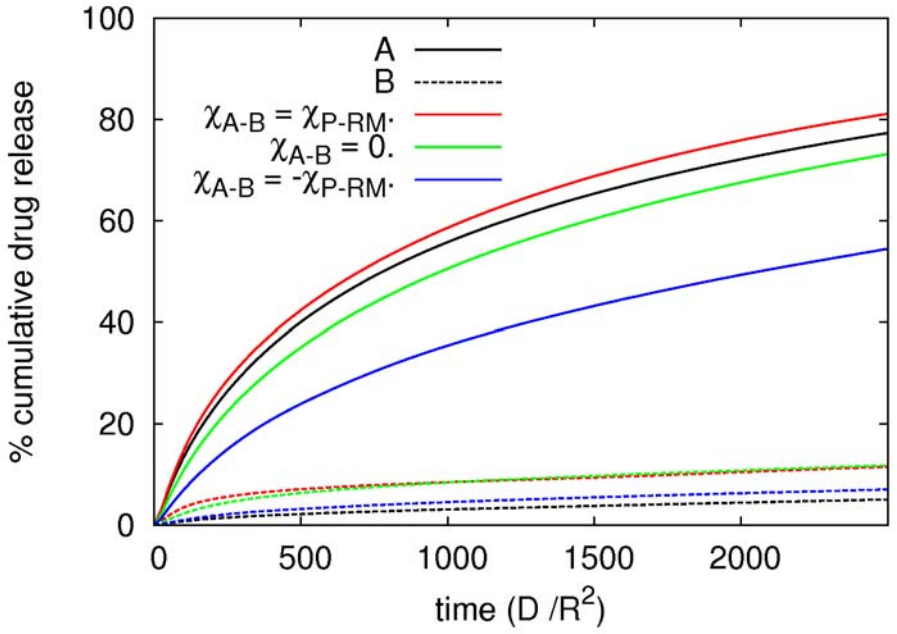

Figure 4.9 Stimulated release pattern of drug A and drug B from individual nanoparticles and co-entrapped nanoparticles.

4.3.4 Pharmacokinetic and tissue distribution studies

Some drugs have been found to alter the pharmacokinetic profile of CsA. The effect of mibefradil (calcium antagonist) on pharmacokinetic profile of Sandimmune® was investigated (Spoendlin *et al*., 1998). Administration of Mibefradil led to significant increase in blood CsA concentrations, which was due to inhibition of CYP3A4, the enzyme responsible for CsA metabolism. Similarly, several CYP3A4 inhibitors like ketoconazole (Gomez *et al*., 1995) have been able to increase CsA blood levels. Moreover several highly lipophilic molecules like probucol have been found to reduce CsA blood levels by reducing the solubility of CsA in aqueous gastrointestinal fluid (Jiko *et al*., 2002).

Considering the above, effect of CoQ10 on Neoral®'s blood profile was investigated by administration of CoQ10 suspension after 15 min of Neoral® administration. Figure 4.10 represents the pharmacokinetic profile of Neoral® and Neoral® with CoQ10 co-administration. As observed from the pharmacokinetic profile and derived parameters (Table 4.5) and tissue concentrations after 72 h (Table 4.6), administration of CoQ10 suspension had no effect on the blood and tissue CsA concentration produced by Neoral®, hence no pharmacokinetic interaction between the two molecules was observed in the given experiment.

The effect of co-entrapping CsA with CoQ10 in PLGA nanoparticles on biodistribution pattern of CsA was investigated. As observed from *in vitro* studies, co-entrapment of CsA with CoQ10 led to a decrease in rate of CsA release, however on *in vivo* profiling, no difference in CsA blood and tissue concentration were observed (Figure 4.10, Table 4.5 and 4.6). No change in AUC, T_{max}, C_{max} and tissue concentration was observed, which was very different to what was observed *in vitro*. Several factors can contribute to this

discrepancy in the release profiles *in vitro* and *in vivo* conditions. Of the several factors, the ability of release medium to provide conditions similar to *in vivo* environment is of prime importance. The release medium used was 5% Labrasol® solution based on its ability to solubilise CoQ10 and CsA. On the other hand, the release of drug *in vitro* is primarily based on diffusion from polymer matrix and polymer degradation, however in body several factors could be of greater consequences like, particle uptake, distribution and clearance. In addition to the above, analytical methods for estimating drug is significant factor as most methods estimate the drug in body as a whole rather than determining the free drug and not the one entrapped in nanoparticles.

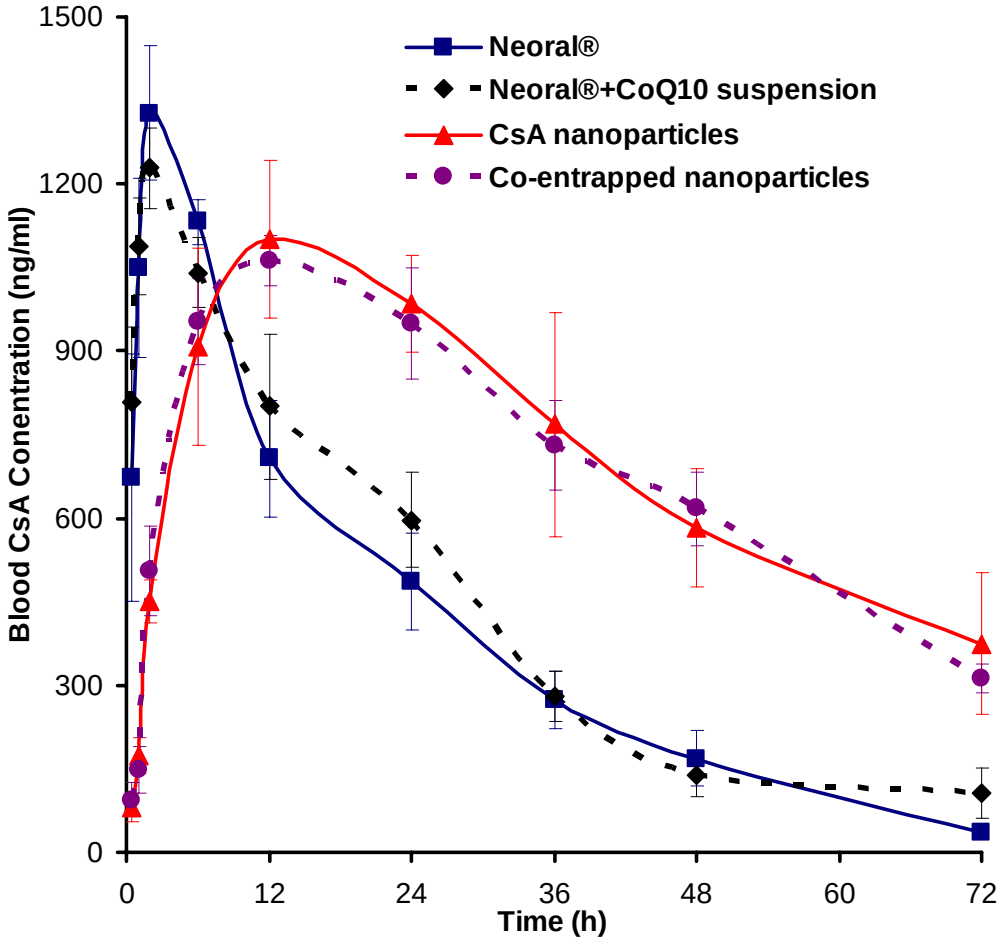

Figure 4.10 Effect of CoQ10 co-administration on Neoral® and co-entrapped nanoparticle blood profile. Neoral® (15 mg/Kg) was administered first followed by CoQ10 suspension (75 mg/Kg) after 15 min. The co-loaded nanoparticles (30% CsA and 70% CoQ10 loading) were administered at 30 mg/Kg of CsA which corresponds to 75 mg/Kg of CoQ10. All values represented as mean±S.E.M. (n=3).

Table 4.5 Effect of co-administration of CoQ10 on pharmacokinetic parameters of CsA

Groups	CsA (mg/Kg)	CoQ10 (mg/Kg)	AUC_{0-72} (ng.h/ml)	C_{max} (ng/ml)	T_{max} (h)
Neoral®	15	-	29046±1437	1328±120	2
Neoral®+CoQ10	15	75	30994±2449	1229±72	2
CsA NPs	30	-	51763±3812	1101±143	12
Co-entrapped NPs	30	75	50763±1411	1062±44	12

All values represented as mean±S.E.M. (n=3).

Table 4.6 Effect of CoQ10 co-administration on tissue concentration of CsA

Tissue	μg/g of tissue			
	Neoral®	Neoral®+CoQ10	CsA NPs	Co-entrapped NPs
Brain	3.4±0.7	2.6±0.7	2.8±1.0	2.4±0.9
Heart	5.0±0.8	5.7±0.9	8.1±2	11.3±2.2
Lung	5.3±0.7	6.3±1.4	11.3±1.8	10.2±1.1
Kidney	9.9±1.6	10.7±1.3	20.3±2.8	17.1±1.4
Spleen	6.9±1.8	8.2±1.4	14.9±1.6	15.4±1.1
Liver	10.7±1.3	13.1±1.1	15.5±1.1	17.1±1.4
Intestine	6.8±0.8	6.3±0.4	7.7±2.4	10.8±1.2

Neoral® (15 mg/Kg) was administered first followed by CoQ10 suspension (75 mg/Kg) after 15 min. The co-entrapped nanoparticles (30% CsA and 70% CoQ10 loading) were administered at 30 mg/Kg of CsA which corresponds to 75 mg/Kg of CoQ10. All values represented as mean±S.E.M. (n=3).

4.3.5 Chronic nephrotoxicity study

The data presented in Chapter 3 of this thesis clearly indicates the potential of nanoparticulate approach in minimising the drug associated toxicity with further scope for improvements. Attempts were made to co-entrap an antioxidant along with CsA in the nanoparticles anticipating positive benefits.

Co-administration of CoQ10 along with Neoral® or as co-entrapped in PLGA nanoparticles had no effect on CsA mediated nephrotoxicity. BUN, PC and glomerular damage index for Neoral® co-administered with CoQ10 were 34.48±1.76 mg/dL, 2.11±0.12 mg/dL and 0.7701±0.0156 while for co-entrapped nanoparticles they were 28.72±1.29 mg/dL, 1.18±0.12 mg/dL and 0.7838±0.006, respectively. Figure 4.11 represents percent change in nephrotoxicity of Neoral® co-administered with CoQ10 suspension and co-entrapped particles in comparison to simple Neoral® and CsA nanoparticles respectively. The BUN, PC and glomerular damage index were similar to simple Neoral® and CsA nanoparticles groups as reported in chapter 3, CoQ10 did not offer any benefits in reducing the toxic effects of CsA.

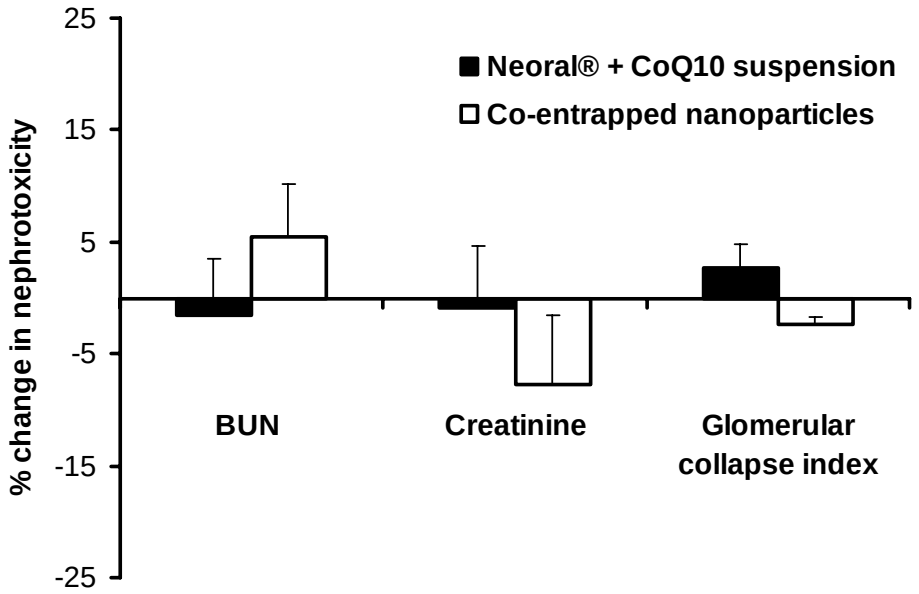

Figure 4.11 Percent change in nephrotoxicity of Neoral® co-administered with CoQ10 suspension and co-entrapped nanoparticles in comparison to simple Neoral® and CsA nanoparticles, respectively. From observed values, co-administration of CoQ10 as suspension or as co-entrapped in PLGA nanoparticles was not able to reduce CsA mediated toxicity. All values represented are mean±S.E.M. (n=6).

Plasma (Figure 4.12) and tissue (Figure 4.13) levels of CsA were determined during 30 day chronic nephrotoxicity study. They were similar to those obtained with simple Neoral® and CsA nanoparticles as shown in chapter 3; further signifying that biodistribution pattern of CsA was unaffected by co-administration of CoQ10. The plasma CoQ10 levels were higher for nanoparticles group to that observed for suspension group, nevertheless offered no benefit (Figure 4.14).

In the literature various attempts have been made to reduce CsA associated nephrotoxicity by antioxidant therapy. Hydroxytyrosol, an antioxidant found in olive oil was investigated for attenuation of CsA toxicity. On i.p. administration at 20 mg/Kg, hydroxytyrosol prevented CsA mediated oxidative stress with partial reversal of structural changes (Capasso *et al*., 2008). Similarly several antioxidants like ellagic acid and EGCG have been found to prevent CsA mediated nephrotoxicity (Sonaje *et al*., 2007; Italia *et al*., 2008). However, CoQ10 administration was not able to prevent CsA mediated nephrotoxicity.

Treatment with CsA in the form of Neoral® is associated with nephrotoxicity and by nanoparticulate approach the CsA associated nephrotoxicity was reduced significantly however, the nanoparticulate formulation was not able to eliminate the nephrotoxicity entirely (Chapter 3) and possibility of developing a completely nephrotoxicity free formulation existed. Considering the fact that antioxidant supplementation was found to completely reverse the nephrotoxic effects of CsA in the chronic rat model (Sonaje *et al*., 2007, Italia *et al*., 2008) we thought about engineering co-entrapped antioxidant-CsA nanoparticles to leverage the benefits of the combination. We hypothesized that co-entrapped CsA-CoQ10 nanoparticles will have multi-faceted advantages. The nanoparticles will improve the oral

bioavailability of CsA and CoQ10, the co-entrapped CoQ10 will significantly lower/eradicate CsA mediated nephropathy and finally the cremophor® EL free formulations would allow exploitation of CsA's complete potential in treatment of diseases like arthritis where CoQ10 would also provide synergistic effects. Therefore, the primary goal was to develop a co-entrapped product that can load both CsA and CoQ10 simultaneously leading to improved oral bioavailability followed by pharmacokinetic and nephrotoxicity studies in rats demonstrating the improved product profile. Using PLGA as polymer matrix and DMAB as stabiliser, CsA-CoQ10 co-loaded nanoparticles were optimised for surfactant concentration, external phase volume, size reduction method and drug loading. The prepared nanoparticles were able to load different dose range of CsA and CoQ10, demonstrating the potential of PLGA matrix in co-entrapping two high molecular weight hydrophobic compounds (Ankola *et al*., 2010). On *in vitro* release, CsA was released at a slower rate in co-entrapped nanoparticles than simple CsA loaded nanoparticles due to increase in the lipophilicity of the PLGA matrix due to the presence of CoQ10. However, CoQ10 was released very slowly, irrespective of the formulation type. The slow release of CoQ10 than CsA could be due its high lipophilicity, making it difficult to partition in aqueous medium based on the logP value of CoQ10 which is 9.9 and is very high compared to CsA with logP of 2.92 and was further supported by the computer stimulation of release profiles (Ankola *et al*., 2010). On nephrotoxic evaluation of co-entrapped nanoparticles, CoQ10 was not able to demonstrate any reduction in nephrotoxicity. The failure of CoQ10 in preventing against CsA mediated nephrotoxicity could be due to several reasons. Of them, the inability of CoQ10 to act against the CsA mediated free radicals could be an important reason and requires further investigations.

However, CoQ10 was found to prevent cisplatin (Sayed-Ahmed *et al*., 1999) and gentamicin (Upanganlawar *et al*., 2006) induced free radical damage. The CoQ10 dose administered to prevent cisplatin and gentamicin induced toxicity were 10 mg/Kg i.p. and 125 mg/Kg orally, respectively. In our present investigation we used a dose of 75 mg/Kg which is significantly lower than that used for prevention of cisplatin induced nephrotoxicity and may have resulted in lower plasma CoQ10 concentrations than those achieved by 10 mg/Kg i.p. dose. 75 mg/Kg of CoQ10 was used in our study as loading of CoQ10 beyond that was not possible in presence of CsA. Considering the above facts, low dose of CoQ10 could have resulted in failure of the therapy. Additionally, administration of CoQ10 in suspension form and as nanoparticulate formulation would have resulted in low oral bioavailability. The suspension form would have demonstrated low oral bioavailability due to the inherent low solubility and permeability of CoQ10 (Chopra *et al*., 1998), while administrating CoQ10 in nanoparticles would have resulted in lower plasma levels due to elimination of PLGA nanoparticles from the body by macrophages before complete release of CoQ10 from the nanoparticles (Moghimi *et al*., 2001). However, several studies have demonstrated an increase in CoQ10 efficacy when entrapped in DMAB stabilised PLGA nanoparticles (Ankola *et al*., 2009; Ratnam *et al*., 2009). CoQ10 loaded PLGA nanoparticles were efficacious than the conventional suspension form and commercial liposomal formulation (Liq-Q-Sorb®) in treatment of hypertension (Ankola *et al*., 2009). Similarly, CoQ10 loaded PLGA nanoparticles were more potent that suspension form in treatment of hyperlipidemia (Ratnam *et al*., 2009) and diabetes (Ratnam *et al*., 2008) in rats.

In spite of the lack of beneficial effect of CoQ10 in reducing CsA mediated nephrotoxicity, the co-entrapped nanoparticles may represent a potent formulation in treatment of arthritis, where CoQ10 has been demonstrated to be effective in preventing the free radical mediated pathophysiology of the disease (Bauerova *et al*., 2005), leading to synergistic effects with CsA. On the other hand, administration of CsA to patients results in hypertension (Taler *et al*., 1999) which can be prevented by CoQ10 loaded in PLGA nanoparticles (Ankola *et al*., 2009). Additionally, renal transplant patients suffer from hyperlipidemia (Tse *et al*., 2004) and CoQ10's potential in preventing hyperlipidemia (Ratnam *et al*., 2009) can be exploited in such patients.

4.4 Conclusions

The current investigation demonstrates a successful development of co-entrapped nanoparticulate formulation of two high molecular weight molecules CsA and CoQ10. Several parameters like surfactant concentration, external phase volume, droplet size reduction method and drug loading governed the nanoparticles characteristics. Presence of CoQ10 in the system affected the entrapment and *in vitro* release behavior of CsA. However, co-entrapped CoQ10 was not able to ameliorate CsA mediated nephrotoxicity.

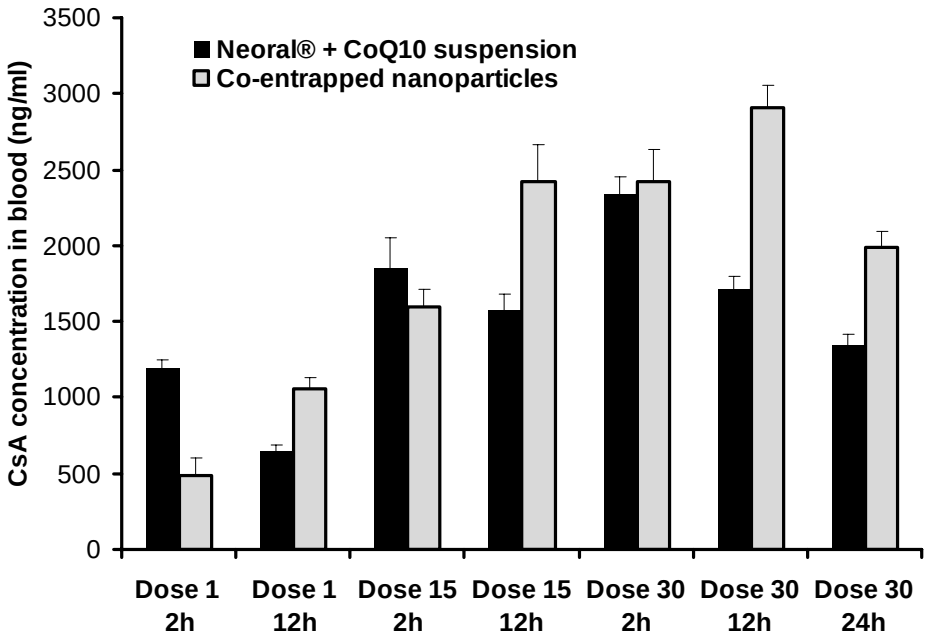

Figure 4.12 Blood CsA levels on co-administration of CoQ10 during the chronic nephrotoxicity study. All values represented are mean±S.E.M. (n=3).

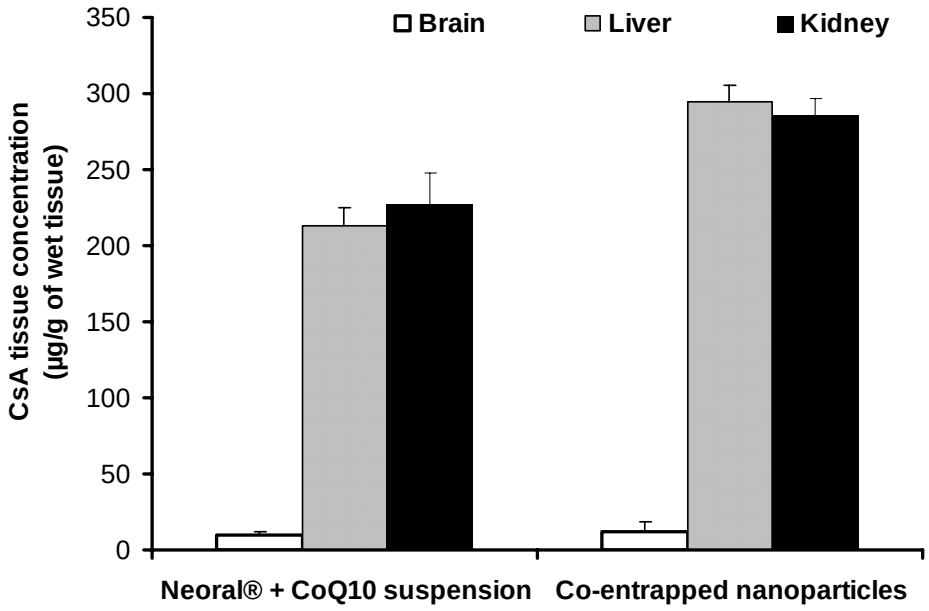

Figure 4.13 CsA levels in brain, liver and kidney observed after 30 days on administration of Neoral® and co-entrapped nanoparticles. All values represented are mean±S.E.M. (n=3).

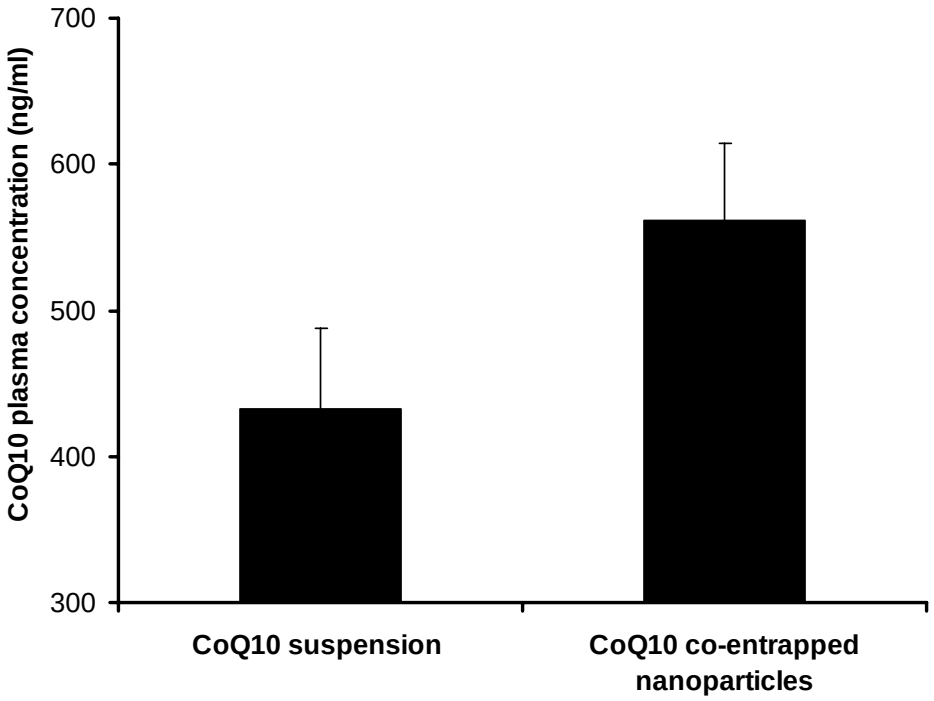

Figure 4.14 Plasma CoQ10 concentrations after 30 days chronic nephrotoxicity study. CoQ10 suspension (75 mg/Kg) was administered after 15 min of Neoral®. The co-entrapped nanoparticles (30% CsA and 70% CoQ10 loading) were administered equivalent 75 mg/Kg CoQ10. All values represented as mean±S.E.M. (n=3).

5. ROLE OF POLYMER ARCHITECTURE ON CICLOSPORIN RELEASE

5.1 Introduction

In recent years, the synthesis of new biodegradable polymers to fulfill unmet needs in healthcare has attained significant interest. Several families of polymers like polyesters, polyurethanes, polyanhydrides, polyamides, poly(amino acids) and polyorthoesters have found interesting applications in catering of medical needs (Schwendeman *et al*., 1997; Middleton and Tipton, 2001; Kim *et al*., 2009). Over the years the focus has shifted towards designing and synthesising biodegradable polymers with tailored properties for specific applications by several approaches which includes developing novel synthetic polymers with unique chemistries to increase the diversity of polymer structure and versatility, designing stimuli sensitive polymer structures and adopting combinatorial and computational approaches in biomaterial design (Nair and Laurencin, 2007; Bajpai *et al*., 2008).

Polymers have found wide applications in drug delivery due to their ability to control and sustain drug release, which has provided an opportunity for improving the potential and reliability of drugs. Among various biodegradable polymers, polyester family which includes PLA, PGA and their copolymer PLGA have been widely explored (Anderson and Shive 1997; Bala *et al*., 2004; Mohamed and Van der Walle, 2008). Over the years many investigations have attempted to functionalise the polyesters to improve their flexibility in terms of entrapping different molecules to modify release. The pegylated polyesters have attracted great deal of attention for their stealth properties as well as their use for loading more hydrophilic drugs (Gref *et al*., 1994; Verrechia *et al*., 1995; Ruan and Feng, 2003; Cerbai *et al*., 2008).

From the foregoing discussion it is clear that PLGA nanoparticles were successful in reducing the nephrotoxicity associated with CsA (Chapter 3) even at 2 times higher dose, required to achieve a C_{max} similar to commercial formulation Neoral®. The C_{max} of any drug from PLGA nanoparticles can be a function of hydrophobicity/molecular weight/copolymer composition of the polymer (Mittal *et al*., 2007). Therefore, we attempted to synthesise a versatile polymer architecture that is more hydrophilic than native PLGA, as well as offer possibility to functionalise and match Neoral®'s C_{max} at a similar or lower dose, as a first step towards meeting clinical requirements.

Many investigators have also tried to enhance the applicability of polyesters by incorporating functional groups into polymer backbone. Many different copolymers of polyesters with different pendant reactive moieties such as carboxyl (Barrera *et al*., 1993; Gimenez *et al*., 2001; Cerbai *et al*., 2008) and amino (Zhao *et al*., 2005) groups have been synthesised. Carboxylated polymers have provided several advantages in designing delivery systems due to versatile nature of carboxyl (COOH) groups. The COOH groups have been explored for various applications from enhancing protein entrapment in nanoparticulate system (Blanco and Alonso, 1997) to utilising its reactivity for polymer drug conjugation (Khandare and Minko, 2006). Recently, a carboxyl–functionalised PLGA–*b*–PEG copolymer was synthesised by direct conjugation of PLGA–COOH with NH_2–PEG–COOH to generate PLGA–*b*–PEG–COOH. Nanoparticles prepared using the above functionalised polymer were conjugated to the A10 RNA aptamer (Apt) that binds to the prostate specific membrane antigen (PSMA). The surface modification with the A10 PSMA Apt significantly enhanced delivery of nanoparticles to tumors (Chenga *et al*., 2007). The negatively ionisable carboxyl functional group has also found to be potential in increasing the calcification properties

of biomaterials (Miyazaki *et al*., 2003). In addition to the functional benefits of COOH, it also aids in faster polymer degradation. The free COOH groups have been found to hasten the hydrolytic degradation rates of polyesters (Tracy *et al*., 1999; Lee *et al*., 2001; Yu and Zhuo, 2003), hence facilitate in faster drug release, in the present case CsA, to achieve desired blood concentrations.

In spite of several advantages of carboxylated polymers, mostly the modifications have been confined to end groups in polymer chain, and not much is known on the introduction of side chain carboxyl groups. Therefore, the present investigation was aimed at the synthesis, characterisation and nanoparticulate application of carboxylated $(ABA)_n$ type multiblock copolymers of PLA and PEG for CsA delivery. These new materials are anticipated to have combination of biodegradability, anti-opsonising and bioadhesive properties. Figure 5.1 represents the architecture of proposed polymer.

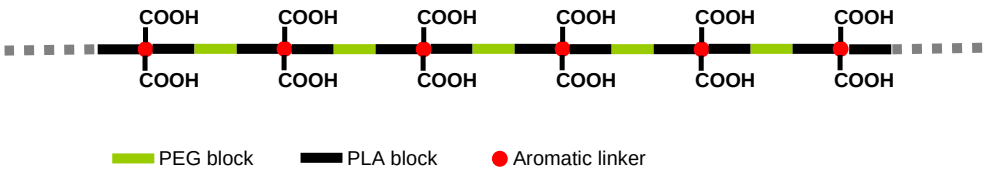

Figure 5.1 Schematic representation of the polymer with side chain carboxylic groups

5.2 Materials and methods

5.2.1 Materials

Toluene (Carlo Erba) was refluxed for 8 h over Na–K alloy under dry nitrogen atmosphere and then distilled, collecting the fraction having b. p. 110 °C. Triethylamine (TEA) (Aldrich) was refluxed for 4 h over CaH_2 under dry nitrogen atmosphere and then distilled collecting the fraction having b. p. 89–90 °C. All other solvents were used as received. Stannous (II) octoate ($SnOct_2$, Aldrich) was used as received. PEG 400 and PEG 1000 (Aldrich) were dried by azeotropic distillation with anhydrous toluene under dry nitrogen atmosphere and used immediately. L–Lactide and D,L–lactide were purchased from Aldrich and used as received.

5.2.2 Prepolymer synthesis

Lactide–ethylene glycol–lactide, triblock copolymers were prepared by ring opening polymerisation. Four different prepolymers were synthesised by varying the lactide content and PEG and data relevant to their composition are reported in Table 5.1 whereas synthesis of pL14 is described in detail as follows. A solution of L–lactide (10 g, 70 mmol), dried PEG 400 (2.0 g, 5.0 mmol) and 0.1% (w/w) stannous octoate (10 ml, 30 mmol) in 20 ml of dry toluene was heated at reflux for 24 h under dry nitrogen atmosphere. A small sample (0.25 ml) was withdrawn from the reaction mixture, dried under vacuum and characterised by nuclear magnetic resonance (NMR) and size exclusion chromatography (SEC). NMR analysis indicated that lactide conversion was 98%. The polymer solution was directly used for chain extension.

5.2.3 Chain extension

Chain extension of lactide–ethylene glycol–lactide triblock copolymers was performed using pyromellitic dianhydride (PMDA). Data relevant to the different experiments are reported in Table 5.2 whereas synthesis of EL14 is described in detail as follows. TEA (1.4 ml, 10 mmol) and PMDA (1.1 g, 5.0 mmol; 1:2:1 copolymer:amine:dianhydride molar ratio) were introduced into the flask containing the pL14 polymer solution under dry nitrogen atmosphere. The mixture was heated at 110 °C for 1 h under stirring, and then toluene was removed under vacuum. The dried polymer was dissolved in dichloromethane, washed with cold 0.5 N HCl and water and then precipitated from dichloromethane solution into diethyl ether. The precipitate was collected by filtration and dried under vacuum to yield 10.8 g (82%) of colorless polymeric product. The polymer was further purified by precipitation from acetone in 5% $NaHCO_3$, washing with water and dried under vacuum.

5.2.4 Size exclusion chromatography

SEC analyses were carried out in chloroform by using a Jasco PU–1580 HPLC pump equipped with two 300 x 7.5 mm PL Mixed–D columns and Jasco 830–RI refractive index detector. Monodispersed polystyrene (Polysciences Inc.) samples were used as calibration standards.

5.2.5 Proton nuclear magnetic resonance analysis

^{1}H-NMR spectra were recorded on 5-10% sample solution at room temperature in $CDCl_3$ (Deuterated chloroform, Sigma) using a Varian Gemini 200 spectrometer and tetramethylsilane (TMS) as internal standard.

5.2.6 Thermal analysis

5.2.6.1 Thermo-gravimetric analysis

Thermo-gravimetric analysis (TGA) analyses were performed under nitrogen atmosphere in the 25–600 ^{0}C range at 10 ^{0}C/min scanning rate on 10–20 mg polymer samples by a Mettler TG 50 instrument. Onset decomposition temperatures (Td) were evaluated at 5% weight loss.

5.2.6.2 Differential scanning calorimetry

Differential scanning calorimetry (DSC) analyses were performed on 8-12 mg samples at 10 ^{0}C/min scanning rate using a Mettler DSC 30. Glass transition temperatures were measured at the inflection point of the thermograms relevant to the second heating cycle. In order to promote crystallisation, samples were either annealed at 85 °C for 2.5 h or cooled down from 160 °C at –0.2 °C/min. Indium and gallium were used as calibration standards.

5.2.7 Polarised optical microscopy

Polarised optical microscopy (POM) analyses were performed by a Reichert–Jung Polivar microscope equipped with polarisers, digital camera, Mettler FP52 hot plate and Mettler FP5 temperature controller. Polymer films cast from 10% dichloromethane solution were heated to 160 ^{o}C and then cooled at -0.2 ^{o}C/ min to room temperature and then observed under polarised light.

5.2.8 *In vitro* degradation

The *in vitro* degradation behavior of polymers was studied in phosphate buffers saline (PBS), pH 7.4 at 37 °C (D'Souza and DeLuca, 2006). 150 mg of polymer powder was dispersed in 10 ml of PBS into test tubes that were vortexed for 20 min. At fixed time intervals the test tubes were vortexed for

10 min, 200 µl of samples were withdrawn, vacuum dried and analysed by SEC.

5.2.9 Preparation of blank nanoparticles and pH titration

The polymer (25 mg) was dissolved in 5 ml of acetone by stirring at 1000 rpm for 30 min. The resulting solution was then added drop wise by a syringe to 20 ml of water under magnetic stirring at 1000 rpm. The preparation was left under stirring at 1000 rpm for 6 h leading to complete evaporation of acetone. The particle size, size distribution and zeta potential were measured on all preparations.

The effect of pH on size and zeta potential of blank nanoparticles was studied. The pH of nanoparticle suspension (5 ml) was adjusted to 1 by addition of 1 N HCl and the suspension was titrated to pH 7.5 with 0.1 N NaOH. The zeta potential was measured at 1±0.5 pH increments at 25 °C.

5.2.10 CsA loaded nanoparticles

Emulsion-diffusion-evaporation technique was used to prepare CsA loaded EL14 nanoparticles as described in section 3.2.2. The effect of drug loading on particle characteristics was studied at 10, 20 and 30 %w/w of polymer load and compared with CsA loaded PLGA nanoparticles.

The particle size and zeta potential measurements were carried out as described in section 3.2.2.1 and the entrapment efficiency was determined as described in section 3.2.2.2.

5.2.11 *In vitro* drug release studies

The *in vitro* release study was performed as described in section 4.2.4. The release of CsA from the EL14 nanoparticles with 20% drug payload was compared with that of native PLGA nanoparticles.

5.2.12 Pharmacokinetic and tissue distribution studies

The pharmacokinetics and tissue distribution studies were carried out as described in section 3.2.3. EL14 nanoparticles with 20% drug payload were used in the study and compared to that of PLGA and Neoral®.

5.3 Results and discussion

5.3.1 Prepolymer synthesis

Linear ABA triblocks copolymers (also referred to as pre–polymers in the following sections) were easily prepared by reaction of lactide with PEG diol in the presence of stannous octoate ($SnOct_2$) as catalyst (Table 5.1). This catalyst was chosen because of its high efficiency in promoting the ring opening polymerisation of lactide, and its approval for biomedical applications by FDA due to its low toxicity (Wong and Mooney, 1997). Pre–polymer samples are named "p" followed by L or DL according to the starting lactide configuration and by two digits indicating the molecular weight of PLA and PEG segments, respectively (4, 5 and 1 correspond to 400, 500 and 1000 Da) based on their theoretical compositions computed from the feed mixtures. Four different pre–polymers were synthesised by varying PLA and PEG chain lengths and by using D,L–lactide and L–lactide. The average molecular weight of triblocks copolymers determined by both SEC analysis and NMR characterisation generally resulted slightly higher than that computed from the composition of the feed mixture. Very likely, this

finding must be attributed to experimental errors. In all cases, the polydispersity index (PDI = M_w/M_n) was in the 1.2–1.3 range.

5.3.2 Chain extension

A few studies have been carried out to convert hydroxyl–terminated triblock copolymers into multiblock copolymers by reaction with diisocyanates and dichlorophosphates (Mao *et al*., 1999; Signori *et al*., 2004). However, these techniques do not provide side–chain functional groups. On the other hand, the molecular weight of recycled poly(ethylene terephthalate) can be extended by reaction with pyromellitic dianhydride (Awaja *et al*., 2004). By following a similar approach, $(ABA)_n$ polymers containing periodically spaced side–chain carboxyl groups were obtained by chain extension of ABA pre–polymers with PMDA in the presence of TEA as catalyst (Figure 5.2). Extended polymer samples are named by replacing the "p" prefix of the corresponding pre–polymers with "E". Preliminary experiments indicated that only a limited increase of the molecular weight was achieved in the presence of either TEA (Run E54T) or $SnOct_2$ (Run E54S), whereas a synergic effect was observed when both TEA and $SnOCt_2$ were present in the reaction mixture (Table 5.2). The dependence of the extent of chain extension on both catalysts can be explained by assuming that lactide polymerisation gives the tin alkoxide of the triblock copolymer. Ring opening of the anhydride then occurs via coordination of the polymeric alkoxide to one of the anhydride carbonyl groups followed by the ring opening. TEA could help by activating the anhydride bonds and/or by removing the octanoic acid formed by reaction of $SnOct_2$ with moisture present in reagents. On an average, the molecular weight of the final polymers was about 6–7 times that of the corresponding pre–polymer. From the adopted pre–polymer/PMDA molar

ratio, one could expect much larger polymer molecular weight. On the other hand, errors made in determining the actual pre–polymer content and composition in the reaction mixture can easily lead to pre–polymer/anhydride ratios different from unity and hence in reduced chain extension.

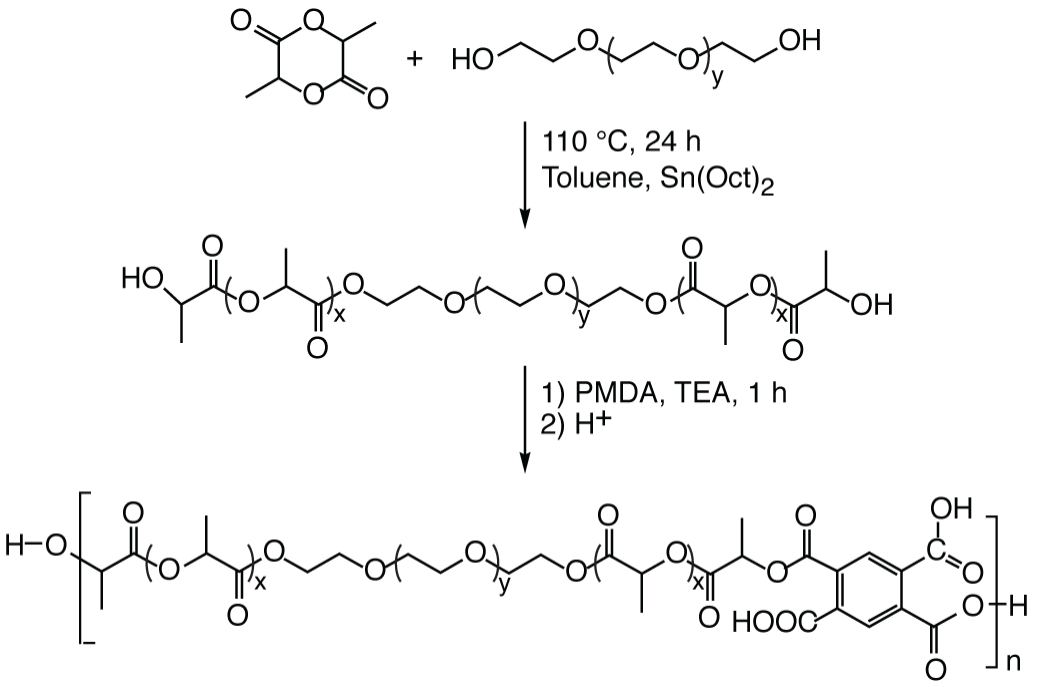

Figure 5.2 Synthetic procedure adopted for the preparation of multiblock copolymers of PLA and PEG containing periodic side–chain carboxyl groups.

Table 5.1 Preparation of ABA–type PLA–PEG–PLA block copolymers

	PEG diol		Lactide		Conversion	Polymer			
Run[a]	M_n	(mmol)	Type	(mmol)	(%)	M_n[b]	M_n[c]	M_n[d]	PDI[d]
pDL54	400	10	D,L	70	>98	1400	1430	1150	1.24
pL54	400	10	L	70	>98	1400	1470	1220	1.30
PL51	1000	10	L	70	>98	2000	2100	1900	1.23
pL14	400	10	L	140	>98	2400	2990	3210	1.21

[a]In the presence of 0.1% (w/w) of $SnOct_2$, for 24 h at reflux. [b] Computed from the feed composition. [c]by NMR. [d]by SEC.

Table 5.2 Preparation of carboxylated chain–extended $(ABA)_n$ polymers by reaction of pre–polymers with PMDA in the presence of TEA and/or $SnOct_2$

	Pre–polymer			Polymer			
Run[a]	Sample	M_n[b]	PDI[b]	Catalyst	Yield (%)	M_n[b]	PDI[b]
E54T	pDL54	1150	1.24	TEA	47	4900	2.32
E54S	pDL54	1150	1.24	$SnOct_2$	36	1900	1.84
EDL54	pDL54	1150	1.24	TEA/$SnOct_2$	71	8700	2.02
EL54	pL54	1220	1.30	TEA/$SnOct_2$	76	7500	2.16
EL51	pL51	1900	1.23	TEA/$SnOct_2$	67	12800	3.21
EL14	pL14	3210	1.21	TEA/$SnOct_2$	82	16300	3.01

[a] At 110 °C for 1 h; polymer/PMDA molar ratio = 1; TEA/PMDA molar ratio = 2; $SnOct_2$ 0.1% (w/w). [b]by SEC.

5.3.3 Proton nuclear magnetic resonance analysis

The ^{1}H–NMR spectra of polymers presented peaks at 1.44 and 5.18 ppm attributable to PLA methyl and methyne protons and at 3.48 ppm due to PEG methylenes. The signal at 3.3 was assigned to water moisture in the deuterated solvent. The peaks at 3.58 and 4.18 ppm were attributed to PEG methylenes linked to hydroxyl end groups and to PLA units (junctions), respectively. In addition to these signals, the ^{1}H–NMR spectra of chain extended polymers presented one peak at 5.35 due to PLA methynes esterified by PMDA (Figure 5.3). Three further small peaks were detected at 7.9, 8.0 and 8.1 ppm, attributable to aromatic protons of pyromellitic diesters. In particular, the peak at 8.0 ppm was assigned to the more symmetric *transoid* isomer whereas signals at 7.9 and 8.1 ppm were assigned to the *cisoid* isomer that contains two non–equivalent aromatic protons H and H' (Figure 5.4). In agreement, the three peaks moved at 8.02, 7.62 and 7.17 ppm when the polymer samples were neutralised with $NaHCO_3$ because of the inductive effect of negatively charged carboxylate groups. Chemical shift evaluation by additive group contributions confirmed the above assignments. Within the limits of experimental errors, the three aromatic proton peaks have 1:2:1 relative intensities, thus suggesting that there is no significant preference for the formation of the *transoid* isomer with respect to the more crowded *cisoid* one. The integrated intensity of the different signals allowed for determining the polymer composition. In all cases, the PMDA/pre–polymer molar ratio resulted close to 0.95. In agreement with SEC analysis, these data indicates that most but not all polymer chains are terminated by one pyromellitic residue. Accordingly, each extended polymer chain contained about 6–7 PMDA molecules, that is, 14–16 free carboxylic groups.

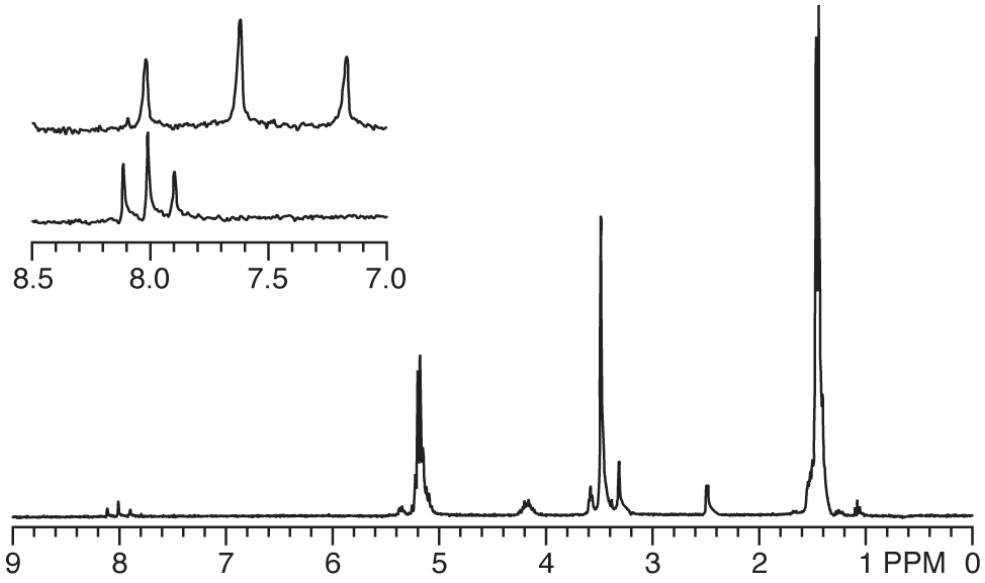

Figure 5.3 ^{1}H NMR spectrum of EL14 polymer sample. The inset presents the aromatic proton region of the polymer after precipitation in 0.5 N HCl (bottom) and in 5% $NaHCO_3$ (top).

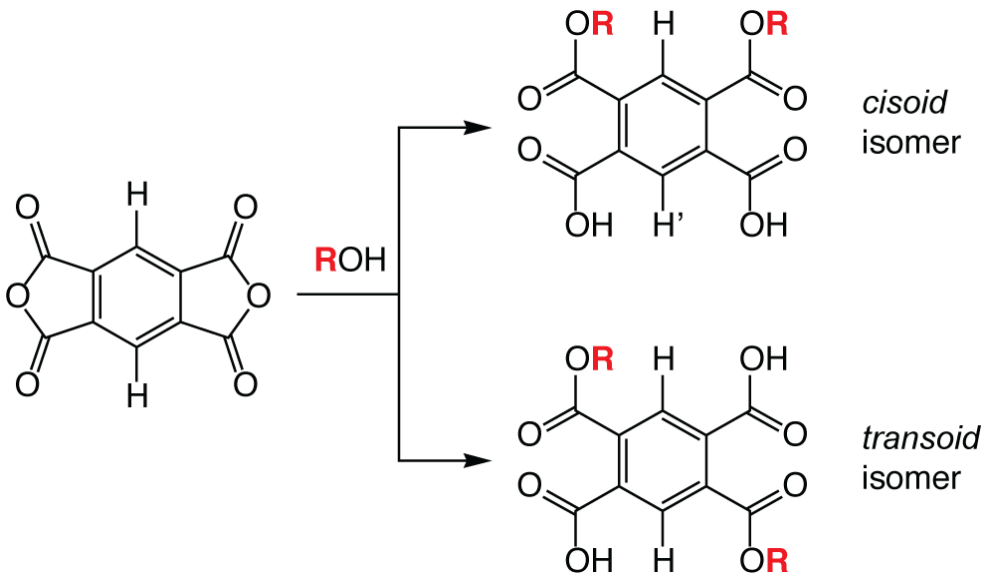

Figure 5.4 Schematic representation of polymer chain extension by reaction of the pre–polymer with PMDA.

5.3.4 Thermal analysis

All polymers and pre–polymers were characterised by TGA and DSC. TGA curves highlighted the occurrence of two decomposition steps. The temperatures at the onset (T_{on}), at the inflection points of the first and second decomposition step (T_{d1} and T_{d2}), the corresponding weight losses (Δw_1 and Δw_2), and the weight residue at 600 °C (WR_{600}) are summarised in Table 5.3. The pre–polymers were found to be appreciably less heat stable than the final polymers. T_{on}, T_{d1} and T_{d2} of the extended polymers were about 100, 50 and 10 °C higher than those of the corresponding pre–polymers, repectively. The weight losses observed for the two decomposition steps closely correspond to the polymer weight content of lactic acid and ethylene glycol units. Moreover, T_{d1} and T_{d2} are in the same range as the decomposition temperatures of PLA and PEG, respectively (D'Antone *et al*., 2001). Accordingly, these two steps can be attributed mainly to the degradation of PLA and PEG blocks. No decomposition step clearly attributable to the thermal degradation of pyromellitic units was detected very likely because of their rather low content in the polymer and/or peak overlap (T_{dPMDA} = 329 °C). In all cases, DSC analysis evidenced the presence of only one glass transition in the temperature range between –100 and 160 °C (Figure 5.5, curve a). On increasing the PLA weight content from 50 to 83%, the Tg of pre–polymers and polymers increased from –34.6 to 16.2 °C and from -9.2 to 43.7 °C, respectively (Table 5.3), in agreement with the larger stiffness and higher Tg (59.1 °C) of PLA blocks (Pan *et al*. 2008).

As indicated, the Tg of the extended polymers was about 30–50 °C higher than that of the corresponding pre–polymers because of both the increased molecular weight and the stiffness of the aromatic chain extender. As expected, both the polymer (EDL54) and pre–polymer (pDL54) containing

racemic PLA blocks did not present any first order transition attributable to polymer crystallisation or melting. The DSC of all other polymer samples also did not display transitions due to polymer crystallisation or melting, in spite of the presence of stereoregular L–lactic acid sequences. Such behavior might be attributed to poly(L–lactic acid) (PLLA) block length that is too short and/or to the crystallisation rate that is too low to allow for the formation of a crystalline phase under the adopted experimental conditions, because of some sort of confinement at the nanometer scale (Delpouve *et al.*, 2008).

To support this hypothesis, the sample EL14 containing the longest stereoregular PLLA blocks and the shortest PEG sequences was heated at 160 °C on a hot stage optical microscope and then cooled down at room temperature at 0.2 °C/min. Optical observation of the sample under cross–polarisers clearly highlighted the presence of typical concentric fringed spherulites (Figure 5.6a). Atomic force microscopy (Figure 5.6b) showed the presence of overlapping spherulites of about 25 μm in diameter and 1700 nm in height.

Table 5.3 Thermal analysis of the investigated pre–polymers and polymers

		DSC		TGA[a]					
Polymer	PLA block (wt–%)	T_g (°C)	ΔC_p (J/g K)	T_{on} (°C)	T_{d1} (°C)	Δw_1 (%)	T_{d2} (°C)	Δw_2 (%)	WR_{600} (%)
pDL54	71	–21.1	0.55	169	303	71	395	28	1
EDL54	71	26.1	0.42	281	347	69	408	28	3
pL54	71	–10.8	0.48	193	295	70	394	28	2
EL54	71	27.2	0.47	279	341	69	410	28	3
pL14	83	16.2	0.28	232	296	80	357	18	2
EL14	83	43.7	0.47	287	344	82	407	16	2
pL51	50	–34.6	0.99	200	296	52	420	44	4
EL51	50	–9.2	0.61	294	340	48	418	49	3

[a] T_{on} is the onset decomposition temperature, evaluated as 5% weight loss; T_{d1} and T_{d2} are the temperatures at the inflection point of the first and second decomposition steps; Δw_1 and Δw_2 are the weight losses of the first and second decomposition steps; WR_{600} is the mass residue at 600 °C.

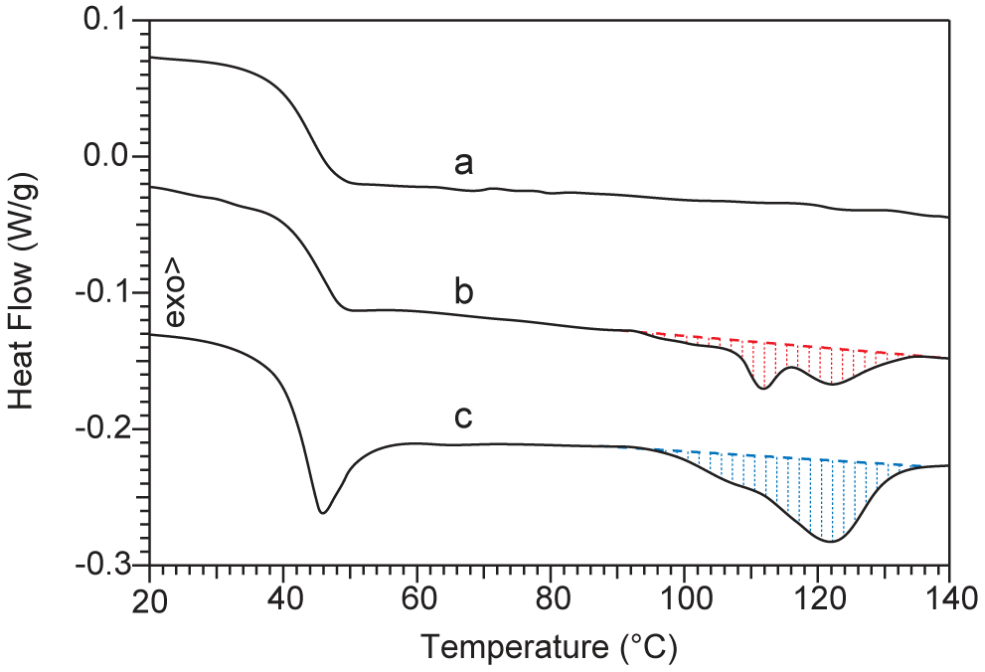

Figure 5.5 DSC thermograms of EL14 polymer sample: a) second heating scan; b) after annealing at 85 °C; c) after cooling from 160 to 25 °C at –0.2 °C/min.

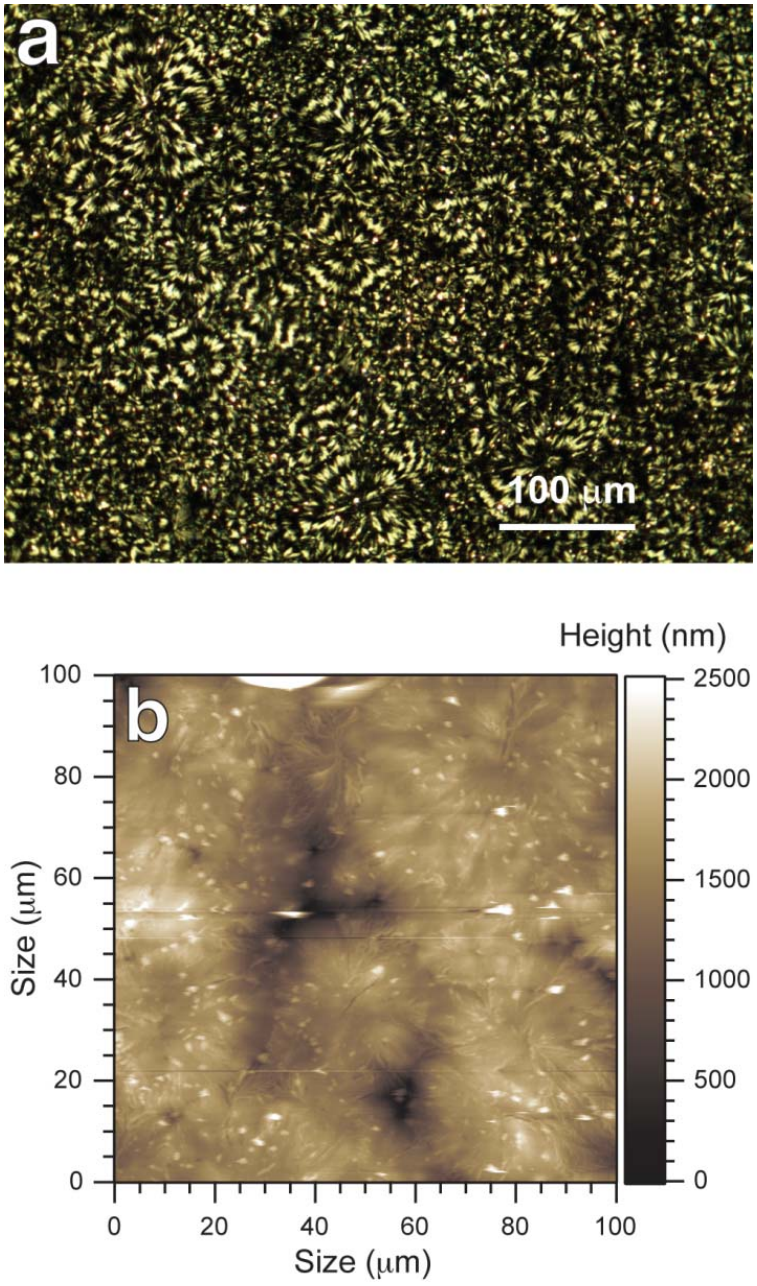

Figure 5.6 Polarised optical microscopy image (a) and AFM topography (b) of EL14 polymer sample cooled from 160 to 25 °C at 0.2 °C/min.

A similar pattern was also observed when a cold EL14 sample was annealed at 85 °C for 2.5 h. It has been reported that PLLA and PLLA segments form ring-banded spherulites in miscible blends and block copolymers. The formation of banded spherulites is attributed to the lamellar twisting along the radial growth direction (Xu *et al*., 2004). It seems therefore reasonable to conclude that the PEG chains are trapped into PLLA spherulites and disturb the regular orientation of crystalline PLLA lamellae.

DSC analysis of the annealed sample showed the occurrence of three overlapping broad melting peaks at 100, 112 and 122 °C with overall ΔH_m = 3.3 J/g (Figure 5.5, curve b). On the other hand, the slowly cooled sample presented a broad melting peak at 122 °C with a shoulder at about 110 °C having overall ΔH_m = 6.3 J/g (Figure 5.5, curve c). This result indicates that more regular crystals are formed when the crystallisation process occurs at higher temperature. In any case, the recorded ΔH_m values were about twenty and ten times lower than that of high molecular weight PLLA, whereas the observed melting temperatures are about 40–50 °C lower (Pan *et al*., 2009). We have to stress, however, that none of the other L–lactic acid polymers and pre–polymers displayed the presence of a crystalline phase, confirming that the formation of polymer crystals is controlled by both chain length and content of PLLA blocks.

5.3.5 *In vitro* degradation

The *in vitro* degradation of EDL54 and EL54 polymer samples containing D,L–lactic acid and L–lactic acid blocks, respectively was investigated in pH 7.4 PBS at 37 °C. The polymers were found to degrade rather quickly, the molecular weight of the PEG segment being reached within about 16 days of degradation (Figure 5.7). The degradation of EL54 and EDL54 followed first

order kinetics with rate constant k 5.4 x 10^{-6} and 7.6 x 10^{-6} s^{-1}, respectively. Unsurprisingly, both polymers have almost the same degradation rate, very likely because the stereoregular EL54 was in an amorphous state.

However, close inspection of SEC traces (Figure 5.8) shows that most of the molecular weight distributions are made by three overlapping peaks roughly corresponding to the molecular weights of the starting extended polymer, the corresponding pre–polymer and the PEG block.

Apparently, the polymer is initially split into ABA blocks because of the easy hydrolysis of pyromellitic ester bonds. Then, ABA blocks are further split into PLA and PEG segments, in accordance with the easier hydrolysis of the ester bond at PLA–PEG junctions as compared to intra chain PLA ester bonds (Hu and Liu, 1994). The hydrolytic degradation was modeled according to two coupled first order kinetics having rate constants k_1 and k_2 as sketched below:

$$A \xrightarrow{k_1} B \xrightarrow{k_2} C$$

To verify this hypothesis, each of the SEC curves was decomposed into three Gaussian components, whose relative area was plotted against time (Figure 5.9) and fitted according to the proposed model. In spite of experimental errors (estimated to be about 10%) and the oversimplified model, the fit is acceptable indicating that the polymer hydrolytic degradation mainly occurs according to the indicated two consecutive steps with similar rate constants k_1 and k_2 of about 2.9 x 10^{-6} and 2.7 x 10^{-6} s^{-1} for both EL54 and EDL54.

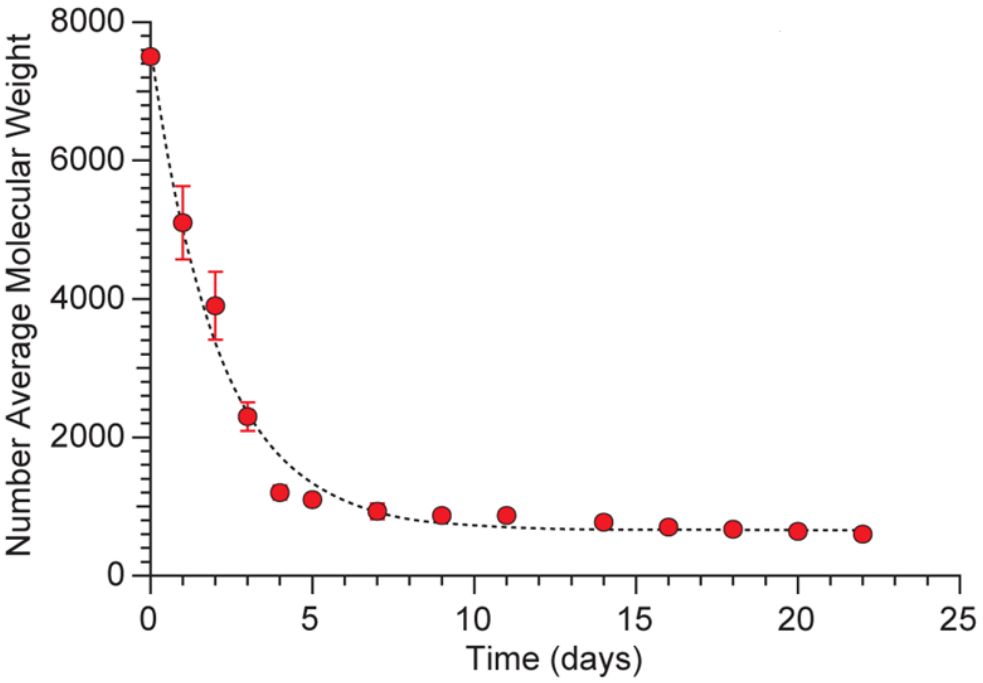

Figure 5.7 Plot of molecular weight vs. time observed during the *in vitro* degradation of EL54. The dashed line represents the best fitting exponential decay.

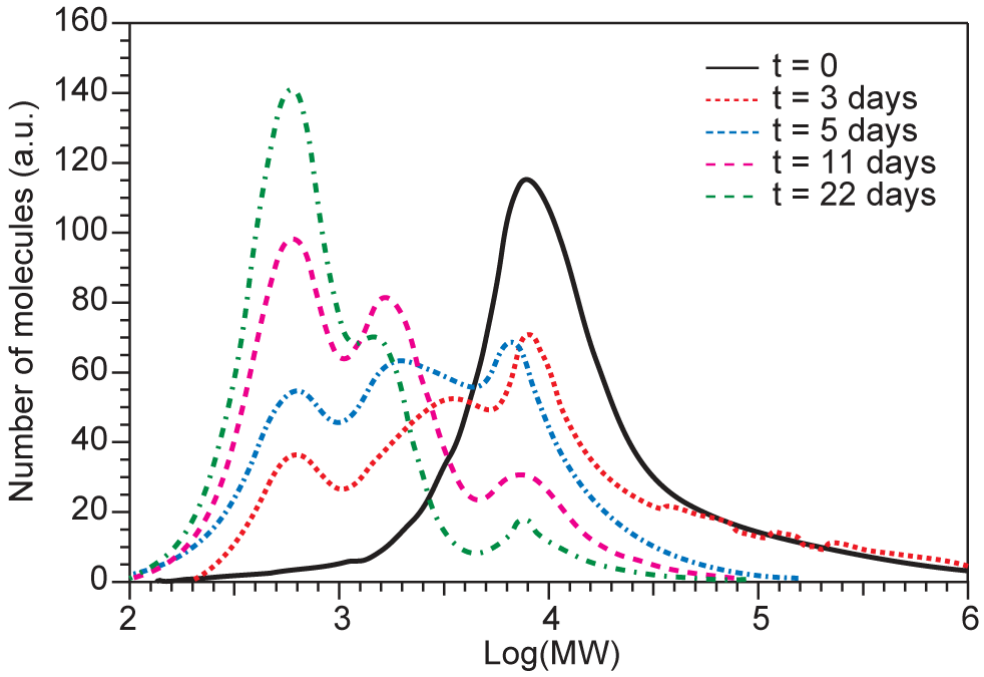

Figure 5.8 SEC traces recorded during the *in vitro* degradation of EL54.

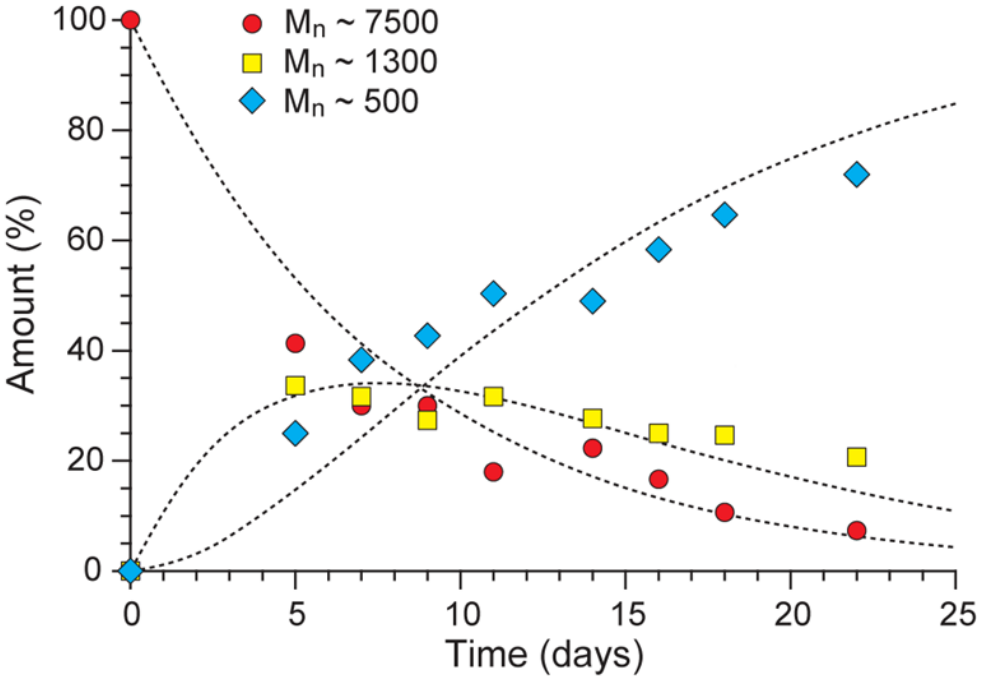

Figure 5.9 Kinetic plot of individual components of SEC curves recorded at different times during the *in vitro* degradation of EL54. A similar plot was also observed for EDL54**.**

5.3.6 Preparation of blank nanoparticles and pH titration

Nanoparticle suspensions were prepared by nanoprecipitation method (Fessi *et al*., 1989). The procedure (also known as solvent displacement method) is better suited for the preparation of nanoparticles loaded with proteic drugs because it does not imply the use of either stabilisers or denaturalizing chlorinated solvents (Chiellini *et al*., 2001). Nanoprecipitation was carried out by slowly adding a diluted acetone solution of the polymer into 5–fold excess of water under magnetic stirring. Interestingly, the polymer containing PEG 1000 blocks (EL51) afforded nanoparticles of about 126 nm, whereas the polymers containing PEG 400 blocks gave nanoparticles of about 50–60 nm (Table 5.4). Within the limits of the narrow range of investigated compositions, the reported behavior suggested that in nanoprecipitation, the particle size was mostly ruled by the length of hydrophilic PEG blocks and was practically independent of the length of PLA segments. This effect can be tentatively attributed to the extent of polymer swelling in water and hence to the PEG content. It is also possible that the polymer hydrophilicity somehow interferes with the interphase mixing that is responsible for particle formation according to the proposed nanoprecipitation mechanism.

The solid residues obtained by centrifugation of nanoparticle suspensions at 10,000 rpm for 5 min were analysed by AFM. Topographic images clearly show the presence of spheroidal nanoparticles having a rather narrow size distribution (Figure 5.10) close to that determined by dynamic light scattering. Moreover, a close up image indicates that the nanoparticle surface is smooth and homogeneous at the nanometer level thus ruling out that nanoparticles are formed by aggregation of smaller particles.

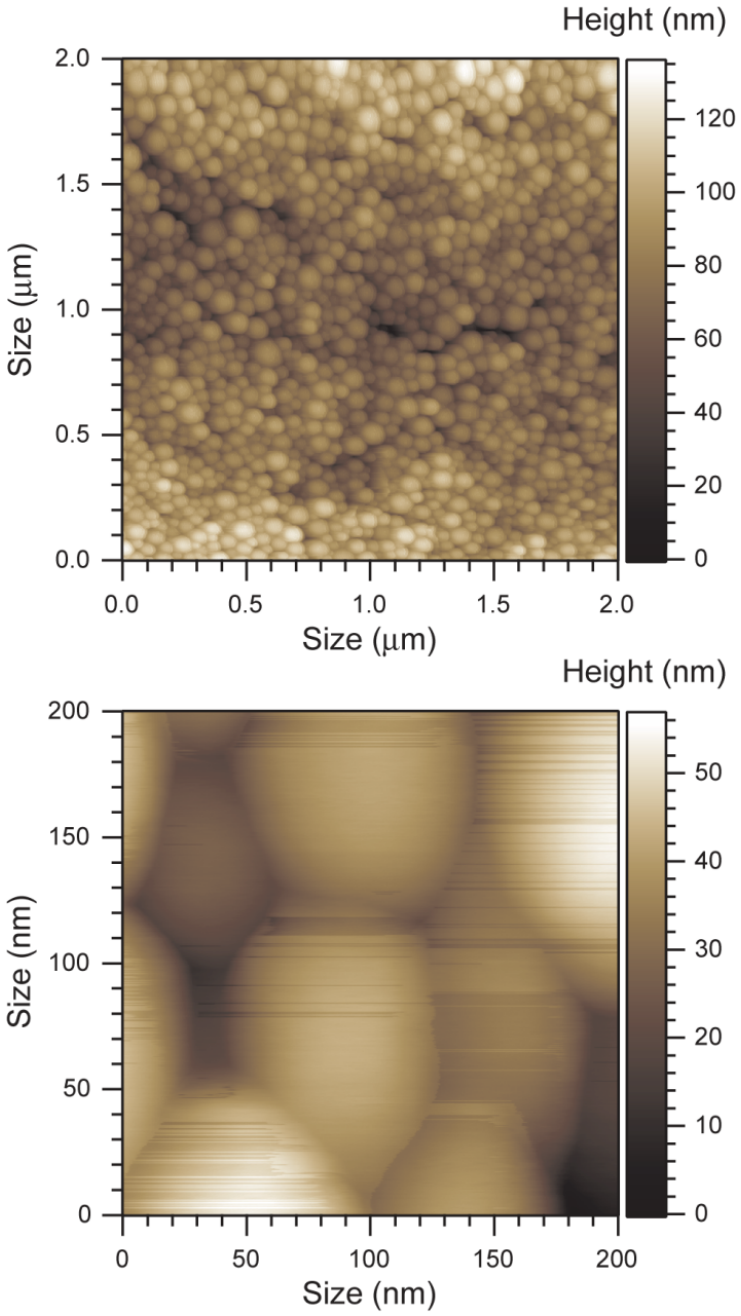

Figure 5.10 AFM topographic images of the pellet obtained by centrifugation at 10,000 rpm for 5 min of nanoparticles prepared by nanoprecipitation of EL14 polymer sample.

The effect of pH on size and zeta potential was investigated by pH titration of the carboxylated nanoparticles prepared by nanoprecipitation (Figure 5.11). Addition of HCl to bring the suspension to pH 1 caused the particle size to increase from about 60 to 700 nm and the zeta potential from about –70 to +2.5 mV. Increasing the pH by addition of NaOH led to a reduction of particle size and to a sharp decrease of the zeta potential. This phenomenon can be explained by considering that at low pH the carboxyl groups are unionized (COOH) with low absolute zeta potential: attenuation of the protective ionic double layer leads to particle aggregation. As the pH increases, the carboxyl groups ionize (COO^-) giving rise to an increase of zeta potential and hence to the electrostatic repulsion of particles leading to smaller nanoparticles. However, the aggregation process is not fully reversible most likely because of adhesion among swollen nanoparticles. In agreement, the particle size decreased from 700 nm to 200 nm and the zeta potential changed from +2.5 to –17.5 mV as the pH increased from 1 to 5. A further increase of the pH above 5 did not cause any significant change of both particle size and zeta potential. This experiment reveals the possibility of designing particles of varying size as a function of the suspension pH.

Table 5.4 Characteristics of nanoparticles prepared by nanoprecipitation

Polymer	Size (nm)	PDI	ZP (mV)
EL51	126±38	0.29±0.08	–44±1
EL14	63±5	0.27±0.09	–51±11
EL54	53±2	0.19±0.01	–64±10
EDL54	56±3	0.26±0.13	–67±9

The ZP was measured in the 2.5–3.3 pH range. All values represented as mean±S.D. (n=3).

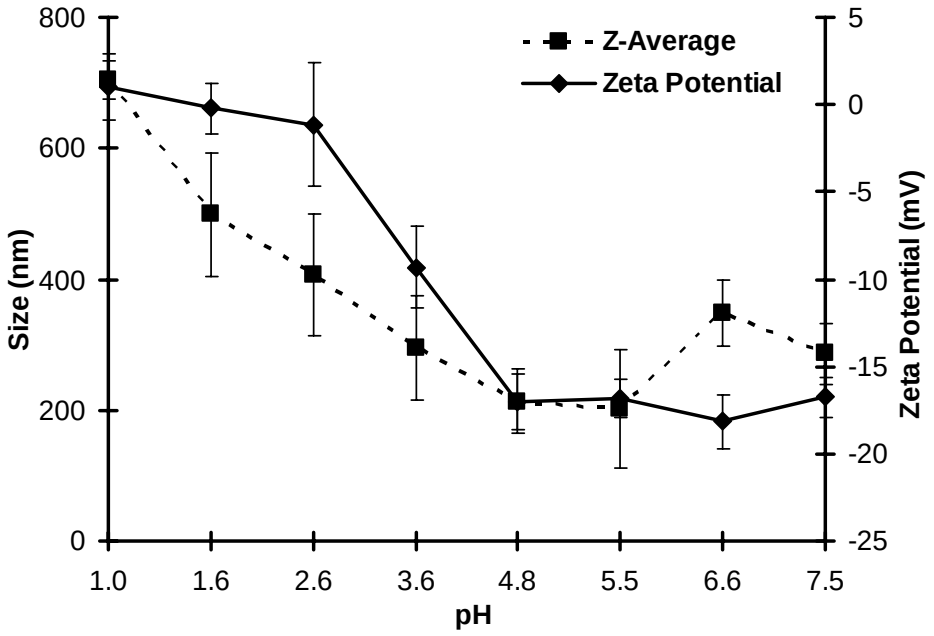

Figure 5.11 Effect of pH on particle size and zeta potential of the carboxylated nanoparticles. All values represented as mean±S.D. (n=3).

5.3.7 CsA loaded nanoparticles

A careful consideration of the polymer and drug properties is needed to optimise drug entrapped nanoparticles as the surfactant and solvent nature can significantly influence the particle characteristics that include size and drug encapsulation. Considering the fact that EL14 had highest MW, it was utilised for nanoparticle preparation. The method previously optimised for PLGA-CsA nanoparticles was adapted with appropriate minor modifications for preparation of EL14 nanoparticles. For PLGA nanoparticles ethyl acetate was the oil phase, however for EL14, ethyl acetate: dichloromethane (4:1) was used for the preparation as small amount of dichloromethane was required for complete dissolution of EL14.

The EL14 and PLGA nanoparticles were prepared by loading different concentrations of CsA (10-30% w/w of polymer weight). A slight increase in particle size from 107 to 119 nm was observed with increase in drug payload from 10-30% (Table 5.5) whereas a significant increase in the entrapment efficiency from 20 to 62% was observed for PLGA. On the other hand, EL14 nanoparticulates did not show any increase in the size however the CsA entrapment decreased. At 10 % loading, EL14 nanoparticles were able to entrap higher amounts of CsA as compared to PLGA. These high entrapments at 10% payload may be due to several possibilities, of which one of the factors could be ionic interaction of CsA with the carboxyl groups present in the side chain of EL14. On the other hand the commercial PLGA has only terminal carboxyl end groups therefore, role of ionic interaction may be negligible as compared to EL14 which would have about 12-16 free carboxyl groups in polymer side chain. Other possibility could be due to better orientation of CsA in the matrix of EL14 than PLGA.

With increasing the load to 30% w/w of polymer, the % entrapment of CsA decreased for EL14 nanoparticles, however an increase was observed for PLGA nanoparticles. The decrease in % entrapment for EL14 could be due to several factors. The lower % entrapment for EL14 could be due to the limitation of the matrix itself owing to its lower molecular weight (16,400) compared to that of PLGA (~40,000). Other reason could be faster saturation of EL14, more hydrophilic matrix to hold highly hydrophobic molecule CsA in comparison to more hydrophobic PLGA. The entrapment of CsA which depends upon the concentration of DMAB can be lowered to increase the CsA entrapment as low entrapment would result in higher polymer administration at desired CsA dose. The nanoparticles prepared using both the polymers were of low PDI (0.08-0.16). The zeta potential was in the range of 71-78 mV for PLGA and 45-59 mV for EL14 nanoparticles at pH 4.1±0.5. The low PDI and high zeta potential indicates the high stability of both the nanoparticulate formulation

In literature, besides PLGA several other polymers have also been explored for preparing CsA loaded nanoparticles. Copolymer of PLA-PEG has been used to prepare CsA loaded NPs (Gref *et al*., 2001). Hyaluronic acid coated PCL particles have been explored for delivery of CsA into the cornea (Yenice *et al*., 2008). In addition to polymers for specific molecules, several polymers for broader drug delivery and biomedical applications have also been synthesized. Several functional polyesters with pendant hydroxyl groups or tailored side chain have been developed (Cerbai *et al*., 2008). Amphiphilic diblock and triblock block copolymers consisting of alternating PEG and PCL segments were synthesised (Signori *et al*., 2005). EL14 also represents a new class of polymer that can effectively entrap CsA, in the form of nanoparticulates in the current circumstances. As 20% loading resulted in

nanoparticles with similar entrapment of CsA in PLGA and EL14 nanoparticles, it was used for *in vitro* and *in vivo* evaluation.

Table 5.5 Characteristics of CsA entrapped nanoparticles

	PLGA			**EL14**		
% Loading	**Size (nm)**	**EE**	**Amt. Entrapped**	**Size (nm)**	**EE**	**Amt. Entrapped**
10	107±7	20±2	1.0±0.1	136±7	51±11	2.5±0.6
20	108±7	46±4	4.6±0.4	139±7	47±3	4.7±0.3
30	119±5	62±4	9.3±0.6	138±4	43±3	6.4±0.5

ZP was measured at pH 4.1±0.5 and was in the range of 71-78 mV for PLGA and 45-59 mV for EL14 nanoparticles. PDI of particles was in the range of 0.08-0.16. All values represented as mean±S.D. (n=3).

5.3.8 *In vitro* drug release studies

The *in vitro* release of drugs from polymeric nanoparticles is mediated by diffusion-cum-degradation process and the recorded release profiles for 20% drug loaded particles are shown in Figure 5.12. A 53% release was recorded at 48 h for EL14 and corresponding to that PLGA recorded 25%. After 48 h, EL14 nanoparticles released about ~7% of drug daily and about 90% by 9th day whereas PLGA nanoparticles released 86% drug by 18th day with ~4% daily release. Several factors could govern the faster release of CsA from EL14 nanoparticles. The hydrophilic nature and low molecular weight of EL14 could have contributed to faster release of CsA from EL14 nanoparticles. Other reasons may also include large amount of surface bound drug on EL14 nanoparticles and faster degradation of the EL14.

The release profile of CsA from both the nanoparticulate formulations were modeled for different release mechanisms mainly; zero order (Najib and Suleiman, 1985), first order (Desai *et al*., 1966), Higuchi's square root plot (Higuchi, 1963), Hixson– Crowell cube root plot (Hixson and Crowell, 1931) and Peppas-Korsmeyer power plot (Korsmeyer *et al*., 1983) (Table 5.6). CsA release from EL14 and PLGA nanoparticles could have followed either Higuchi's model (diffusive) or first order release based on higher correlation coefficient (R) and lower sum of squared errors (χ^2). No conclusive differences between Higuchi's model (diffusive) or first order release were found particularly if experimental errors (5-10%) were taken into account. However, if data for less than 85% release are considered, the release of CsA from EL14 nanoparticles fits exceptionally well with the Higuchi model. To further confirm, fitting to Peppas-Korsemeyer gave diffusional coefficient (n) = 0.47 for EL14 nanoparticles (n < 0.5, Fickian diffusion), indicating a diffusive release mechanism. The somewhat larger n = 0.685 was observed

for PLGA nanoparticles indicating a small deviation from the diffusive model, suggesting that diffusion is accompanied by erosion ($n > 0.5$, non-Fickian diffusion). The difference between the two polymers can be attributed to: hydration of hydrophilic EL14 nanoparticles which facilitates drug diffusion; limited diffusion inside rather hydrophobic PLGA nanoparticles and hence a diffusion/erosion mechanism. The faster but controlled release from EL14 nanoparticles would help in achieving higher CsA blood levels in comparison to PLGA but at a controlled C_{max}.

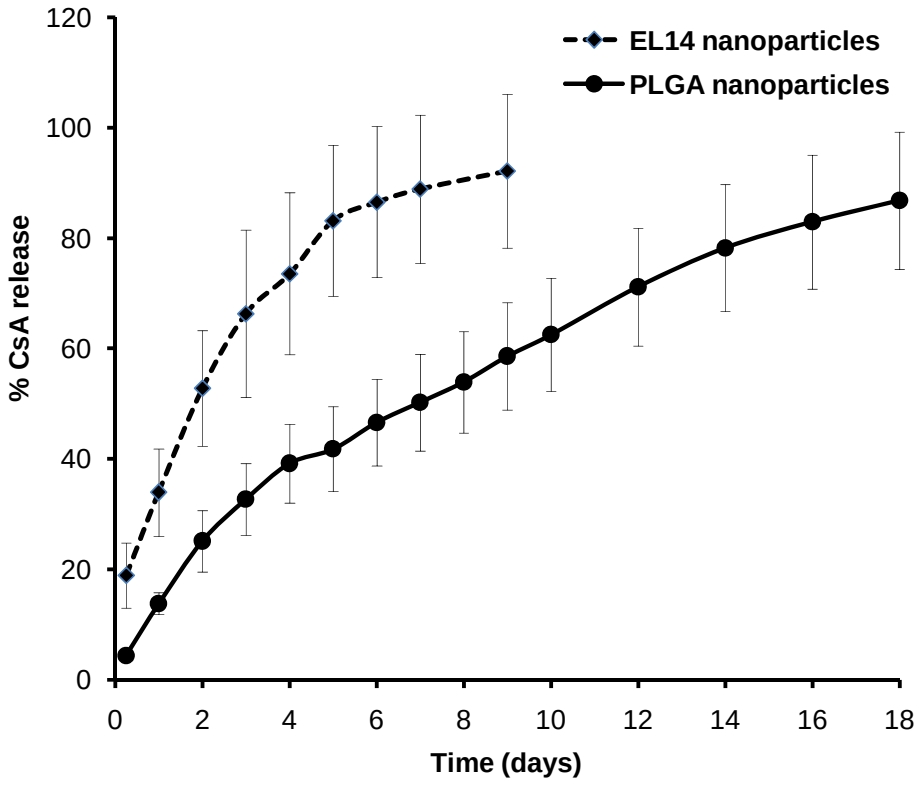

Figure 5.12 *In vitro* release pattern of CsA from EL14 and PLGA nanoparticles. All values represented as mean±S.D. (n=3).

Table 5.6 *In vitro* release data fit to models

Kinetic Model	Equation	Parameters [a]	PLGA NPs	EL14 NPs [b]
Zero order	$Q_t = k_0 t$	R	0.972	0.914
		χ^2	1590	1516
		k_0	5.78	9.72
Higuchi	$Q_t = k_H t^{1/2}$	R	0.997	0.988 (0.999)
		χ^2	155	260 (11.9)
		k_H	21.5	34.5 (37.0)
First order	$\ln Q_t = \ln Q_0 - k_1 t$	R	0.994	0.990
		χ^2	105.1	62.1
		k_1	0.0912	0.388
Hixon-Crowell	$Q_0^{1/3} - Q_t^{1/3} = k_{HC} t$ $Q_t^{1/3} = Q_0^{1/3} - k_{HC} t$	R	0.800	0.733
		χ^2	44565	43164
		k_{HC}	0.165	0.337
Peppas-Korsmeyer	$\frac{Q_t}{Q_0} = k_{PK} t^n$ $\ln Q_t = \ln Q_0 k_{PK} + n \ln$	R	0.994	0.993
		χ^2	187.8	200.8
		k_{PK}	0.170	0.366
		n	0.685	0.470

[a] Q_t is the amount of drug released at time t; Q_0 is the initial amount of the drug in the formulation; n is the diffusional coefficient; k_0, k_1, k_H, k_{HC}, and k_{PK} are the release rate constants for zero-order, first-order, Higuchi, Hixson-Crowell, and Peppas-Korsmeyer rate equations respectively. n-diffusional coefficient in Peppas-Korsmeyer rate equations; R is the correlation coefficient and χ^2 is the sum of squared errors. [b] Values in parentheses refers to release values lower than 85%.

5.3.9 Pharmacokinetic and tissue distribution studies

Pharmacokinetics and tissue distribution studies are noteworthy in assessment of a delivery system as they provide valuable information about the safety and efficacy of the formulations and also help in estimating clinical doses. Comparison of nanoparticulate formulation with currently marketed formulation of CsA would provide additional information on therapeutic implications of the new formulations. Considering the above, the pharmacokinetic profile of EL14 and PLGA nanoparticles of CsA were compared with currently marketed CsA formulation Neoral®. The blood CsA levels with time for Neoral®, EL14 and PLGA nanoparticles on oral administration at 15 mg/Kg are shown in Figure 5.13 and the derived pharmacokinetics parameters in Table 5.7.

Entrapment of CsA into EL14 and PLGA nanoparticles resulted in the sustained release of the drug in comparison to the Neoral® which is a micro-emulsion based formulation. The T_{max} for Neoral® was 2 h while that for EL14 and PLGA nanoparticles were 12 and 24 h, respectively. The C_{max} of the formulations varied widely, depending upon the ability of the formulation to sustain the CsA release. C_{max} were 1328, 1006 and 682 ng/ml for Neoral®, EL14 and PLGA nanoparticles, respectively. Neoral® resulted in a quick absorption profile while PLGA nanoparticles sustained the release of CsA longer than EL14 nanoparticles. By 72 h after administration, EL14 and PLGA nanoparticles had similar blood levels. The relative bioavailability of EL14 and PLGA nanoparticles were 126 and 120% respectively in comparison to Neoral® and 105 for EL14 nanoparticles in comparison to PLGA nanoparticles.

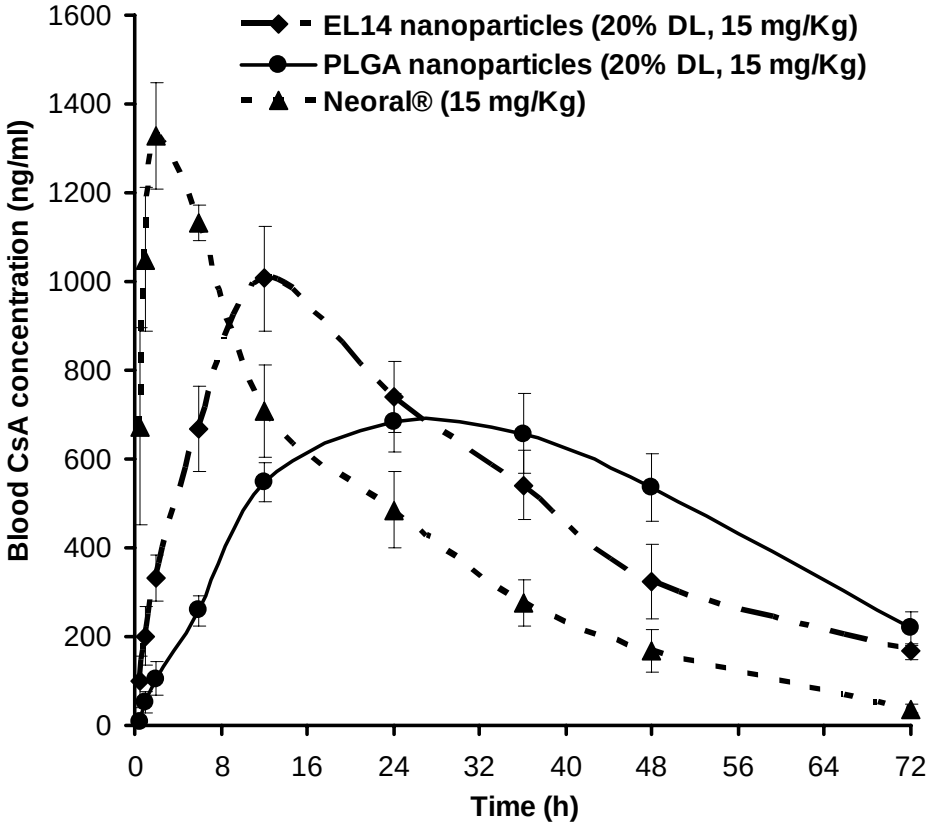

Figure 5.13 Comparative *in vivo* plasma concentration vs. time profiles of CsA administered orally as Neoral®, CsA nanoparticles of EL14 and PLGA at 15 mg/Kg. All values reported are mean±S.E.M. (n=3).

Table 5.7 Pharmacokinetic parameters

Groups	AUC_{0-72}	C_{max}(ng/ml)	T_{max} (h)	Relative Bioavailability*	Relative Bioavailability**
Neoral®	29046±1437	1328±120	2	100	-
PLGA	34854±2157	682±66	24	120	100
EL14	36616±2843	1006±119	12	126	105

*In relative to Neoral®, **In relative to PLGA. All data represented as mean±S.E.M. (n=3).

After 72 h on oral administration, the animals were sacrificed and tissue concentration determined to have an insight on biodistribution (Table 5.8). For Neoral® the concentrations for all the organs, except brain were lower than PLGA and EL14 nanoparticles. For brain, Neoral® had highest CsA concentration followed by EL14 and PLGA nanoparticles respectively, which may be due the fact that free CsA penetrated blood brain barrier more easily than that entrapped in polymeric particles. When both the nanoparticulate formulations were compared with each other, EL14 nanoparticles produced higher CsA tissue levels at lower blood CsA levels than PLGA nanoparticles. This may be due to the ability of EL14 nanoparticles to distribute more in tissues as observed by higher tissue distribution coefficient (*Kp*) as depicted in Table 5.9. From the observed kinetic and tissue profile it was clear that the nature of polymer matrix played a key role in determining the performance of given delivery system. EL14 in comparison to PLGA generated a kinetic profile which is much closer to Neoral®.

This report illustrates the synthesis and systematic characterisation of carboxylated $(ABA)_n$ type multiblock copolymers of lactic acid (A) and ethylene glycol (B) and its application in nanoparticulate delivery of CsA. The synthesis involved ring opening polymerisation of lactide initiated by PEG diol, followed by chain extension with PMDA leading to incorporation of 12–16 free carboxylic acid groups in the polymer matrix. The polymers were found to be degradable and well suited for the preparation of nanoparticle suspensions and in oral delivery of CsA.

The carboxyl functionalisation of the polymer could be beneficial for drug delivery applications. Recently, the ability of particles exposing different surface functional groups such as, phenyl, carboxyl, amine, dialkyl phosphonate, ester, and hydroxyl groups to adhere to live malignant cells

was investigated (McNamee *et al*., 2007). Carboxyl groups showed the highest adhesion to B16F10 cells. The high adhesion of carboxyl groups to malignant cell was due to vander Waals attraction, hydrogen bonding, and significant chemical binding, due to reactions between the carboxylic acid and the hydroxyl group of integrins and glycoproteins which are over expressed on the cancer cell surface (McNamee *et al*., 2007). Taking into account the above results, the prepared carboxylated polymers when processed into nanoparticulates would offer the adhesiveness required for attachment to cancerous cells and would present a new polymer for loading chemotherapeutic agents. In addition to stronger adhesion of the delivery system to cancerous cells, the side–chain carboxyl groups can be exploited for binding targeting molecules like A10 RNA aptamer which binds to the prostate specific membrane antigen (Chenga *et al*., 2007) and for linking drug molecules (Khandare and Minko, 2006). Furthermore, the ionic interaction between the carboxylated polymer and proteins would lead to better entrapment of proteins (Blanco and Alonso, 1997). Due to higher acidic nature of the polymer due to the presence of carboxyl groups, the basic drugs would solubilise more in the polymer (Tatavarti *et al*., 2004) and result in higher entrapment. Finally, the ability of the synthesised polymers to form nanoparticles would also offer advantages of nano–drug delivery making them promising materials for biomedical applications.

The synthesised polymer when explored for oral delivery of CsA, demonstrated controlled delivery of CsA compared to Neoral® and PLGA nanoparticles with higher bioavailability. In the literature several studies have demonstrated the correlation of CsA concentrations to the incidence of side effects. The toxicities are found to depend on C_{max} and the AUC of the drug. In a recent study in pediatrics with stable renal transplant it was found

that hypertrichosis was related to AUC, whereas the tremors were more related to C_{max} of CsA (David-Neto *et al*., 2000). Similar facts have also been established in acute nephrotoxicity caused by CsA where decrease in glomerular filtration rate was closely related to the C_{max} and not AUC (Perico *et al*., 1992). It was further suggested that hypertrichosis and tremor can be prevented by maintaining the $AUC_{0\text{-}4} \leq 4200$ ng/ml per h and $C_{max} \leq 900$ ng/ml respectively (David-Neto *et al*., 2000). In circumstances to the above, EL14 nanoparticles could be a preferred formulation for CsA delivery as observed C_{max} was in the desired range, unlike Neoral® which exceeded the limit significantly by ~400 ng/ml. The current commercial formulation of CsA experiences erratic bioavailability due to its extensive metabolism in the gut, making it difficult to predict trough levels (Lindholm and Kahan, 1993). The better bioavailability of CsA in the form of EL14 nanoparticles could be due the protective role of PEG present in the polymer chain which has been found to have protective effects on proteins and peptides in gastric fluids (Tobio *et al*., 2000). The decreased gut-wall metabolism would allow better therapeutic monitoring of CsA. Compared to PLGA nanoparticles, EL14 nanoparticles achieved the desired C_{max} at half the dose. This dose reduction may provide significant increase in cost benefits ratio as result of less amount of CsA required, hence cheaper formulation with lower toxicity resulting in better therapeutics with increased patient compliance.

CsA is a substrate and inhibitor of P-gp and can modulate and reverse multidrug resistance and improve chemotherapy. However, its use is limited due to its low binding efficiency which necessitates the use of high dose, hence resulting in toxicity (Tan *et al*., 2000). In view of this, CsA loaded EL14 nanoparticles would be an attractive strategy to derive maximum beneficial effects of CsA due to the possibility of adhesion of carboxylated

nanoparticles to cancerous cells leading to increased binding (McNamee *et al*., 2007) and requirement of low dose of CsA as a result of improved oral bioavailability.

In general, CsA with its ability in treatment of wide variety of disease is an interesting molecule of medical research today. The current developed nanoparticulates unlocks the advancement in drug delivery technology that would result in better management of transplants patients and treatment of autoimmune disorders, with simultaneous reduction in the associated adverse effects of CsA.

5.4 Conclusions

The current report illustrates the synthesis and nanoparticulate applications of multiblock copolymers containing periodically spaced side–chain carboxyl groups. The carboxylated EL14 nanoparticles were able to successfully deliver CsA at a comparable profile to that achieved by Neoral®, particularly C_{max}. This is essentially a step close to clinical needs.

Table 5.8 Tissue concentration of CsA at 72 h on oral administration.

Tissue	μg/g of tissue		
	Neoral®	**PLGA**	**EL14**
Blood	0.04±0.01	0.22±0.04	0.17±0.02
Brain	3.4±0.7	1.9±0.2	2.7±1.1
Heart	5.0±0.8	6.4±1.5	6.8±0.8
Lung	5.3±0.7	8.9±3.6	10.7±0.6
Kidney	9.9±1.6	14.0±1.3	15.3±1.5
Spleen	6.9±1.8	9.3±2.1	10.8±1.2
Liver	10.7±1.3	11.7±0.8	16.4±1.1
Intestine	6.8±0.8	7.5±1.5	7.7±1.2

All data represented as mean±S.E.M. (n=3).

Table 5.9 Tissue distribution coefficient

Tissue	K_p	
	PLGA	**EL14**
Blood	1	1
Brain	9	16
Heart	29	41
Lung	40	64
Kidney	64	91
Spleen	42	64
Liver	53	98
Intestine	34	46

6. SUMMARY AND FUTURE WORK

6.1 Summary

The results presented in this work testify the potential of polymeric nanoparticles for oral delivery of CsA. CsA loaded PLGA nanoparticles were prepared at different loading ratios and were investigated for their pharmacokinetic behaviour. Dose dependent pharmacokinetic evaluation of CsA loaded PLGA nanoparticles demonstrated an increase in the C_{max} and AUC_{0-72}, however with decreased relative bioavailability with increasing the dose from 15 to 45 mg/Kg. With increasing the loading from 10 to 30%, an increase in C_{max} and AUC_{0-72} was observed with corresponding increase in relative bioavailability. Nanoparticulate formulations of CsA demonstrated higher tissue concentrations than those observed by Neoral® except for brain at an equal dose. The nanoparticulate formulation of CsA (30% loading at 30 mg/Kg), which demonstrated similar C_{max} to Neoral®, were found to be significantly less nephrotoxic than the Neoral®.

Antioxidant adjuvant CoQ10 was explored further to reduce the nephrotoxicity. CoQ10 co-entrapped PLGA nanoparticles were successfully prepared using emulsion-diffusion-evaporation method using DMAB as a stabiliser. Comprehensive characterisation of the co-entrapped nanoparticles revealed that the surfactant concentration, external phase volume, droplet size reduction method and drug loading concentration can all influence the characteristics of co-loaded nanoparticles. The semi-quantitative solubility study demonstrated a strong influence of CoQ10 on CsA entrapment which was thought to be due to increase in the lipophilicity of the overall system. The *in vitro* dissolution profile indicated the influence of CoQ10 on CsA release to that of individual nanoparticles of CsA, however this effect was not observed *in vivo*. The co-entrapped CoQ10 does not seem to have any

additional affect on the nephrotoxicity behaviour in comparison to that of native CsA nanoparticles, suggesting the inability of CoQ10 to ameliorate the nephrotoxicity at the given dose or CoQ10 is as such ineffective in scavenging such free radical mediated toxicity.

New polymer architecture was explored to modify the release of CsA from nanoparticles to reduce its dose and match the blood profile of Neoral®. Multiblock copolymers containing periodically spaced side–chain carboxyl groups were synthesised successfully by a two–step synthesis involving the preparation of ABA triblock pre–polymers of lactic acid (A block) and ethylene glycol (B block) followed by chain extension to $(ABA)_n$ multiblock copolymers by reaction with PMDA. The synthesised polymers were thoroughly characterised by NMR, TGA and DSC. Chain extension resulted in the incorporation of free carboxylic groups in polymer backbone and in a six fold increase of molecular weight. The polymers were found to be fast degrading in water following first order kinetics. The carboxylated nanoparticles of EL14 were successfully able to entrap CsA. On *in vitro* release, EL14 nanoparticles released CsA faster compared to native PLGA nanoparticles. On *in vivo* evaluation, the EL14 nanoparticles were successfully able to deliver CsA via oral route at a controlled rate, demonstrating a higher C_{max}, a faster T_{max} and enhanced tissue levels to that of PLGA particles; however the overall bioavailability of the nanoparticulates were similar and higher than Neoral®.

The developed PLGA and EL14 nanoparticulate formulations of CsA will provide a safer and more effective alternative to Neoral® which would enhance the quality of patient life and permit the use of CsA in the treatment of a wide variety of immune disorders and would be an attractive proposition for pharmaceutical companies.

The current project explores the possibility of delivering CsA orally using polymeric nanoparticles. For the transport of polymeric nanocarriers across the GIT, the paracellular and the transcellular routes have been suggested (Florence, 2004; des Rieux *et al*., 2006). The paracellular route for nanoparticle translocation is very limited because of the very small surface area of the intercellular spaces and due to tightness of the intercellular junctions (pore diameter 3-10 Å) (Jung *et al*., 2000). However, using cationic polymers such as chitosan, the paracellular transport of drugs can be increased (Schipper *et al*., 1997) through ionic interactions between the polymer and the cell membrane which results in opening of tight junctions (van der Lubben *et al*., 2001). Transcellular transport of nanoparticles takes place through the receptor mediated and the adsorptive endocytosis. Receptor mediated transport is based on the principle of ligand binding to receptors on cell surface to initiate endocytotic uptake while adsorptive endocytosis is based on simple physical adsorption of nanoparticles onto cell surface. The transcellular uptake of polymeric nanoparticles has been shown to occur through two types of intestinal cells, the enterocytes and the M cells. Most studies show that majority of the nanoparticles are taken up by M cells, however, it constitutes only a small ratio of GIT surface area and the uptake process is found to be saturable in nature (Jani *et al*., 1990; Desai *et al*., 1996; Shakweh *et al*., 2004; Florence, 2005; des Rieux *et al*., 2006).

The extent of uptake of nanoparticles from GIT has been demonstrated to be small and varied. It was demonstrated that particles in the range of 50-100 nm were observed to an extent of 30% (Jani *et al*., 1990). However, the uptake represented the amount of polystyrene particles absorbed and adsorbed from rat mucosa (Florence, 1997). Desai *et al*., studies the effect of size on uptake of PLGA nanoparticles in Caco-2 cells. The uptake efficiency at 100 μg/ml

concentration of 100 nm particles was 41% while 1 μm and 10 μm demonstrated 15 and 6% uptake efficiency, respectively (Desai *et al*., 1997). On administration of radio labelled polymethyl methacrylate nanoparticles, the total concentration of the nanoparticles in the body was 1% of the dose at 2 h and total uptake remained very low (< 10% at 130 nm particle size) (Araujo, *et al*., 1990). Similarly, low uptake of 1.9-2.3% of PLGA nanoparticles of 133 nm in size was observed after 1 h of oral administration in mice (Le Ray *et al*., 1994).

However, most of the studies assessing the transport of nanoparticles across the intestinal wall were performed using Caco-2 cells or in animals and relevance of these transport models to predict their behavior in human is an ongoing debate, as clinical studies are very much missing (Florence, 2005; des Rieux *et al*., 2006; Florence 2007).

However, considering the above facts, it seems only a small proportion of administered nanoparticles can reach systemic circulation. Additionally, once taken up, the nanoparticles are countered with macrophages which results in their rapid clearance from systemic circulation (Moghimi *et al*., 2001). However, in the present dissertation, large quantities of CsA was delivered to systemic circulation by polymeric nanoparticles. At 15 mg/Kg dose of CsA, PLGA and EL14 nanoparticles demonstrated higher bioavailability than commercial formulation Neroal® with prolonged *in vivo* release, indicating towards the possibility of different mechanism(s) involved in delivery of CsA to systemic circulation by DMAB stabilised nanoparticles.

Considering the fact that cationic polymers can open the tight junctions (Jung *et al*., 2000), the DMAB stabilised cationic nanoparticles on oral administration can modify the membrane permeability, resulting in opening of the tight junctions and translocation of nanoparticles, hence delivering

CsA to systemic circulation. However, the ability of DMAB stabilised nanoparticles to affect tight junctions requires additional investigations. Additionally, the cationic nanoparticles/polymers have been found to demonstrate mucoadhesive properties (Schipper *et al*., 1997; Jung *et al*., 2000). In view of this, DMAB stabilised nanoparticles can attach to the mucus, resulting in increased uptake by intestinal enterocytes. Furthermore, the attachment of DMAB stabilised nanoparticles to mucus may improve the intestinal residence time and can release CsA, causing an increased local CsA concentration at the site of absorption (Haas and Lehr, 2002; Bernkop-Schnurch *et al*., 2003). Besides mucoadhesive property of DMAB, its P-gp inhibiting nature should be explored as it may help in reducing the high variability in CsA absorption (Lown *et al*., 1992; Fricker *et al*., 1996).

Recently it was reported that DMAB modified nanoparticles penetrated the endothelial cells better with enhanced uptake compared to other cationic surfactants and PVA. The higher penetration and uptake was facilitated by interactions of the di-chains of the cationic DMAB with cell membrane, signifying the role of surface charge and molecular structure of the surfactant in uptake of nanoparticles across the cell membrane (Peetla and Labhasetwar, 2009) and could be one of the mechanism involved in higher uptake of DMAB stabilised PLGA nanoparticles.

During nanoparticle preparation it was observed that CsA's solubility was dependent upon the DMAB concentration in aqueous phase (Italia *et al*., 2007; Ankola *et al*., 2010) which may be due to micellar solubilisation of CsA by DMAB. On administration of the nanoparticles orally, DMAB bound to the surface of PLGA nanoparticles may help further in solubilising CsA in the GIT and hence improving the oral absorption. However, the amount of DMAB bound to PLGA nanoparticles was < 20 μM (Bhardwaj *et al*., 2009)

which is significantly lower than the critical micellar concentration of DMAB which is ~2.5 mM (Fontana *et al*., 2003), hence a very negligible effect of DMAB's role in solubilising the CsA in GIT may be predicted but requires further investigations.

Overall, the mechanisms involved in delivery of drugs to systemic circulation by DMAB stabilised nanoparticles remains far from explored and requires further investigation based on the above hypothesized mechanisms.

6.2 Future perspectives

The current report establishes the role of polymeric nanoparticles in oral delivery of CsA. The polymeric nanoparticles were prepared by emulsion diffusion evaporation method. However, the method suffers from several limitations which prevent its successful implementation for commercialisation. The limitation of method includes inability to load high dose of drugs into the nanoparticles along with low batch size. Additionally, the method results in nanoparticles with a size distribution of 50-500 nm, which is considerably large. Use of high pressure homogenisation should be explored to obtain narrow size distribution of nanoparticles with high drug loading and large batch size (Kwon *et al*., 2002; Kharb *et al*., 2006). Further limiting the scale-up of nanoparticles is absence of an efficient purification method. Centrifugation has been routinely used in purification of nanoparticles but is burdensome in nature and less efficient. Therefore, an efficient purification system is required for separation of free drug and impurities. Several methods like dialysis and gel filtration have been investigated but with limited success for large-scale productivity. Ultrafiltration should be explored for particle purification for its swiftness and high particle recovery along with its ability to handle large volume (Tsao *et al*., 2009).

Apart from technological limitations in producing large quantities of nanoparticles, the nanoparticulate technology suffers from the limitations of bioanalytical methods in determining the bioavailable drug in body. Most methods determine the free drug as well as the drug entrapped in nanoparticles, making it difficult to predict the pharmacokinetic/pharmacodynamic correlation of the formulation (Zhao *et al*., 2009). Currently, ultrafiltration, micro-dialysis, ultracentrifugation and

gel chromatography have been exploited to determine the free and bound drug in blood or plasma but have been found to be less efficient due to very limited amount of plasma/blood available for drug determination along with their expansive and time consuming nature (Zhang and Musson, 2006; Wang *et al*., 2008). Recently, a simple and efficient liquid-liquid extraction method was developed and validated for determination of non-encapsulated hydrophobic pyrene in plasma (Zhao *et al*., 2009) and should be explored further to estimate free CsA.

Additionally, determination of the extent of nanoparticle uptake from GIT is critical to the success of the technology. Biodistribution experiments are important in determining localisation pattern of nanoparticles and in estimating the amount of nanoparticle uptake. Tissue distribution studies can be performed by tagging the nanoparticles with radiolabels, contrast agents or dyes that would allow the detection of nanoparticle/polymer concentration within the tissues over time and moreover help in estimating the free drug and bound drug in the body. Radio-labelling of PLGA nanoparticles can be done by either entrapping/coupling a radio-active material like ^{125}I (Panagi *et al*., 2001; Hau and Sun, 2006). The effect of dose on biodistribution of PLGA nanoparticles was studied by entrapping ^{125}I bound to cholesterylaniline (Panagi *et al*., 2001). The technique can be easily tailored to study biodistribution pattern of DMAB stabilised PLGA nanoparticles. ^{14}C radio-labelling technique can be utilised to study the biodistribution and *in vivo* degradation behaviour of PLGA nanoparticles but ^{14}C radio-labelling technique is expansive and associated with high radiation pollution and ^{125}I remains the preferred technique (Hau and Sun, 2008). Recently Technetium-99m (^{99m}Tc) radionuclide has been preferred due to its ideal physical

properties in studying *in vivo* uptake and behaviour of PLGA nanoparticles (Stevanovic *et al*., 2009).

Another common technique to study and quantify the biodistribution pattern of polymeric nanoparticles is to entrap a fluorophore or fluorophore-labelled drug derivative or use a flurophore-labelled polymer and consequently image the system using fluorescence microscopy. Several fluorescence probes like 6-coumarin (Panyam *et al*., 2003) and rhodamine (Betancourt *et al*., 2009) have been widely investigated. However, the fluorescent technique has been associated with low contrast, high background noise, photo-bleaching and confounding fluorescence from animal tissues. Recently, a new technique based on Raman spectroscopy has been investigated. The technique was used to study the intra-cellular distribution and degradation behavior of PLGA nanoparticles (Cherneko, *et al*., 2009).

A great deal has been said about the effect of size on nanoparticle uptake from GIT. However, most studies demonstrating the effect of size has been performed using Z-average obtained from dynamic light scattering technique rather than taking into the account the size distribution curve. Similar studies were also performed in the current work; however effect of size distribution should be carefully investigated. Using the above particle tracking techniques, detailed investigation about effect of particle size on kinetics of uptake and their biodistribution, retention and excretion should be performed.

Additionally, one of the major hurdles in nanoparticulate delivery is their rapid elimination from the body by macrophages of liver and spleen (Moghimi *et al*., 2001; Owens and Peppas, 2006). However, using DMAB as stabiliser, prolonged drug concentrations were observed. This prolonged circulation could be due to the ability of DMAB stabilised nanoparticles to

avoid interaction with opsonin proteins and escaping phagocytic uptake however, requires mechanistic understanding of its role. The plasma protein adsorption on DMAB stabilised nanoparticles in rat and human blood can be studied using 2-D PAGE analysis and MALDI-TOF MS and rate of protein adsorption can be studied using Protein Lab-on-chip® technology as it is highly specific and rapid in nature (Kim *et al*., 2007). Several techniques have been investigated to study the uptake of nanoparticles by macrophages. The macrophagocytic uptake of DMAB stabilised polymeric nanoparticles can be studied *in vitro* using human monocytes or monocytes derived macrophages and quantification of their uptake by fluorescence-based flow cytometry (Nahrendorf *et al*., 2008; Bouno *et al*., 2009).

The biocompatibility and biodegradability are important prerequisites for polymers used in drug delivery. The newly synthesised carboxylated polymers should be screened for biocompatibility and biodegradability. Lactate dehydrogenase (LDH) and 3-(4,5-dimethylthiazol-2-yl)-2,5-diphenyltetrazolium bromide (MTT) assay (Bhardwaj *et al*., 2009) should be performed to determine biocompatibility of the polymers. The carboxylated polymers are synthesized using aromatic dianhydride, which has limited information about its toxicity. Possibility of carrying out the chain extension using aliphatic dianhydride should be investigated because of their better *in vivo* degradability (Muller *et al*., 2001).

In addition to the above, the future work should focus on nephrotoxic screening of CsA loaded EL14 nanoparticles. The nephrotoxic study of CsA loaded EL14 nanoparticles would provide additional information on role of polymeric nanoparticles and their ability to reduce CsA nephrotoxicity. Further, the PLGA and EL14 nanoparticles can be evaluated in various transplant and disease models to get an insight of their therapeutic potential

in preventing graft rejection and treatment of autoimmune disorders. A systematic regulatory toxicology screening should be carried out.

The effect of CoQ10 dose should be investigated and other antioxidants that can have dual function of minimising the hypertension as well as nephrotoxicity (Ankola *et al*., 2007; Sonaje *et al*., 2007; Italia *et al*., 2009) should be screened for co-encapsulation. Eventually, stability testing of the most successful formulations need to be carried out according to the regulatory requirements setting the ground for clinical trials.

REFERENCES

Aberg, F., Appelkvist, E. L., Dallner, G. and Ernster, L., 1992. Distribution and redox state of ubiquinone in rat and human tissues. Arch. Biochem. Biophy., 295, 230-234.

Ahmad, Z., Pandey, R., Sharma, S. and Khuller, G. K., 2006. Pharmacokinetic and pharmacodynamic behaviour of antitubercular drugs encapsulated in alginate nanoparticles at two doses. Int. J. Antimicrob. Agents, 27, 409-416.

Aliabadi, H. M., Brocks, D. R. and Lavasanifar, A., 2005. Polymeric micelles for the solubilization and delivery of cyclosporine A: pharmacokinetics and biodistribution. Biomaterials, 26, 7251-7259.

Aliabadi, H. M., Elhasi, S., Brocks, D. R. and Lavasanifar, A., 2008. Polymeric micellar delivery reduces kidney distribution and nephrotoxic effects of Cyclosporine A after multiple dosing. J. Pharm. Sci., 97, 1916-1926.

Allemann, E., Leroux, J. C. and Gurny, R., 1998. Polymeric nano- and microparticles for the oral delivery of peptides and peptidomimetics. Adv. Drug Del. Rev., 34, 171-189.

Al-Meshal, M. A., Khidr, S. H., Bayomi, M. A. and Al-Angary, A. A., 1998. Oral administration of liposomes containing cyclosporine: a pharmacokinetic study. Int. J. Pharm., 168, 163-168.

Amidon, G. L., Lennernas, H., Shah, V. P. and Crison, J. R., 1995. A theoretical basis for biopharmaceutic drug classification: The correlation of in vitro drug product dissolution and in vivo bioavailability. Pharm. Res., 12, 413-420.

Anderson, J. M. and Shive, M. S., 1997. Biodegradation and biocompatibility of PLA and PLGA microspheres. Adv. Drug Del. Rev., 28, 5-24.

Andersson, M., Aberg, F., Teclebhran, H., Edlund, C. and Appelkvist, E. L., 1995. Age-dependent modification in the metabolism of mevalonate pathway lipids in rat brain. Mech. Ageing. Dev., 85, 1-14.

Andoh, T. F. and Bennett, W. M., 1998. Chronic cyclosporine nephrotoxicity. Curr. Opin. Nephrol. Hypertens., 7, 265-270.

Andrieux, K. and Couvreur, P., 2009. Polyalkylcyanoacrylate nanoparticles for delivery of drugs across the blood-brain barrier. Wiley Interdiscip. Rev. Nanomed. Nanobiotechnol., 1, 463-474.

Ankola, D. D., Durbin, E. W., Buxton, G. A. Schäfer, J., Bakowsky U. and Kumar, M. N. V. R., 2010. Preparation, characterization and in silico modeling of biodegradable nanoparticles containing Cyclosporine A and Coenzyme Q10. Nanotechnology, 21, doi:10.1088/0957-4484/21/6/065104

Ankola, D. D., Viswanad, B., Bhardwaj, V., Ramarao, P. and Kumar, M. N. V. R., 2007. Development of Potent Oral Nanoparticulate Formulation of Coenzyme Q10 for Treatment of Hypertension: Can the Simple Nutritional Supplements be used as First Line Therapeutic Agents for Prophylaxis/Therapy? Euro. J. Pharm. Biopharm., 67, 361-369.

Apanay, D. C., Neylan, J. F., Ragab, M. S. and Sgoutas, D. S., 1994. Cyclosporine increases the oxidizability of low-density lipoproteins in renal transplant recipients. Transplantation, 58, 663-669.

Arujo, L., Sheppard, M., Lobenberg, R. and Kreuter, J., 1999. Uptake of PMMA nanoparticles from the gastrointestinal tract after oral administration to rats: modification of the body distribution after suspension in surfactant solution and in oil vehicle. Int. J. Pharm., 176, 209-224.

Awaja, F., Daver, F. and Kosior, E., 2004. Recycled poly(ethylene terephthalate) chain extension by a reactive extrusion process. Polym. Eng. Sci., 44, 1579–1587.

Bach, J. F., 1999. The contribution of cyclosporine A to the understanding and treatment of autoimmune diseases. Transplant. Proc., 31, S16-S18.

Bajpai, A. K., Shukla, S. K., Bhanu, S. and Kankane, S., 2008. Responsive polymers in controlled drug delivery. Prog. Polym. Sci., 33, 1088–1118.

Bala, I., Bhardwaj, V., Hariharan, S., Sitterberg, J., Bakowsky, U. and Kumar, M. N. V. R., 2005. Design of Biodegradable Nanoparticles: A Novel Approach to Encapsulate Poorly Soluble Phytochemical Ellagic acid. Nanotechnology, 16, 2819-2822.

Bala, I., Hariharan, S. and Kumar, M. N. V. R., 2004. PLGA Nanoparticles in Drug Delivery: The State of the Art. Crit. Rev. Ther. Drug Carrier Syst., 21, 387-422.

Barrera, D. A., Zylstra, E., Lansbury, P. T. and Langer, R., 1993. Synthesis and RGD peptide modification of a new biodegradable co polymer; poly(lactic acid-co-lysine). J. Am. Chem. Soc., 115, 11010-11021.

Bauerova, K., Kucharska, J., Mihalova, D., Navarova, J., Gvozdjakova, A. and Sumbalova, Z., 2005. Effect of Coenzyme Q10 supplementation in at model of adjuvant arthritis. Biomed. Pap. Med. Fac. Univ. Palacky Olomouc. Czech Repub. 149, 501–503.

Beal, M. F., 1999. Coenzyme Q10 and its potential for treatment of neurodegenerative diseases. Biofactors, 9, 261-266.

Bekerman, T., Golenser, J. and Domb, A., 2004. Cyclosporin nanoparticulate lipospheres for oral administration. J. Pharm. Sci., 93, 1264-1270.

Bernkop-Schnurch, A., Kast, C. E. and Guggi, D., 2003. Permeation enhancing polymers in oral delivery of hydrophilic macromolecules: thiomer/GSH systems. J. Control. Release, 93, 95–103.

Betancourt, T., Shah, K. and Brannon-Peppas, L., 2009. Rhodamine-loaded poly(lactic-co-glycolic acid) nanoparticles for in vitro interactions with breast cancer cells. J. Mater. Sci. Mater. Med., 20, 387-395.

Bhagavan, H. N. and Chopra, R. K., 2006. Coenzyme Q10: Absorption, tissue uptake, metabolism and pharmacokinetics. Free Radic. Res., 40, 445-453.

Bhagavan, H. N. and Chopra, R. K., 2007. Plasma coenzyme Q10 response to oral ingestion of coenzyme Q10 formulations. Mitochondrion, 7, S78-S88.

Bhardwaj, V., Ankola, D. D., Gupta, S. C., Schneider, M., Lehr, C.-M. and Kumar, M. N. V. R., 2009. PLGA nanoparticles stabilized with cationic surfactant: Safety studies and application in oral delivery of paclitaxel to treat chemical induced breast cancer in rat. Pharm. Res., 26, 2495-2503.

Bhardwaj, V., Hariharan, S., Bala, I., Lamprecht, A., Kumar, N., Panchagnula, R. and Kumar, M. N. V. R., 2005. Pharmaceutical aspects of polymeric nanoparticles for oral delivery. J. Biomed. Nanotechnol., 1, 235-258.

Blanco, M. D. and Alonso, M. J., 1997. Development and characterization of protein-loaded poly(lactide-co-glycolide) nanospheres. Eur. J. Pharm. Biopharm., 43, 287-294.

Borel, J. F., Feurer, C., Glubler, H. U. and Stahelin, H., 1976. Biological effects of Cyclosporine A; a new antilymphocytic agent. Agents Actions, 6, 468-475.

Brown, B. G., Zhao, X.-Q., Chait, A., Fisher, L. D., Cheung, M. C., Morse., J. S., Dowdy, A. A., Marino, E. K., Bolson, E. L. and *et al*., 2001.

Simvastatin and niacin, antioxidant vitamins, or the combination for the prevention of coronary disease. N. Engl. J. Med., 345, 1583-1592.

Bruno, C., Anzinger, J. J., Amar, M. and Kruth, H. S., 2009. Fluorescent pegylated nanoparticles demonstrate fluid-phase pinocytosis by macrophages in mouse atherosclerotic lesions. J. Clin. Invest., 119, 1373-1381.

Brynskov, J., Freund, L., Rasmussen, S. N., Lauritsen, K., de Muchadell, O. S., Williams, N., MacDonald, A. S., Tanton, R., Molina F. and *et al*., 1989. A placebo-controlled, double-blind, randomized trial of cyclosporine therapy in active chronic Crohn's disease. N. Engl. J. Med., 321, 845-850.

Bunjes, H., Drechsler, M., Koch, M. H. J. and Westesen, K., 2001. Incorporation of the model drug Ubidecarenone into solid lipid nanoparticles. Pharm. Res., 18, 287-293.

Burdmann, E. A., Andoh, T. F., Nast, C. C., Evan, A., Connors, B. A., Coffman, T. M., Lindsley, J. and Bennett, W. M., 1995. Prevention of experimental cyclosporin-induced insterstitial fibrosis by losartan and enalapril. Am. J. Physiol., 269, F491–F499.

Buxton, G. A. and Clarke, N., 2007. Drug diffusion from polymer core–shell nanoparticles. Soft Matter, 3, 1513-1517.

Cahn, J. W. and Hilliard, J. E., 1958. Free energy of a nonuniform system. I. Interracial free energy. J. Chem. Phys., 28, 258-267.

Capasso, G., Di, G. C. I., Della, R. F., Manna, C., Ciarcia, R., Florio, S., Perna, A., Pollastro, R. M., Damiano, S. and *et al*., 2008. In vivo effect of the natural antioxidant hydroxytyrosol on cyclosporine nephrotoxicity in rats. Nephrol. Dial. Transplant., 23, 1186–1195.

Cecka, J. M. and Terasakai, P. I., 1991. The UNOS Scientific Renal Transplant Registry. Clin. Transpl., 1-11.

Cerbai, B., Solaro, R. and Chiellini, E., 2008. Synthesis and Characterization of Functional Polyesters Tailored for Biomedical Applications. J. Polym. Sci. A: Polym. Chem., 46, 2459–2476.

Chander, V., Tirkey, N. and Chopra, K., 2005. Resveratrol, a polyphenolic phytoalexin protects against cyclosporine-induced nephrotoxicity through nitric oxide dependent mechanism. Toxicology, 210, 55–64.

Chen, H. and Langer, R., 1998. Oral particulate delivery: status and future trends. Adv. Drug Del. Rev., 34, 339-350.

Chenga, J., Teply, B. A., Sherifi, I., Sung, J., Luther, G., Gu, F. X., Nissenbaum, E. L., Moreno, A. F. R., Langer, R. and Farokhzad, O. C., 2007. Formulation of functionalized PLGA–PEG nanoparticles for in vivo targeted drug delivery. Biomaterials, 28, 869–876.

Chernenko, T., Matthaus, C., Milane, L., Quintero, L., Amiji, M. and Diem, M., 2009. Label-free raman spectral imaging of intracellular delivery and degradation of polymeric nanoparticle systems. ACS Nano, 3, 3552-3559.

Chiellini, E., Chiellini, E. E., Chiellini, F. and Solaro, R., 2001. Targeted Administration of Proteic Drugs. I. Preparation of Polymeric Nanoparticles. J. Bioact. Compat. Polym., 16, 441–465.

Chiu, Y. Y., Higaki, K., Neudeck, B. L., Barnett, J. L., Welage, L. S. and Amidon, G. L., 2003. Human Jejunal Permeability of Cyclosporin A: Influence of Surfactants on P-Glycoprotein Efflux in Caco-2 Cells. Pharm. Res., 5, 749-756.

Chopra, R., Goldmann, R., Siantra, S. and Bhagava, H., 1998. Relative bioavailability of Coenzyme Q10 formulations in human subjects. Int. J. Vitam. Nutr. Res., 68, 109-113.

Conger, J. D., Kim, G. E. and Robinette, J. B., 1994. Effect of AngII, ETA, and TxA2 receptor antagonists on cyclosporin A renal vasoconstriction. Am. J. Physiol., 267, F443-F449.

Conklin, K. A., 2005. Coenzyme Q10 for Prevention of Anthracycline-induced cardiotoxicity. Integrative Cancer Therapies., 4, 110-130.

Crane, F. L., 2001. Biochemical functions of coenzyme Q10. J. Am. Coll. Nutr., 20, 591–598.

Crane, F. L., Hatefi, Y., Lester, R. I., and Widmer, C., 1957. Isolation of a quinone from beef heart mitochondria. Biochim. Biophys. Acta, 25, 220–221.

Cristol, J. P., Vela, C., Maggi, M. F., Descomps, B. and Mourad, G., 1998. Oxidative stress and lipid abnormalities in renal transplant recipients with or without chronic rejection. Transplantation, 65, 1322-1328.

Czogalla, A., 2009. Oral cyclosporine A – the current picture of its liposomal and other delivery systems. Cell. Mol. Bio. Lett., 14, 139-152.

D'Antone, S., Bignotti, F., Sartore, L., D'Amore, A., Spagnoli, G. and Penco, M., 2001. Thermogravimetric investigation of two classes of block copolymers based on poly(lactic-glycolic acid) and poly(e-caprolactone) or poly(ethylene glycol). Poly. Degrad. Stab., 74, 119-124.

D'Souza, S. S. and DeLuca, P. P., 2006. Methods to assess in vitro drug release from injectable polymeric particulate system. Pharm. Res., 23, 460-474.

Dai, J., Nagai, T., Wang, X., Zhang, T., Meng, M. and Zhang, Q., 2004. pH-sensitive nanoparticles for improving the oral bioavailability of cyclosporine A. Int. J. Pharm., 280, 229-240.

Damgé, C., Maincent, P. and Ubrich N., 2007. Oral delivery of insulin associated to polymeric nanoparticles in diabetic rats. J. Control. Release, 117, 163-170.

David-Neto, E., Lemos, F. B. C., Furusawa, E. A., Schwartzman, B. S., Cavalcante, J. S., Yagyu, E. M., Romano, P. and Ianhez L. E., 2000. Impact of Cyclosporin A Pharmacokinetics on the Presence of Side Effects in Pediatric Renal Transplantation. J. Am. Soc. Nephrol., 11, 343–349.

de Mattos, A. M., Olyaei, A. J. and Bennett, W. M., 2000. Nephrotoxicity of immunosuppressive drugs: long-term consequences and challenges for the future. Am. J. Kidney Dis., 35, 333-346.

Delie, F., 1998. Evaluation of nano- and microparticle uptake by the gastrointestinal tract. Adv. Drug Del. Rev., 34, 221-233.

Delpouve, N., Saiter, A., Mano, J. F. and Dargent, E., 2008. Cooperative rearranging region size in semi-crystalline poly(L-lactic acid). Polymer, 49, 3130–3135.

des Rieux, A., Fievez, V., Garinot, M., Scheider, Y.-J. and Preat, V., 2006. Nanoparticles as potential oral delivery systems of proteins and vaccines: A mechanistic approach. J. Control. Rel., 116, 1-27.

Desai, M. P., Labhasetwar, V., Amidon, G. L. and Levy, R. J., 1996. Gastrointestinal uptake of biodegradable microparticles: effect of particle size. Pharm. Res., 13, 1838-1845.

Desai, M. P., Labhasetwar, V., Walter, R. J., Levy, R. J. and Amidon, G. L., 1997. The mechanism of uptake of biodegradable microparticles in Caco-2 cells is size dependent. Pharm. Res., 14, 1568-1573.

Desai, S. J., Singh, P., Simonelli, A. P. and Higuchi, W. I., 1966. Investigation of factors influencing release of solid drug dispersed in wax matrices. III. Quantitative studies involving polyethylene plastic matrix. J. Pharm. Sci., 55, 1230-1234.

Digiesi, V., Cartini, F., Oradei, A., Bisi, G., Guarino, G. C., Brocchi, A., Bellandi, F., Mancini, M. G. and Littaru, G. P., 1994. Coenzyme Q10 in essential hypertension. Mol. Aspects Med., 15, S257-S263.

Djamali, A., Reese, S., Yracheta, J., Oberely, T., Hullett, D. and Backer, B., 2005. Epithelial-to-mesenchymal transition and oxidative stress in chronic allograft nephropathy. Am. J. Transplant., 5, 500-509.

Dunn, C. J., Wagstaff, A. J., Perry, C. M., Plosker, G. L. and Goa, K. L., 2001. Cyclosporin: An updated review of the pharmacokinetic properties, clinical efficacy and tolerability of a microemulsion-based formulation (Neoral®) in organ transplantation. Drugs, 61, 1957-2016.

Durak, I., Karabacak, H. I., Buyukkocak, S., Cimen, M. Y., Kacmaz, M., Omeroglu, E. and Ozturk, H. S., 1998. Impaired antioxidant defense system in the kidney tissues from rabbits treated with cyclosporine. Protective effects of vitamins E and C. Nephron., 78, 207-211.

Dye, D. and Watkins, J., 1980. Suspected anaphylactic reaction to cremophor EL. Br. Med. J., 280, 1353.

El-Shabouri, M. H., 2002. Positively charged nanoparticles for improving the oral bioavailability of cyclosporine-A. Int. J. Pharm., 249, 101-108.

El-Tayar, N., Mark, A. E., Vallat, P., Brunne, R. M., Testa, B. and van Gunsteren, W. F., 1993. Solvent-dependent conformation and hydrogen-bonding capacity of cyclosporin A: evidence from partition coefficients and molecular dynamics simulations. J. Med. Chem., 36, 3757-3764.

Elzinga, L. W., Rosen, S. and Bennett, W. M., 1993. Dissociation of glomerular filtration rate from tubulointerstitial fibrosis in experimental chronic cyclosporine nephropathy; the role of sodium intake. J. Am. Soc. Nephrol., 4, 214–221.

Emery, R. W., Cork, R., Christensen, R., Levinson, M. M., Icenogle, T. B., Riley, J., Ott, R. A. and Copeland, J. G., 1986. Cardiac transplant patient at one year. Cyclosporine vs conventional immunosuppression. Chest, 90, 29-33.

European multicentre trial group, 1983. Cyclosporin in cadaveric renal transplantation: one-year follow-up of a multicentre trial. Lancet, 2, 986-989.

Fahr, A., 1993. Cyclosporine clinical pharmacokinetics. Clin. Pharmacokinet., 24, 472-495.

Fahr, A., Holz, M. and Fricker, G., 1995. Liposomal formulations of Cyclosporin A: influence of lipid type and dose on pharmacokinetics. Pharm. Res., 12, 1189-1197.

Faulds, D., Goa, K. L., and Benfield, P., 1993. Cyclosporin. A review of its pharmacodynamic and pharmacokinetic properties, and therapeutic use in immunoregulatory disorders. Drugs, 45, 953-1040.

Fessi, H., Puisieux, F., Devissaguet, J. P., Ammoury, N. and Benita, S., 1989. Nanocapsule formation by interfacial polymer deposition following solvent displacement. Int. J. Pharm. 55, R1–R4.

Florence, A. T., 1997. The oral absorption of micro- and nanoparticulates: Neither Exceptional Nor Unusal. Pharm. Res., 14, 259-266.

Florence, A. T., 2004. Issues in oral nanoparticle drug carrier uptake and targeting. J. Drug Target., 12, 65-70.

Florence, A. T., 2005. Nanoparticle uptake by the oral route: Fulfilling its potential? Drug Discov. Today Technol., 2, 75-81.

Florence, A. T., 2007. Pharmaceutical nanotechnology: More than size Ten topic for research. Int. J. Pharm., 339, 1-2.

Flory, P. J., 1953. Principles of Polymer Chemistry, Cornell University Press New York.

Folkers, K., Langsjoen, P., Willis, R., Richardson, P. Xia, L. J., Ye, C. Q. and Tamagawa, H., 1990. Lovastatin decreases coenzyme Q10 levels in humans. Proc. Natl. Acad. Sci., 87, 8931-8934.

Folkers, K., Wolaniuk, A., Vadhanavikit, S., Sakmato, N., Takemura, K., Baker, L. and Richardson, P. C., 1986. Biomedical and clinical research on coenzyme Q10 with emphasis on cardiac patients. In: Folkers. K., Yamamura, Y., eds. Biomedical and Clinical Aspects of Coenzyme Q. Amsterdam: Elsevier, p. 375–391.

Fontana, A., De Maria, P., Siani, G. and Robinson, B. H., 2003. Kinetics of breakdown of vesicles from dididecyldimethylammonium bromide induced by single chain surfactants and by osmotic stress in aqueous solution. Colloids Surf. B: Biointerface, 32, 365-374.

Francis, M. F., Cristea, M., Yang, Y. and Winnik, F. M., 2005. Engineering polysaccharide-based polymeric micelles to enhance permeability of cyclosporine A across Caco-2 cells. Pharm. Res., 22, 209-219.

Freeman. D., Grant, D., Levy, G., Rochon, J., Wong, P.-Y., Altraif, I. and Asfar, S., 1995. Pharmacokinetics of a new oral formulation of cyclosporine in liver transplant recipients. Ther. Drug Monit., 17, 213–216.

Freise, C. E., Liu, T., Hong, K. L., Osorio, R. W., Papahadjopoulos, D., Ferrell, L., Ascher, N. L. and Roberts, J. P., 1994. The increased efficacy and decreased nephrotoxicity of a cyclosporine liposome. Transplantation, 57, 928-932.

Fricker, G., Drewe, J., Huwyler, J., Gutmann, H. and Beglinger, C., 1996. Relevance of p-glycoprotein for the enteral absorption of cyclosporin A: in vitro in vivo correlation. Br. J. Pharmacol., 118, 1841-1847.

Gebert, A., Rothkotter, H. J. and Pabst, R., 1996. M cells in Peyer's patches of the intestine. Int. Rev. Cytol., 167, 91-159.

Ghasemian, S. R., Light, J. A., Currier, C., Sasaki, T. M. and Aquino, A., 2001. Tacrolimus vs Neoral in renal and renal/pancreas transplantation. Clin. Transplant., 13, 123–125.

Gimenez, S., Ponsart, S., Coudane, J. and Vert, M., 2001. Synthesis, properties and in vitro degradation of carboxyl-bearing PCL. J. Bioact. Compt. Polym., 16, 32-37.

Gomez, D., Wacher, V., Tomlanovich, S., Herbert, M. and Benet, L., 1995. The effects of ketoconazole on the intestinal metabolism and bioavailability of cyclosporine. Clin. Pharmacol. Ther., 58, 15–19.

Gorantla, V. S., Barker, J. H., Jones, J. W., Prabhune, K., Maldonado, C. and Granger, D. K., 2000. Immunosuppressive agents in transplantation: mechanisms of action and current anti-rejection strategies. Microsurgery, 20, 420-429.

Górecki, D. C., Jakóbisiak, M., Kruszewski, A. and Laser, W., 1991. Evidence that liposome incorporation of Cyclosporine reduces its toxicity and potentiates its ability to prolong survival of cardiac allografts in mice. Transplantation, 52, 766-769.

Grant, D., Kneteman, N., Tchervenkov, J., Roy, A., Murphy, G., Tan, A., Hendricks, L., Guilbault, N. and Levy, G., 1999. Peak cyclosporine levels (Cmax) correlate with freedom from liver graft rejection: results of a prospective, randomized comparison of neoral and sandimmune for liver transplantation (nof-8)1,2. Transplantation, 67, 1133-1137.

Greenberg, S. and Frishman, W. H., 1990. Coenzyme Q10: A new drug for cardiovascular disease. J. Clin. Pharmacol., 30, 590–608.

Gref, R., Luck, M., Quellec, P., Marchand, M., Dellacherie, E., Harnisch, S., Blunk, T. and Muller, R. 2000. 'Stealth' corona-core nanoparticles surface modified by polyethylene glycol (PEG): influences of the corona (PEG chain length and surface density) and of the core composition on phagocytic uptake and plasma protein adsorption. Colloids Surf. B: Biointerf., 18, 301-313.

Gref, R., Minamitake, Y., Peracchia, M. T., Trubetskoy, V., Torchilin, V. and Langer, R., 1994. Biodegradable long-circulating nanospheres. Science, 263, 1600–1603.

Gref, R., Quellec, P., Sanchez, A., Calvo, P., Dellacherie, E. and Alonso, M. J., 2001. Development and characterization of CyA-loaded poly(lactic acid)-poly(ethylene glycol)PEG micro- and nanoparticles. Comparison with conventional PLA particulate carriers. Eur. J. Biopharm. Pharm., 51, 111-118.

Guarrero, Q., Allemann, E., Fessi, H. and Doelker, E., 1996. Influence of stabilizing agents and preparative variables on the formation of poly(-lactic acid) nanoparticles by an emulsification-diffusion technique. Int. J. Pharm., 143, 133-141.

Guo, J., Ping, Q. and Chen, Y., 2001. Pharmacokinetic behavior of cyclosporin A in rabbits by oral administration of lecithin vesicle and sandimmun neoral. Int. J. Pharm., 216, 17-21.

Gursoy, R. N. and Benita, S., 2004. Self-emulsifying drug delivery systems (SEDDS) for improved oral delivery of lipophilic drugs. Biomed. Pharmacother., 58, 173-182.

Guzman, M., Molpeceres, J. Garcia, F., Aberturas, M. R. and Rodriguez, M., 1993. Formation and characterization of cyclosporine-loaded nanoparticles. J. Pharm. Sci., 82, 498–502.

Haas, J. and Lehr, C. M., 2002. Developments in the area of bioadhesive drug delivery systems. Expert Opin. Biol. Ther., 2, 287–298.

Hamel, A. R., Hubler, F., Carrupt, A., Wenger, R. M. and Mutter, M., 2004. Cyclosporin A prodrugs: design, synthesis and biophysical properties. J. Peptide Res., 63, 147-154.

Hans, M. L. and Lowman. A. M., 2002. Biodegradable nanoparticles for drug delivery and targeting. Curr. Opin. Solid State Mater. Sci., 6, 319-327.

Hansen, J. M., Fogh-Andersen, N., Christensen, N. J. and Strandgaard, S., 1997. Cyclosporine-induced hypertension and decline in renal function in healthy volunteers. J. Hypertens., 15, 319–326.

Hariharan, S., Bhardwaj, V., Bala, I., Sitterberg, J., Bakowsky, U. and Kumar, M. N. V. R., 2006. Design of estradiol loaded PLGA nanoparticulate formulations: a potential oral delivery system for hormone therapy Pharm. Res., 23, 184-196.

Hau, N. and Sun, J., 2006. Synthesis and application of PLGA labeled with ^{125}I. Nuclear Sci. Techniq., 17, 48-52.

Hau, N. and Sun, J., 2008. Body distribution of poly(D,L-lactide-co-glycolide) copolymer degradation products in rats. J. Mater. Sci. Mater. Med., 19, 3243-3248.

Hebert, M. F., 1997. Contributions of hepatic and intestinal metabolism and P-glycoprotein to cyclosporine and tacrolimus oral drug delivery. Adv. Drug. Deliv. Rev., 27, 201-214.

Higuchi, T., 1963. Mechanism of sustained action medication, theoretical analysis of rate of release of solid drugs dispersed in solid matrices. J. Pharm. Sci. 52, 1145-1149.

Hixson, A. W. and Crowell, J. H., 1931. Dependence of reaction velocity upon surface and agitation: I— Theoretical consideration. Ind. Eng. Chem., 23, 923-931.

Ho. V. C., Griffiths, C. E. M., Albrecht, G., Vanaclocha, F., Leon-Dorantes, G., Atakan, N., Reitamo, S., Johannesson, A., Mork, N. J. and *et al*., 1999. Intermittent short courses of cyclosporin (Neoral®) for psoriasis unresponsive to topical therapy: a 1-year multicentre, randomized study. Br. J. Dermatol., 141, 283-291.

Hong, J. C., Kahan, B. D., 2000. Sirolimus-induced thrombocytopenia and leukopenia in renal transplant recipients: Risk factors, incidence, progression, and management. Transplantation, 69, 2085-2090.

Hu, D. S.-G. and Liu, H.-J., 1994. Structural analysis and degradation behavior in polyethylene glycol/poly(L-lactide) copolymers J. Appl. Polym. Sci., 51, 473–482.

Hussain, N., Jaitley, V. and Florence, A. T., 2001. Recent advances in the understanding of uptake of microparticulates across the gastrointestinal lymphatics. Adv. Drug Del. Rev. 50, 107-142.

Iacono, A. T., Smaldone, G. C., Keenan, R. J., Diot, P., Dauber, J. H., Zeevi, A., Burckart, G. J. and Griffith, B. P., 1997. Dose-related reversal of acute lung rejection by aerosolized cyclosporine. Am. J. Crit. Care Med., 155, 1690-1698.

Igarashi, T., Nakajima, Y., Tanaka, M. and Otake, S., 1974. Effect of coenzyme Q10 on experimental hypertension in rats and dogs. J. Pharmacol. Exp. Ther., 189, 149-156.

Igarashi, T., Tanabe, Y., Nakajima, Y., Kobayashi, M., Tanaka, M. and Ohtake, S., 1972. Effect of coenzyme Q10 on experimental hypertension in the desoxycorticosterone acetate-saline loaded rats. Folia Pharamacol. Jap., 68, 460-472.

Italia, J. L., Bhardwaj, V. and Kumar, M. N. V. R., 2006. Disease, destination, dose and delivery aspects of cyclosporine: The state of the art. Drug Discov. Today, 11, 846-854.

Italia, J. L., Bhatt, D K., Bhardwaj, V., Tikoo, K. and Kumar, M. N. V. R., 2007. PLGA nanoparticles for oral delivery of cyclosporine: Nephrotoxicity and pharmacokinetic studies in comparison to Sandimmune Neoral®. J. Control. Rel., 119, 197-206.

Italia, J. L., Datta, P., Ankola D. D. and Kumar, M. N. V. R., 2008. Nanoparticles enhance per oral bioavailability of poorly available molecules: Epigallocatechin gallate nanoparticles ameliorates cyclosporine induced nephrotoxicity in rats at three times lower dose than oral suspension. J. Biomed. Nanotechnol., 4, 304-312.

Jani, P. U., McCarthy, D. E. and Florence, A. T., 1992. Nanosphere and microsphere uptake via Peyer's patches: observation of the rate of uptake in rat after a single oral dose. Int. J. Pharm., 86, 239-246.

Jani, P., Halbert, G. W., Langridge, J. and Florence, A.T. 1990. Nanoparticle uptake by the rat gastrointestinal mucosa: quantitation and particle size dependency. J. Pharm. Pharmacol., 42, 821–826.

Jiko, M., Yano, I., Wakasugi, H., Saito, H. and Inui, K., 2002. Evaluation of pharmacokinetic interaction between cyclosporin A and probucol in rats. Pharm. Res., 9, 1362-1367.

Jung, T., Kamm, W., Breitenbach, A., Kaiserling, E., Xiao, J. X. and Kissel, T., 2000. Biodegradable nanoparticles for oral delivery of peptides: is there

a role for polymers to affect mucosal uptake? Eur. J. Pharm. Biopharm., 50, 147-160.

Kahan, B. D., 1989. Cyclosporine. N. Engl. J. Med., 321, 1725-1738.

Kahan, B. D., 2004. Therapeutic Drug Monitoring of Cyclosporine: 20 Years of Progress. Transplant. Proc., 36, 378S-391S.

Kahan, B. D., 2008. Fifteen years of clinical studies and clinical practice in renal transplantation: reviewing outcomes with *de novo* use of sirolimus in combination with cyclosporine. Transplant. Proc., 40, S17-S20.

Kaikkonen, J., Nyyssonen, K., Porkkala-Sarataho, E., Poulsen, H. E., Metsa-Ketela, T., Hayn, M., Salonen, R., Salonen, J. T., 1997. Effect of oral coenzyme Q10 supplementation on the oxidation resistance of human VLDL+LDL fraction: absorption and antioxidative properties of oil and granule-based preparations. Free Radic. Biol. Med., 22, 1195–1202.

Kalaria, D. R., Sharma, G., Beniwal, V. and Kumar, M. N. V. R., 2009. Design of biodegradable nanoparticles for oral delivery of Doxorubicin: In vivo pharmacokinetics and toxicity studies in rats. Pharm. Res., 26, 492-501.

Kato, T., Yoneda, S., Kako, T., Koketsu, M., Hayano, I. and Fujinmani, T., 1990. Reduction in blood viscosity by treatmentwith coenzyme Q10 in patients with ischemic heart disease. Int. J. Clin. Pharmacol. Ther. Toxicol. 28, 123-126.

Kelly, P. A., Wang, H., Napoli, K. L., Kahan, B. D. and Strobel, H. W., 1999. Metabolism of cyclosporine by cytochromes P450 3A9 and 3A4. Eur. J. Drug Metab. Pharmacokinet., 24, 321-328.

Khandare, J. and Minko, T., 2006. Polymer–drug conjugates: Progress in polymeric prodrugs. Prog. Polym. Sci., 31, 359–397.

Kharb, V., Bhatia, M., Dureja, H. and Kaushik, D., 2006. Nanoparticle technology for the delivery of poorly water-soluble drugs. Pharm. Technol., Feb 2.

Kim, H. R., Andrieux, K., Delomenie, C., Chacun, H., Appel, M., Desmaele, D., taran, F., Goeorgin, D., Couvreur, P. and Taverna, M., 2007. Analysis of plasma protein adsorption onto PEGlyated nanoparticles by complementary methods: 2-DE, CE and Protein Lab on chip system. Electrophoresis, 28, 2252-2261.

Kim, S. T., Jang, D. J., Kim, J. H., Park, J. Y., Lim, J. S., Lee, S. Y., Lee, K. M., Lim, S. J. and Kim, C. K., 2009. Topical administration of cyclosporin A in a solid lipid nanoparticle formulation. Pharmazie, 64, 510-514.

Kim, S., Kim, J. H., Jeon, O., Kwon, I. C. and Park, K., 2009. Engineered polymers for advanced drug delivery. Eur. J. Pharm. Biopharm., 71, 420–430.

Kitchell, J. P. and Wise, D. L., 1985. Poly(lactic/glycolic acid) biodegradable drug-polymer matrix systems. Methods Enzymol., 112, 436-448.

Kommuru, T. R., Gurley, B., Khan, M. A. and Reddy, I. K., 2001. Self-emulsifying drug delivery systems (SEDDS) of coenzyme Q10: formulation development and bioavailability assessment. Int. J. Pharm., 212, 233-246.

Korsmeyer, R. W., Gurny, R., Doelker, E. M., Buri, P. and Peppas, N. A., 1983. Mechanism of solute release from porous hydrophilic polymers. Int. J. Pharm., 15, 25-35.

Kreuter, J., Ramge, P., Petrov, V., Hamm, S., Gelperina, S. E., Engelhardt, B., Alyautdin, R., von Briesen, H. and Begley, D. J., 2003. Direct evidence that polysorbate-80-coated poly(butylcyanoacrylate) nanoparticles

deliver drugs to the CNS via specific mechanisms requiring prior binding of drug to the nanoparticles. Pharm. Res., 20, 409-416.

Kronbach, T., Fischer, V. and Meyer, U. A., 1988. Cyclosporine metabolism in human liver: identification of a cytochrome P-450III gene family as the major cyclosporine-metabolizing enzyme explains interactions of cyclosporine with other drugs. Clin. Pharmacol. Ther., 43, 630-635.

Kumari, A., Yadav, S. K. and Yadav, S. C., 2010. Biodegradable polymeric nanoparticles based drug delivery systems. Colloids Surf. B: Biointerf., 1, 1-18.

Kunitomo, M., Yamaguchi, Y., Kagota, S. and Otsubo, K., 2008. Beneficial effect of Coenzyme Q10 on increased oxidative and nitrative stress and inflammation and individual metabolic components developing in a rat model of metabolic syndrome. J. Pharmacol. Sci., 107, 128-137.

Kwon, H. Y., Lee, J. Y., Sung, W. C. and Jang, Y., 2001. Preparation of PLGA nanoparticles containing estrogen by emulsification-diffusion method. Colloids Surf. A: Physicochem. Eng. Asp., 182, 123-130.

Kwon, S. S., Nam, Y. S., Lee, J. S., Ku, B. S., Han, S. H., Lee, J. Y. and Chang, I. S., 2002. Preparation and characterization of coenzyme Q10-loaded PMMA nanoparticles by a new emulsification process based on microfluidization. Coll. Surf. A: Physico. Eng. Asp., 210, 95-104.

Lai, J., Lu, Y., Yin, Z., Hu, F. and Wu, W., 2010. Pharmacokinetics and enhanced oral bioavailability in beagle dogs of cyclosporine A encapsulated in glyceryl monooleate/poloxamer 407 cubic nanoparticles. Int. J. Nanomedicine, 5, 13-23.

Lai, S. K., O'Hanlon, D. E., Harrold, S., Man, S. T., Wang, Y. Y., Cone, R. and Hanes, J., 2007. Rapid transport of large polymeric nanoparticles in

fresh undiluted human mucus. Proc. Natl. Acad. Sci. USA, 104, 1482-1487.

Lallemand, F., Perottet, P., Felt-Baeyens, O., Kloeti, W., Philippoz, F., Marfurt, J., Besseghir, K. and Gurny, R., 2005. A water-soluble prodrug of cyclosporine A for ocular application: a stability study. Eur. J. Pharm. Sci., 26, 124-129.

Lallemand, F., Varesio, E., Felt-Baeyens, O., Bossy, L., Hopfgartner, G. and Gurny, R. 2007. Biological conversion of a water-soluble prodrug of cyclosporine A. Eur. J. Pharm. Biopharm., 67, 555-561.

Lamprecht, A., Ubrich, N., Perez, M. H., Lehr, C. M. and Hoffman, M., 2000. Influences of process parameters on nanoparticle preparation performed by a double emulsion pressure homogenisation technique. Int. J. Pharm., 196, 177-182.

Lanese, D. M. and Conger, J. D., 1993. Effects of endothelin receptor antagonist on cyclosporine-induced vasoconstriction in isolated rat renal arterioles. J. Clin. Invest., 91, 2144-2149.

Langsjoen, P. H., Langsjoen, P. H. and Folkers, K., 1993. Isolated diastolic dysfunction of the myocardium and its response to CoQ10 treatment. Clin. Investig., 71, S140–S144.

Le Ray, A. M., Vert, M., Gautier, J. C. and Benoit, J. P., 1994. Fate of [^{14}C]poly(DL-lactide-co-glycolide) nanoparticles after intravenous and oral administration to mice. Int. J. Pharm., 106, 201-211.

Lee, D. B., 1997. Cyclosporine and the renin-angiotensin axis. Kidney Int., 52, 248-260.

Lee, E. J., Lee, S. W., Choi, H. G. and Kim, C. K., 2001. Bioavailability of cyclosporin A dispersed in sodium lauryl sulfate-dextrin based solid microspheres. Int. J. Pharm., 218, 125-131.

Lee, S., Kim, S., Han, Y. and Kim, Y., 2001. Synthesis and degradation of end-group -functionalized polylactide. J. Polym. Sci. Polym. Chem., 39, 973-985.

Legg, B. and Rowland, M., 1987. Cyclosporin: measurement of fraction unbound in plasma. J. Pharm. Pharmacol., 39, 599-603.

Legg, B., Gupta, S. K., Rowland , M., Johnson, R. W. and Solomon, L. R., 1998. Cyclosporin: pharmacokinetics and detailed studies of plasma and erythrocyte binding during intravenous and oral administration. Eur. J. Clin. Pharmacol., 34, 451-460.

Lexis, L. A., Fenning, A., Brown, L., Fassett, R. G. and Coombes, J. S., 2006. Antioxidant Supplementation Enhances Erythrocyte Antioxidant Status and Attenuates Cyclosporine-Induced Vascular Dysfunction. Am. J. Transplant., 6, 41-49.

Lichtiger, S., Present, D. H., Kornbluth, A., Gelernt, I., Bauer, J., Galler, G., Michelassi, F. and Hanauer S., 1994. Cyclosporine in severe ulcerative colitis refractory to steroid therapy. N. Engl. J. Med., 330, 1841-1845.

Lindhlom, A., 1991. Factors influencing the pharmacokinetics of cyclosporine in man. Ther. Drug Monit., 13, 465-477.

Lindholm, A., and Kahan, B. D., 1993. Influence of cyclosporine pharmacokinetics, trough concentrations, and AUC monitoring on outcome after kidney transplantation. Clin. Pharmacol. Ther., 54, 205-218.

Ling, H., Li, X., Jha, S., Wang, W., Karetskaya, L., Pratt, B. and Ledbetter, S., 2003. Therapeutic role of TGF-betaneutralizing antibody in mouse cyclosporin A nephropathy: morphologic improvement associated with functional preservation. J. Am. Soc. Nephrol., 14, 377-388.

Littaru, G. P. and Tiano, L., 2010. Clinical aspects of coenzyme Q10: an update. Nutrition, 26, 250-254.

Lockwood, K., Moesgard, S. and Folkers, K., 1994. Partial and complete regression of breast cancer in patients in relation to dosage of coenzyme Q10. Biochem. Biophys. Res. Commun., 199, 1504-1508.

Lown, K. S., Mayo, R. R., Leichtman, A. B., Hsiao, H. L. Turgeon, D. K., Schmiedlin-Ren, P., Brown, M. B., Guo, W. and Rossi, S. J., 1992. Role of intestinal P- glycoprotein (mdr1) in interpatient variation in the oral bioavailability of cyclosporine. Clin. Pharmacol. Ther., 62, 248-260.

Malyszko, J., Malyszko, J. S., Pawlak, K. and Mysliwiec, M., 1996. The coagulo-lytic system and endothelial function in cyclosporine-treated kidney allograft recipients. Transplantation, 62, 828-830.

Manchala, R., 2010. M.S. Thesis. Methods to quantify Coenzyme Q10 in biological samples by liquid chromatography-mass spectrometry. Strathclyde Institute of Pharmacy and Biomedical Sciences, University of Strathclyde, Glasgow. UK.

Manez, R., Jain, A., Marino, I. R. and Thomson, A. W., 1995. Comparative evaluation of tacrolimus (FK506) and cyclosporine a as immunosuppressive agents. Transplant. Rev. 9, 63–76.

Mao, H., Kadiyala, I., Leong, K. W., Zhao, Z. and Dang, W., 1999. In Encyclopedia of controlled drug delivery; Mathiowitz, E., Ed.; Wiley – Interscience: New York, vol. 1, pp 45–60.

McCarthy, M. F. 1999. Coenzyme Q versus hypertension: does CoQ decreases endothelial superoxide generation? Med. Hypotheses, 53, 300-304.

McNamee, C. E., Aso, Y., Yamamoto, S., Fukumori, Y., Ichikawa, H. and Higashitani, K., 2007. Chemical groups that adhere to the surfaces of living malignant cells. Pharm. Res. 24, 2370–2380.

Meena, A. K., Ratnam, D. V., Chandraiah, G., Ankola, D. D., Ramarao, P. and Kumar, M. N. V. R., 2008. Oral Nanoparticulate Atorvastatin Calcium is More Efficient and Safe in Comparison to Lipicure® in Treating Hyperlipidemia. Lipids, 43, 231-241.

Mehta, M. U., Venkataramanan, R., Burckart, G. J., Ptachcinski, R. J., Delamos, B., Stachak, S., Heil, D. H. V., Iwatsuki, S. and Starzl, T. E., 1998. Effect of bile on cyclosporine absorption in liver transplant patients. Br. J. Clin. Pharmacol., 25, 579-584.

Merion, R. M., White, D. J. G., Thiru, S., Evans, D. B. and Calne R. Y., 1984. Cyclosporine: five years' experience in cadaveric renal transplantation. N. Engl. J. Med., 310, 148-154.

Mervaala, E. M. A., Pere, A.-K., Lindgren, L., Laakso, J., Teräväinen, T.-L., Karjala, K., Vapaatalo, H., Ahonen, J. and Karppanen, H., 1997. Effects of dietary sodium and magnesium on cyclosporine A-induced hypertension and nephrotoxicity in spontaneously hypertensive rats. Hypertension, 29, 822–827.

Middleton, J. C. and Tipton, A. J., 2001. Synthetic biodegradable polymers as orthopedic devices. Biomaterials, 21, 2335–2346.

Mihatsch, M. J., Antonovych, T., Bohman, S. O., Habib, R., Helmchen, U., Noel, L. H., Olsen, S., Sibley, R. K., Kemeny, E. and *et al*., 1994. Cyclosporin A nephropathy: Standardization of the evaluation of kidney biopsies. Clin. Nephrol., 41, 23-32.

Mihatsch, M. J., Thiel, G. and Ryffel, B., 1988. Histopathology of cyclosporine nephrotoxicity. Transplant. Proc., 3, 759–771.

Mittal, G. and Kumar, M. N. V. R., 2009. Impact of polymeric nanoparticles on oral pharmacokinetics: A dose-dependent case study with estradiol. J. Pharm. Sci., 98, 3730-3734.

Mittal, G., Sahana, D. K., Bhardwaj, V. and Kumar, M. N. V. R., 2007. Estradiol loaded PLGA nanoparticles for oral administration: Effect of polymer molecular weight and copolymer composition on release behavior in vitro and in vivo. J. Control. Rel., 119, 77-85.

Miyazaki, T., Ohtsuki, C., Akioka, Y., Tanihara, M., Nakao, J., Sakaguchi, Y. and Konagaya, S., 2003. Apatite Deposition on Polyamide Films Containing Carboxyl Group in a Biomimetic Solution. J. Mater. Sci. Mater. Med., 2003, 14, 569–574.

Moghimi, S. M., Hunter, A. C. and Murray, J. C., 2001. Long-circulating and target-specific nanoparticles: Theory to practice. Pharmacol. Rev., 53, 283-318.

Mohamed, F. and Van der Walle, C. F., 2008. Engineering Biodegradable Polyester Particles with Specific Drug Targeting and Drug Release Properties. J. Pharm. Sci., 97, 71-87.

Mora-Huertas, C. E., Fessi, H. and Elaissari, A., 2010. Polymer-based nanocapsules for drug delivery. Int. J. Pharm., 385, 113-142.

Morrisett, J. D., Abdel-Fattah, G., Hoogeveen, R., Mitchell, E., Ballantyne, C. M., Pownall, H. J., Opekun, A. R., Jaffe, J. S., Oppermann, S. and *et al*., 2002. Effects of sirolimus on plasma lipids, lipoprotein levels and fatty acid metabolism in renal transplant patients. J. Lipid Res. 43, 1170-1180.

Mueller, E. A., Kovark, J. M., van Bree, J. B., Tetzloff, W., Grevel, J. and Kutz, K., 1994. Improved dose linearity of cyclosporine pharmacokinetics from a microemulsion formulation. Pharm. Res., 11, 301–304.

Mueller, R. H., Runge, S., Ravelli, V., Mehnert, W., Thunemann, A. F. and Souto, E. B., 2006. Oral bioavailability of cyclosporine: solid lipid nanoparticles (SLN®) versus drug nanocrystals. Int. J. Pharm., 317, 82-89.

Muller, R.-F., Kleeberg, I. and Deckwer, W.-D., 2001. Biodegradation of polyesters containing aromatic constitutents. J. Biotechnol., 30, 87-95.

Myers, B. D., Sibley, R., Newton, L., Tomlanovich, S. J., Boshkos, C., Stinson, E., Luetcher, J. A., Whitney, D. J., Krasny D. and *et al*., 1988. The long-term course of cyclosporine-associated chronic nephropathy. Kidney Int., 33, 590–600.

Nahrendroff, M., Zhang, H., Hembrador, S., Panizzi, P., Sosnovik, D. E., Aikawa, E., Libby, P., Swirski, F. K. and Weissleder, R., 2008. Nanoparticle PET-CT Imaging of Macrophages in Inflammatory Atherosclerosis. Circulation, 117, 379-387.

Nair, L. S. and Laurencin, C. T., 2007. Biodegradable polymers as biomaterials. Prog. Polym. Sci., 32, 762-798.

Najib, N and Suleiman, M., 1985. The kinetics of drug release from ethyl cellulose solid dispersions. Drug Dev. Ind. Pharm., 11, 2169-2181.

Nehilla, B. J., Bergkvist, M., Popat, K. C. and Desai, T. A., 2008. Purified and surfactant-free coenzyme Q10-loaded biodegradable nanoparticles. Int. J. Pharm., 348, 107-114.

Neu, M., Sitterberg, J, Bakowsky, U. and Kissel, T., 2006. Stabilized Nanocarriers for Plasmids Based Upon Cross-linked Poly(ethylene imine). Biomacromolecules, 12, 3428-3438.

Newton, C., Gebhardt, B. M. and Kaufman, H. E., 1988. Topically applied cyclosporine in azone prolongs corneal allograft survival. Invest. Opthalmol. Vis. Sci., 29, 208-215.

Okamoto, H., Kawaguchi, H., Togashi, H., Masaru, M., Saito, H. and Yasuda, H., 1991. Effect of coenzyme Q10 on structural alterations in the renal membrane of stroke-prone spontaneously hypertensive rats. Biochem. Med. Metab. Biol., 45, 216-226.

Origlia, N., Migliori, M., Panichi, V., Filippi, C., Bertelli, A., Carpi, A. and Giovannini, L., 2006. Protective effect of L-propionylcarnitine in chronic Cyclosporine-A induced nephrotoxicity. Biomed. Pharmacother., 60, 77–81.

Owens, D. E. and Peppas, N. A., 2006. Opsonization, biodistribution, and pharmacokinetics of polymeric nanoparticles. Int. J. Pharm., 307, 93-102.

Pan, P., Liang, Z., Zhu, B., Dong, T. and Inoue, Y., 2009. Blending Effects on polymorphic crystallization of Poly(l-lactide). Macromolecules, 42, 3374–3380.

Pan, P., Zhu, B., Kai, W., Dong, T. and Inoue, Y., 2008. Polymorphic Transition in Disordered Poly(L-lactide) Crystals Induced by Annealing at Elevated Temperatures, Macromolecules, 41, 4296-4304.

Panagi, Z., Beletsi, A., Evangelatos G., Livaniou, E., Ithakissios, D. S. and Avgoustakis K., 2001. Effect of dose on the biodistribution and pharmacokinetics of PLGA and PLGA–mPEG nanoparticles. Int. J. Pharm., 221, 143–152.

Panyam, J. and Labhasetwar, V., 2003. Biodegradable nanoparticles for drug and gene delivery to cells and tissue. Adv. Drug Del. Rev., 55, 329-347.

Panyam, J., Sahoo, S. K., Prabha, S., Bargar, T. and Labhasetwar, V., 2003. Fluorescence and electron microscopy probes for cellular and tissue uptake of poly(, -lactide-co-glycolide) nanoparticles. Int. J. Pharm., 262, 1-11.

Panyam, J., Williams, D., Dash, A., Leslie-Pelecky, D. and Labhasetwar, V., 2004. Solid-state solubility influences encapsulation and release of hydrophobic drugs from PLGA/PLA nanoparticles. J. Pharm. Sci., 93, 1804-1814.

Peetla, C. and Labhasetwar, V., 2009. Effect of molecular structure of cationic surfactants on biophysical interactions of surfactant-modified nanoparticles with a model membrane and cellular uptake. Langmuir, 25, 2369-2377.

Perico, N., Dadan, J., Remuzzi, G., 1990. Endothelin mediates the renal vasoconstriction induced by cyclosporine in the rat. J. Am. Soc. Nephrol., 1, 76-83.

Perico, N., Ruggenenti, P., Gaspari, F., Mosconi, L., Benigni, A., Amuchastegui, C. S., Gasparini, F. and Remuzzi, G., 1992. Daily renal hypoperfusion induced by cyclosporine in patients with renal transplantation. Transplantation, 54, 56–60.

Petcher, T. J., Weber, H. and Ruegger, A., 1976. Crystal and molecular structure of an iodo-derivative of the cyclic undecapeptide cyclosporin A. Helv. Chim. Acta., 59, 1480-1489.

Pollard, S. G., 2004. Pharmacologic Monitoring and Outcomes of Cyclosporine. Transplant. Proc., 36, 404S–407S.

Quiles, J. L., Ochoa, J. J., Huertas, J. R. and Mataix, J., 2004. Coenzyme Q supplementation protects from age-related DNA double-strand breaks and increases lifespan in rats fed on a PUFA-rich diet. Exp. Gerontol., 39, 189-194.

Quinn, P. J., Fabisiak, J. P. and Kagan, V. E., 1999. Expansion of antioxidant activity of vitamin E by Coenzyme Q. Biofactors, 9, 149-154.

Ratnam, D. V., Chandraiah, G., Meena, A. K., Ramarao, P. and Kumar M. N. V. R., 2009. The co-encapsulated antioxidant nanoparticles of ellagic acid and coenzyme Q10 ameliorates hyperlipidemia in high fat diet fed rats. J. Nanosci. Nanotechnol., 9, 6741-6746.

Ratnam, D. V., Chandraiah, G., Sonaje, K., Viswanad, B., Bhardwaj, V., Ramarao, P. and Kumar M. N. V. R., 2008. A Potential Therapeutic Strategy for Diabetes and Its Complications in the Form of Co-Encapsulated Antioxidant Nanoparticles (NanoCAPs) of Ellagic Acid and Coenzyme Q10: Preparation and Evaluation in Streptozotocin Induced Diabetic Rats. J. Biomed. Nanotech., 4, 33-43.

Reiter, M., Rupp, K., Baumeister, P., Zieger, S. and Harreus, U., 2009. Antioxidant effects of quercetin and coenzyme Q10 in mini organ cultures of human nasal mucosa cells. Anticancer Res., 29, 33-39.

Reynolds, N. J. and Al-Daraji, W. I., 2002. Calcineurin inhibitors and sirolimus: mechanisms of action and applications in dermatology. Rev. Clin. Exp. Dermatol., 27, 555–561.

Rezzani, R., 2004. Cyclosporine A and adverse effects on organs: histochemical studies. Prog. Histochem. Cytochem., 39, 85–128.

Ritschel, W. A., Adolph, S., Ritschel, B. G. and Schroeder, T., 1990. Improvement of peroral absorption of cyclosporin A by microemulsions. Methods Find. Exp. Clin. Pharmacol., 12, 127–134.

Rosenfeldt, F. L., Haas, S. J., Krum, H., Hadj, A., Ng, K., Leong, J. Y. and Watts, G. F., 2007. Coenzyme Q10 in the treatment of hypertension: a meta-analysis of the clinical trials. J. Hum. Hypertens., 21, 297–306.

Ruan, G. and Feng, S. S., 2003. Preparation and characterization of poly(lactic acid)–poly(ethylene glycol)–poly(lactic acid) (PLA–PEG–PLA)

microspheres for controlled release of paclitaxel. Biomaterials, 24, 5037–5044.

Ruiz-Ortega, M. and Egido, J., 1997. Angiotensin II modulates cell growth-related events and synthesis of matrix proteins in renal interstitial fibroblasts. Kidney Int., 52, 1497-1510.

Sahana, D. K., Mittal, G., Bhardwaj, V. and Kumar, M. N. V. R., 2008. PLGA nanoparticles for oral delivery of hydrophobic drugs: influence of organic solvent on nanoparticle formation and release behavior in vitro and in vivo using estradiol as a model drug. J. Pharm. Sci., 97, 1530-1542.

Sall, K., Stevenson, O. D., Mundorf, T. K. and Reis, B. L., 2000. Two multicenter, randomized studies of the efficacy and safety of cyclosporine ophthalmic emulsion in moderate to severe dry eye disease. CsA phase 3 study group. Ophthalmology, 107, 631-639.

Sayed-Ahmed, M. M., Khattab, M., Khalifa, A., El-Khabany, M. and Osman, A. M., 1999. Potenial promise of using L-carnitine and Coenzyme Q10 as protective agents against Cisplatin-induced nephrotoxicity. J. Egyptian National Cancer Institute, 11, 167-173.

Scheiber, S. L. and Crabtree, G. R., 1992. The mechanism of action of cyclosporin A and FK506. Rev. Immunol. Today, 13, 136-42.

Schipper, N. G., Olsson, S., Hoogstraate, J. A., de Boer, A. G., Varum, K. M. and Artursson, P., 1997. Chitosans as absorption enhancers for poorly absorbable drugs 2: mechanism of absorption enhancement. Pharm. Res., 14, 923-929.

Schumacher, A. and Nordheim, A., 1992. Progress towards a molecular understanding of cyclosporin A-mediated immunosuppression. Clin. Investig., 70, 773-779.

Schwendeman, S., Costantino, H. R., Gupta, R. K. and Langer, R., 1997. Peptide, protein and vaccine delivery from implantable polymeric systems: Processes and challenges, in Controlled Drug Delivery: Challenges and Strategies. Park, K. Eds., American Chemical Society: Washington D.C. p. 229-267.

Shah, N. M., Parikh, J., Namdeo, A., Subramanian, N. and Bhowmick, S., 2006. Preparation, characterization and in vivo studies of proliposomes containing cyclosporine A. J. Nanosci. Nanotechnol., 6, 2967-2973.

Shaikh, J., Ankola, D. D., Beniwal, V., Singh, D. and Kumar, M. N. V. R., 2009. Nanoparticle encapsulation improves oral bioavailability of curcumin by at least 9 fold when compared to curcumin administered with piperine as absorption enhancer. Eur. J. Pharm. Sci., 37, 223-230.

Shakweh, M., Ponchel, G. and Fattal, E., 2004. Particle uptake by Peyer's patches: a pathway for drug and vaccine delivery, Expert. Opin. Drug Deliv., 1, 141–163.

Sharma, A., Pandey, R., Sharma, S. and Khuller, G. K., 2004. Chemotherapeutic efficacy of poly (DL-lactide-co-glycolide) nanopaticule encapsulated antitubercular drugs at sub-theraputic dose against experimental tuberculosis. Int. J. Antimicrob. Agents, 24, 599-604.

Shihab, F. S., Bennett, W. M., Yi, H. and Andoh, T. F., 2002. Pirfenidone treatment decreases transforming growth factor-beta1 and matrix proteins and ameliorates fibrosis in chronic cyclosporine nephrotoxicity. Am. J. Transplant., 2, 111-119.

Shono, Y., Nishihara, H., Matsuda, Y., Furukawa, S., Okada, N., Fujita, T. and Yamamoto, A., 2004. Modulation of intestinal P-glycoprotein function by cremophor EL and other surfactants by an in vitro diffusion chamber

method using the isolated rat intestinal membranes. J. Pharm. Sci., 93, 877-885.

Signori, F., Chiellini, F. and Solaro, R., 2005. New self-assembling biocompatible–biodegradable amphiphilic. Polymer, 46, 9642–9652.

Smeesters, C., Giroux, L., Vinet, B., Arnoux, R., Chaland, P., Corman, J., St Louis, G. and Daloze, P., 1988. Efficacy of incorporating cyclosporine into liposomes to reduce its nephrotoxicity. Can. J. Surgery, 31, 34–36.

Sonaje, K., Italia, J. L., Sharma, G., Bhardwaj, V., Tikoo, K. and Kumar, M. N. V. R., 2007. Development of biodegradable nanoparticles for oral delivery of ellagic acid and evaluation of their antioxidant efficacy against cyclosporine A-Induced nephrotoxicity in rats. Pharm. Res., 24, 899-908.

Speiser, P. and Kreuter, J., 1976. In vitro studies of poly(metylmethacrylate) adjuvants. J. Pharm. Sci., 65, 1624-1627.

Spoendlin, M., Peters, J., Welker, H., Bock, A. and Thiel, G., 1998. Pharmacokinetic interaction between oral cyclosporin and mibefradil in stabilized post-renal-transplant patients. Nephrol. Dial. Transplant., 13, 1787–1791.

Starzl, T. E., Klintmalm, G. B., Porter, K. A., Iwatsuki, S. and Schroter G. P., 1981. Liver transplantation with use of cyclosporin A and prednisone. N. Engl. J. Med. 30, 266-269.

Stevanovic, M., Maksin, T., Petkovic, J., Filipic, M. and Uskokovic, D., 2009. An innovative, quick and convenient labeling method for the investigation of pharmacological behavior and the metabolism of poly(DL-lactide-coglycolide) nanospheres. Nanotechnology, 20, 335102.

Stonecipher, K., Perry, H. D., Gross, R. H. and Kerney, D. L., 2005. The impact of topical cyclosporine A emulsion 0.05% on the outcomes of

patients with keratoconjunctivitis sicca. Curr. Med. Res. Opin., 21, 1057-1063.

Sullivan, P. G., Thompson, M. and Scheff, S. W., 2000. Continuous infusion of cyclosporin A postinjury significantly ameliorates cortical damage following traumatic brain injury. Exp. Neurol. 161, 631-637.

Suzuki, N., Sakane, T. and Tsunematsu, T., 1990. Effects of a novel immunosuppressive agent, FK506 on human B-cell activation. Clin. Exp. Immunol., 79, 240–245.

Taler, S. J., Textor, S. C., Canzanello, V. J. and Schwartz, L., 1999. Cyclosporin-induced hypertension. Incidence, pathogenesis and management. Drug Safety, 20, 437–449.

Tam, J. S., McConvillie, J. T., Williams, R. O. and Johnston, K. P., 2008. Amorphous Cyclosporin Nanodispersions for Enhanced Pulmonary Deposition and Dissolution. J. Pharm. Sci., 97, 4915-4933.

Tan, B., Piwnica-Worms, D. and Ratner, L., 2000. Multidrug resistance transporters and modulation. Curr. Opin. Oncol. 12, 450–458.

Tanaka, C., Kawai, R. and Rowland, M., 2000. Dose-dependent pharmacokinetics of cyclosporin A in rats: events in tissues. Drug Metab. Dispos., 28, 582-589.

Tatavarti, A. S., Mehta, K. A., Augsburger, L. L. and Hoag, S. W., 2004. Influence of methacrylic and acrylic acid polymers on the release performance of weakly basic drugs from sustained release hydrophilic matrices. J. Pharm. Sci., 93, 2319-2331.

The Canadian multicentre transplant study group, 1986. A randomized clinical trial of cyclosporine in cadaveric renal transplantation: analysis at three years. N. Engl. J. Med., 314, 1219-1225.

Theil, G., Hermle, M., and Brunner, F. P., 1986. Acutely impaired renal function during intravenous administration of cyclosporine A: a cremophore side effect. Clin. Nephrol., 25, S40-S42.

Thunemann, A. F. and General, S., 2001. Nanoparticles of a polyelectrolyte–fatty acid complex: carriers for Q10 and triiodothyronine. J. Control. Release., 75, 237-247.

Tobio, M., Gref, R., Sanchez, A., Langer, R. and Alonso, M. J., 1998. Stealth PLA– PEG nanoparticles as protein carriers for nasal administration. Pharm. Res., 15, 270-275.

Tobio, M., Sanchez, A., Vila, A., Soriano, I., Evora, C., Vila-Jato J. L. and Alonso, M. J., 2000. The role of PEG on the stability in digestive fluids and in vivo fate of PEG-PLA nanoparticles following oral administration. Colloids Surf. B: Biointerf., 18, 315–323.

Toki, K., Kyo, M., Takahara, S., Hatori, M., Morozumi, K., Ichimaru, N., Wang, J.-D., Ding, X.-Q., Miyamoto, M. and *et al*., 1999. Histopathologic findings in routine biopsies of renal transplant allografts. Transplant. Proc., 31, 2655-2658.

Toronto Lung Transplant Group, 1986. Unilateral lung transplantation for pulmonary fibrosis. N. Engl. J. Med., 314, 1140-1145.

Touw, C. R., Hakkaart-Van Roijen, L., Verboom, P., Paul, C., Rutten, F. F. and Finlay, A. Y., 2001. Quality of life and clinical outcome in psoriasis patients using intermittent cyclosporine. Br. J. Dermatol., 144, 967-972.

Tracy, M., Ward, K., Firouzabadian, L., Wang, Y., Dong, N., Qian, R. and Zhang Y., 1999. Factors affecting the degradation rate of poly(lactide-co-glycolide) microspheres in vivo and in vitro. Biomaterials, 20, 1057-1062.

Tsao, T. M., Wang, M. K. and Huang, P. M., 2009. Automated ultrafiltration device for efficient collection of environmental nanoparticles from aqueous suspensions. Soil Sci. Soc. Am. J., 73, 1808-1816.

Tse, G., Blankschtein, D., Shefer, A. and Shefer, S., 1999. Thermodynamic prediction of active ingredient loading in polymeric microparticles. J. Control. Rel., 60, 77-100.

Tse, K. C., Lam, M. F., Yip, P. S., Li, F. K., Lai, K. N. and Chan, T. M., 2004. A long-term study on hyperlipidemia in stable renal transplant recipients. Clin. Transplant. 18, 274–280.

Tugwell, P., Bombardier, C., Tugwell, P., Gent, M., Bennett., K. J., Roberts, R. S. Ludwin, D., Bensen, W. G., Carette, S. and *et al*., 1990. Low dose cyclosporin versus placebo in patients with rheumatoid arthritis. Lancet, 355, 1051-1055.

Ubrich, N., Bouillot, P. Pellerin, C., Hoffman, M. and Maincent., P., 2004. Preparation and characterization of propranolol hydrochloride nanoparticles: a comparative study. J. Control. Rel., 97, 291-300.

Upaganlawar A. B., Farswan, M., Rathod, S. P. and Balaraman, R., 2006. Protective role of CoQ10 on gentamicin induced nephrotoxicity in rats. The Indian Pharmacist, 5, 105-107.

van der Lubben, I., Verhoef, J. C., Borchard, G. and. Junginger, H. E., 2001. Chitosan and its derivatives in mucosal drug and vaccine delivery, Eur. J. Pharm. Sci., 14, 201–207.

Varela, M. C., Guzman, M., Molpeceres, J., del Rosario Aberturas, M., Rodriguez-Puyol, D. and Rodriguez-Puyol, M., 2001. Cyclosporine-loaded polycaprolactone nanoparticles: immunosuppression and nephrotoxicity in rats. Eur. J. Pharm. Sci., 12, 471-478.

Venkataram, S., Awni, W. M., Jordan, K. and Rahman, Y. E., 1990. Pharmacokinetics of two alternative dosage forms for cyclosporine: liposomes and intralipid. J. Pharm. Sci., 79, 216-219.

Verrechia, T., Spenlehauer, G., Bazile, D. V., Murry-Brelier, A., Archimbaud, Y. and Veillard, M., 1995. Non-stealth (poly(lactic acid/albumin) and stealth (poly(lactic acid–polyethylene glycol)) nanoparticles as injectable drugs carriers. J. Control. Rel., 36, 49–51.

Vila, A., Sanchez, A., Tobio, M., Calvo, P. and Alonso, M. J., 2002. Design of biodegradable particles for protein delivery. J. Control. Rel., 78, 15-24.

Walker, P. D., Barri, Y. and Shah, S. V., 1999. Oxidant mechanisms on gentamicin nephrotoxicity. Ren. Fail., 21, 433–442.

Wang, X., Chi, N. and Tang, X., 2008. Preparation of estradiol chitosan nanoparticles for improving nasal absorption and brain targeting. Eur. J. Pharm. Biopharm., 70, 735-740.

Wasko M. C. M., Hubert, H. B., Lingala, V B., Elliott, J. R., Luggen, M. E., Fries, J. F. and Ward, M. W., 2007. Hydroxychloroquine and Risk of Diabetes in Patients With Rheumatoid Arthritis. JAMA, 298, 187-193.

Weis, M., Mortensen, S. A., Rassing, M. R., Moller, S. J., Poulsen, G. and Rasmussen, S. N., 1994. Bioavailability of four oral Coenzyme Q10 formulations in healthy volunteers. Mol. Aspects Med., 15, S273-S280.

Wenger, R. M., 1984. Total synthesis of 'cyclosporin A' and 'cyclosporin H', two fungal metabolites isolated from species Tolypocladium Inflatum Gams. Helv. Chim. Acta. 67, 503-515.

Wong, W. H. and Mooney, D. J., 1997. In Synthetic Biodegradable Polymers Scaffolds; Atala, A., Mooney, A., Eds., Birkhauser: Boston p 51-82.

Woo, J. S., Piao, M. G., Li, D. X., Ryu, D. S., Choi, J. Y., Kim., J. A., Kim, J. H., Jin, S. G., Kim, D. D. and *et al*., 2007. Development of cyclosporin A-

loaded hyaluronic microsphere with enhanced oral bioavailability. Int. J. Pharm., 10, 134-141.

Woodroffe, R., Yao. G. L., Meads, C., Bayliss, S., Ready, A., Raftery, J. and Taylor, R. S., 2005. Clinical and cost-effectiveness of newer immunosuppressive regimens in renal transplantation: a systematic review and modelling study. Health Technol. Assess., 9, 21.

Wu, C.-Y., Benet, L. Z., Hebert, M. F., Gupta, S. K., Rowland, M., Gomez, D. Y. and Wacher, V. J., 1995. Differentiation of absorption and first-pass gut and hepatic metabolism in humans: Studies with cyclosporine. Clin. Pharmacol. Therap., 58, 492-497.

Xu, J., Guo, B.-H., Zhang, Z.-M., Zhou, J.-J., Jiang, Y., Yan, S., Li, L., Wu, Q., Chen, G.-Q. and Schultz, J. M., 2004. Direct AFM Observation of Crystal Twisting and Organization in Banded Spherulites of Chiral Poly(3-hydroxybutyrate-co-3-hydroxyhexanoate). Macromolecules, 37, 4118–4123.

Yamagami, T., Shibata, W. and Folkers, K., 1986. Bioenergitics in clinical medicine. Administration of coenzyme Q10 to patients with essential hypertension. Res. Commun. Chem. Pathol. Pharmacol., 14, 721-727.

Yenice, I., Mocan, M. C., Palaska, E., Bochot, A., Bilensoy, E., Vural, I. Irkeç, M. and Hincal, A. A., 2008. Hyaluronic acid coated poly-3-caprolactone nanospheres deliver high concentrations of cyclosporine A into the cornea. Exprimental Eye Res., 87, 162-167.

Yu, F. and Zhuo, R., 2003. Synthesis, characterization, and degradation behavior of end-group -functionalized poly(trimethylene carbonate)s. Polym. J., 35, 671-676.

Yuce, A., Atessahin, A. and Ceribasi, A. O., 2008. Amelioration of Cyclosporine A –induced Renal, hepatic and Cardiac damages by ellagic acid in rats. Basic Clin. Pharmacol. Toxicology, 103, 186–191.

Zhang, J. and Musson, D. G., 2006. Investigation of high-throughput ultrafiltration for the determination of an unbound compound in human plasma using liquid chromatography and tandem mass spectrometry with electrospray ionization. J. Chromatography B, 843, 47-56.

Zhao, J., Quan, D., Liao, K. and Wu, Q., 2005. PLGA- (L-Asp-alt-diol)(x)-PLGAs with different contents of pendant amino groups: synthesis and characterisation. Macromol. Biosci., 5, 636-643.

Zhong, Z., Arteel, G. E., Connor, H. D., Yin, M., Frankenberg, M., Stachlewitz., Raleigh, J. A., Mason, R. P. and Thurman, R. G., 1998. Cyclosporin A increases hypoxia and free radical production in rat kidneys: prevention by dietary glycine. Am. J. Physiol. Renal Physiol., 275, F595-F604.